Stellingen behorende bij het proefschrift "Positron Moderation and Reemission Experiments"

1. De waarde van het gemiddelde energieverlies per botsing van een positron met vast argon zoals genoemd door Gullikson en Mills is fout.
   E. M. Gullikson en A. P. Mills Jr, Phys. Rev. Lett. 57, 376 (1986) en hoofdstuk 3 van dit proefschrift.

2. De negatieve werkfunktie van de halfgeleiders SiC en GaN voor positronen maakt hen veelbelovende kandidaat-materialen voor veld-geassisteerde moderatie op kamertemperatuur.
   Hoofdstuk 4 van dit proefschrift.

3. Pyrolytisch BN heeft een positieve werkfunctie voor positronen.
   Hoofdstuk 4 van dit proefschrift.

4. De gewoonte om bij de berekening van implantatieprofielen van positronen de kristallijne effecten niet in rekening te brengen is een mogelijke verklaring voor de slechte beschrijving van implantatieprofielen in dunne lagen.
   Hoofdstuk 5 van dit proefschrift.

5. Als positronen een wolfraamoppervlak bereiken vanuit vacuüm met een energie kleiner dan de absolute waarde van de negatieve werkfunktie van dat materiaal, zal een significante fractie worden gereflecteerd.
   Hoofdstuk 6 van dit proefschrift.

6. Een veelbelovende alternatieve methode om een zeer heldere positronenbundel te verkrijgen is het opslaan van positronen in een ionenval, waarna de positronen worden gekoeld voordat de val wordt geopend.
   S. J. Gilbert, C. Kurz, R. G. Greaves en C. M. Surko, Appl. Phys. Lett. 70, 15 (1997)

7. De gebonden toestand van twee positronen en een elektron wordt Ps^+ genoemd. Strikt genomen is Ps_2^+ een betere naam.

8. Tijdens het etsen van staal met zoutzuur kan de interne waterstofdruk in interne holtes (zogenaamde blow-holes) zo ver oplopen dat het staal gedeformeerd wordt.
   O. Dankert, R. van Meenen, A. van Veen, J. Zijp en A. A. Kamperman, wordt   gepubliseerd

9. Het aantal studenten dat kiest voor een beta-studie is een goede maat voor de maatschappelijke status van natuurwetenschappers.

10. Auto's van buitenlands fabrikaat zouden moeten worden verboden aangezien ze meer doden per jaar veroorzaken dan de nieuwe variant van de Creutzfeldt-Jacob ziekte die heeft geleid tot het importverbod van Brits rundvlees.

11. De gezamenlijke markt van de Europese Unie heeft het verhuizen binnen de Unie nog niet zo eenvoudig gemaakt als het verhuizen binnen één van de lidstaten nu is.

12. Er zit veel fysica in een glas bier.
   "Clouds in a Glass of Beer" van Craig F. Bohren, John Wiley and Sons, New York 1987

Propositions (stellingen) belonging to the thesis "Positron Moderation and Reemission Experiments"

1. The value of the average positron energy loss per collision below the inelastic threshold in solid argon reported by Gullikson and Mills is in error.
    E. M. Gullikson and A. P. Mills Jr, Phys. Rev. Lett. 57, 376 (1986) and chapter 3 of this thesis.

2. The negative positron workfunctions of the wide bandgap semiconductors SiC and GaN make them promising candidates for Field Assisted Moderation (FAM) at room temperature.
    Chapter 4 of this thesis.

3. Pyrolytic BN has a positive positron workfunction.
    Chapter 4 of this thesis.

4. The failure of standard positron implantation profiles to take crystalline effects into account could possibly explain why they do not describe implantation in thin films very well.
    Chapter 5 of this thesis.

5. When positrons impinge on a tungsten surface with an energy less than the absolute value of the negative workfunction of that material, a significant fraction will be reflected from the surface.
    Chapter 6 of this thesis.

6. A promising alternative method to achive a high brightness beam of positron is to first store the positrons in an ion trap and subsequently cool the stored particles prior to their controlled release from the trap.
    S. J. Gilbert, C. Kurz, R. G. Greaves and C. M. Surko, Appl. Phys. Lett. 70, 15   (1997)

7. The bound state of two positrons and an electron is traditionally called Ps^+. A more stringently correct name would be Ps_2^+.

8. Loading extended voids in steel (e.g. blow-holes) with hydrogen during etching with hydrocloric acid can cause very high internal pressures. After the loading the material might become deformed.
    O. Dankert, R. van Meenen, A. van Veen, J. Zijp and A. A. Kamperman, to be published

9. The number of students who choose to study science is a good measure of the percieved status of scientists in society.

10. Foreign made cars should be banned as they cause more deaths per year than caused by the new variant of Creutzfeldt-Jacob Disease, which has led to the banning of British beef.

11. The rules of the European Unions for a single labour market have not yet made it as easy to move between the countries of the union as within one country.

12. Many physics lessons can be learned from a glas of beer.
    "Clouds in a Glass of Beer" by Craig F. Bohren, John Wiley and Sons, New York 1987

Positron Moderation and Re-emission Experiments

Positron Moderation and Re-emission Experiments

PROEFSCHRIFT

ter verkrijging van de graad van doctor
aan de Technische Universiteit Delft,
op gezag van de Rector Magnificus Prof. ir. K. F. Wakker,
in het openbaar te verdedigen ten overstaan van een commissie,
door het College van Promoties aangewezen,
op maandag 8 juni 1998 om 13.30 uur

door

Lars Varming JØRGENSEN

Cand. Scient. in de Natuurkunde

geboren te Bramdrup, Denemarken

Dit proefschrift is goedgekeurd door de promotoren:
Prof. dr. A. van Veen
Prof. dr. ir. H. van Dam
Prof. dr. ir. P. Kruit

Samenstelling promotiecommisie:

Rector Magnificus, voorzitter	
Prof. dr. A. van Veen	RU Groningen, promotor
Prof. dr.ir. H. van Dam	TU Delft, promotor
Prof. dr. ir. P. Kruit	TU Delft, promotor
Dr. M. Charlton	University College London, U.K.
Prof. dr. J. Th. M. de Hosson	RU Groningen
Prof. dr. ir. C. W. E. van Eijk	TU Delft
Prof. dr. W. Th. Wenckebach	TU Delft

TABLE OF CONTENTS

List of publications related to this thesis:

Chapter 3:

"Field assisted positron moderation by surface charging of rare gas solids"
> J. P. Merrison, M. Charlton, B. I. Deutch and L. V. Jørgensen, J. Phys.: Condens. Matter **4**, L207 (1992)

"Studies of positron moderation in surface charged rare gas solids"
> J. P. Merrison, M. Charlton, B. I. Deutch and L. V. Jørgensen, Hyp. Int. **76**, 305 (1993)

"Positron dynamics in surface charged solid argon"
> L. V. Jørgensen, J. P. Merrison, B. I. Deutch, M. Charlton and G. O. Jones, Phys. Rev. B **52**, 12402 (1995)

Chapter 4:

"Positron re-emission from epitaxially grown β-SiC"
> L. V. Jørgensen, A. van Veen and H. Schut, Nucl. Instr. and Meth. in Phys. Res. B **119**, 487 (1996)

"Investigation of vacancies in GaN by positron annihilation"
> L. V. Jørgensen, A. C. Kruseman, H. Schut, A. van Veen, M. Fanciulli and T. D. Moustakas, MRS Fall Meeting 1996, III-V Nitrides, Mat. Res. Soc. Proc. **449**, 853 (1997)

"GaN - a new material for positron moderation"
> A. van Veen, L.V. Jørgensen and H. Schut, to be published

Chapter 5:

"A rectifying tungsten-molybdenum foil for positron remoderation"
> L. V. Jørgensen, A. van Veen, H. Schut and J. Chevallier, J. Appl. Phys. **81**, 2725 (1997)

"Positron transmission remoderation using bi-layered rectifying foils"
> L. V. Jørgensen, A. van Veen, H. Schut, and J. Chevallier, Mat. Sci. Forum **255-257**, 647 (1997)

Chapter 6:

"Evidence of very low energy positron reflection off tungsten surfaces"
> L. V. Jørgensen, F. Labohm, H. Schut, and A. van Veen, submitted to J.Phys.: Condens. Matter

Other publications:

"Thermal activation of positronium from thin Ag(100) films in backscattering and transmission geometries"
> M. R. Poulsen, M. Charlton, J. Chevallier, B. I. Deutch, L. V. Jørgensen and G. Laricchia, J. Phys.: Condens. Matter **3**, 2849 (1991)

"Positronium formation from silver"
> M. R. Poulsen, M. Charlton, B. I. Deutch, L. V. Jørgensen and G. Laricchia, Hyp. Int. **76**, 309 (1993)

"Antihydrogen synthesis by the reaction of antiprotons with excited state positronium atoms"
> B. I. Deutch, M. Charlton, M. H. Holzscheiter, P. Hvelplund, L. V. Jørgensen, H. Knudsen, G. Laricchia, J. P. Merrison and M. R. Poulsen, Hyp. Int. **76**, 153 (1993)

"Morphologies and growth modes of FeSi and β-FeSi$_2$ layers prepared by rapid thermal annealing"
> P. H. Amesz, L. V. Jørgensen, M. Libezny, J. Poortmans, J. Nijs, A. van Veen, H. Schut and J. Th. M. de Hosson, MRS Fall Meeting 1995, Silicide Thin Films - Fabrication, Properties and Applications, Mat. Res. Soc. Proc. **402**, 373 (1996)

"Hydrogen formation by proton impact on positronium"
> J. P. Merrison, H. Bluhme, J. Chevallier, B. I. Deutch, P. Hvelplund, L. V. Jørgensen, H. Knudsen, M. R. Poulsen, and M. Charlton, Phys. Rev. Lett. **78**, 2728 (1997)

"Monitoring of the thermal annealing of HDP-Si oxides by positron annihilation and thermal desorption spectrometry"
> H. Schut, A. van Veen, L. V. Jørgensen, O. Dankert, K. T. Westerduin, A. H. Reader, and J. C. Oberlin, Microelectronic Engeneering **33**, 357 (1997)

"Trapping of nitrogen at the Fe-AlN precipitate interface studied by the Positron Doppler Broadening Technique"
> H. Schut, A. van Veen, L. V. Jørgensen, S. van der Zwaag, and N. Geerlofs, Mat. Sci. Forum **255-257**, 427 (1997)

"Conversion electron Mossbauer spectroscopy and positron annihilation study of pseudomorfic Fe$_{0.5}$Si"
> M. Fanciulli, L.V. Jørgensen, G. Weyer, A. van Veen, H. von Kaenel and N. Onda, to be published

"Microscopic environment of Sn in pseudomorphic Si(1-x)Sn(x) thin films"
C. Ridder, L.V. Jørgensen, M. Fanciulli, A. Nylandsted Larsen, G. Weyer, H. Schut, and A. van Veen, to be published

LIST OF SYMBOLS

a	in-plane lattice constant for hexagonal crystal structure [Å]
A_+	positron affinity [eV]
B	magnetic field [T]
B_r	reduced brightness [A/(sr m^2 keV)]
c	velocity of light [2.9979 × 10^8 m/s]
c	inter-plane lattice constant for hexagonal crystals structure [Å]
$c(z)$	steady state positron distribution as a function of depth [m^{-3}]
d	positron beam diameter [m]
d	sample thickness [m]
dE	average energy loss per collision due to phonon interactions [eV]
D	surface diplole barrier [eV]
D_+	positron diffusivity in defect-free material [m^2/s]
e	elementary charge [1.6022 × 10^{-19} C]
E	(initial) energy of implanted positron [keV]
E	photon energy [keV]
E	electric field [V/m]
E_a	activation energy for positronium formation [eV]
E_b	binding energy of the positron to the surface potential well [eV]
E_{Ps}^{BAr}	bulk inelastic positronium formation threshold for argon [eV]
E_{Ps}^{cAr}	effective positronium threshold at the surface of contaminated argon [eV]

E_{Ps}^{O2} effective positronium threshold at the surface of O_2 coated argon [eV]

f_{bulk} fraction of implanted positrons that annihilate in the bulk [-]

f_{e+} fraction of implanted positrons that are reemitted as free positrons [-]

f_i fraction of implanted positrons that annihilate in layer i [-]

f_{Ps} fraction of implanted positrons that annihilate as positronium [-]

$f_{surface}$ fraction of implanted positrons that annihilate at the surface [-]

F_{e+} fraction of the total beam that are reemitted as free positrons [-]

$F_s(E)$ fraction of implanted positrons that reach the surface [-]

k   Boltzmanns constant [1.380662×10^{-23} J/K]

l_s scattering length [m]

L   diffusion length [m]

m mass of particle [kg]

m shape parameter for the Makhovian implantation profile [-]

m_0, m_e electron rest mass [kg]

n exponential constant in the formula for the mean implantation depth [-]

$n_i(z)$ depth dependant defect concentration [m^{-3}]

P_l longitudinal momentum component [kg m/s]

P_t transverse momentum component [kg m/s]

$P(z,E)$ implantation profile [-]

r_0 classical electron radius [m]

R   reflection coefficient [-]

S S- or Shape annihilation lineshape parameter [-]

S_i S parameter for annihilation in the layer i [-]

$S_{surface}$ S parameter for annihilation at the surface [-]

t time [s]

T   temperature [K]

V_{grid} potential on grid [V]

W W- or Wing annihilation lineshape parameter

z depth below surface [m]

$<z>$ mean implantation depth [m]

z_0 penetration parameter [m]

Z	atomic number of material [-]
α	constant in the formula for the mean implantation depth [g cm^{-2} (keV)$^{-n}$]
Γ	annihilation rate [1/s]
$\Gamma(x)$	Euler's gamma function [-]
δ	change in surface dipole barrier caused by adsorption [eV]
Δ	dipole potential step between two metals in contact [eV]
ΔE	photon energy shift [keV]
$\Delta E_+^{A,B}$	difference in ground state positron energy across the interface between material A and B [eV]
Δm	mass difference [kg]
ΔV	potential shift [V]
$\Delta \phi_-$	electron workfunction difference between two materials [eV]
ϵ	electric field [V/m]
ϵ_{e+}	the surface branching rate to free positrons [-]
ϵ_{Ps}	the surface branching rate to positronium [-]
$\epsilon_{surface}$	the surface branching rate to the surface state [-]
ϵ_r	relative dielectric constant [-]
η	the fraction of positrons backscattered from a surface [-]
Θ	angular deviation from collinearity [rad]
Θ_D	Debye temperature [K]
λ_b	bulk annihilation rate [1/s]
μ_+	positron mobility [m^2/V s]
μ_-	electron chemical potential [eV]
μ_+	positron chemical potential [eV]
v_d	positron drift velocity [m/s]
v_t	specific positron trapping rate for a defect [1/s]
v_{th}	mean velocity during thermalization [m/s]
ρ	mass density [kg/m^3]
$\rho_-(\mathbf{r})$	electron probability density at position $\mathbf{r}$ [1/m^3]
$\rho_+(\mathbf{r})$	positron probability density at position $\mathbf{r}$ [1/m^3]

τ	positron lifetime [s]
τ	characteristic time of the system (chapter 6) [s]
τ_i	time between collisions [s]
τ_{sc}	average time between collisions [s]
ϕ_-	electron workfunction [eV]
ϕ_+	positron workfunction [eV]
Ω	solid angle [sr]

LIST OF ABBREVIATIONS

ADC	Analog-to-Digital Converter
bcc	body centered cubic
BNL	Brookhaven National Laboratory
CCD	Charge Coupled Device
CPT	Charge - Parity - Time
CVD	Chemical Vapor Deposition
DC	Direct Current
E-BEAM	The Electrostatic Positron Beamline at Delft
ECR	Electron Cyclotron Resonance
FG	Function Generator
FWHM	Full Width at Half Maximum
LED	Light Emitting Diode
LEPD	Low Energy Positron Diffraction
MBE	Molecular Beam Epitaxy
MCP	Multi Channel Plate
MOS	Metal - Oxide - Semiconductor
o-Ps	ortho-positronium
PALS	Positron Annihilations Lifetime Spectroscopy
POSH	POSitrons at the HOR-reactor - The reactor based positron beamline at Delft
ppmv	parts per million volume

p-Ps	para-positronium
PRM	Positron Reemission Microscope
Ps	Positronium
q-Ps	quasi-positronium
RGS	Rare Gas Solid
SEM	Scanning Electron Microscope
SI	Semi Insulating
TFA	Timing Filter Amplifier
TTL	Transistor-Transistor Logic
UV	Ultra Violet
VEP	Variable Energy Positron beamline at Delft (The magnetic beamline)
VEPFIT	Variable Energy Positron Fitting and Modelling Program
2D-ACAR	Two-dimensional Angular Correlation of Annihilation Radiation

CHAPTER 1

INTRODUCTION

1.1. General and motivation

Positron techniques have proved to be a major tool in the study of defects in materials. The positron's unique ability to trap at vacancies and open volume defects makes it an interesting probe of such defects (see e.g. Schultz and Lynn 1988 and refs. therein). Its high sensitivity to such defects over a very wide range of defect concentrations and defect sizes makes it a valuable probe of electron densities and momenta in the vicinity of such defects as well as in the bulk of solids (see Fig. 1.1). By using a beam of monoenergetic positrons a depth profile of vacancy type defects can be obtained and, in principle, a complete three dimensional map of the defects can be made.

It is with such high resolution defect profiling in mind that a positron microprobe facility is under construction at the Interfaculty Reactor Institute at Delft University of Technology (Seijbel 1995, van Veen *et al.* 1994). After moderation of positrons from a nuclear reactor based source and subsequent fourfold remoderation the resulting positron beam will be focused to a final spot size of 100 nm. This beam will be injected into a standard Philips Scanning Electron Microscope. By having the positron beam coming in from the side and being deflected onto the column axis of the
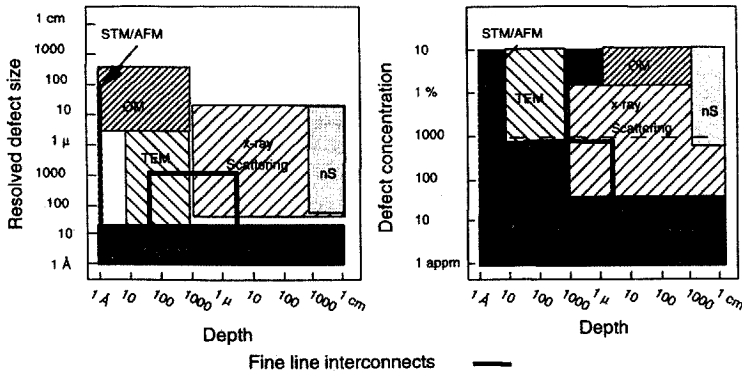
Fig. 1.1. The power of positron spectroscopy techniques for general vacancy defect analysis compared to other relevant techniques. OM: Optical Microscopy, nS: neutron scattering, TEM: Transmission Electron Microscopy, STM: Scanning Tunneling Microscopy, AFM: Atomic Force Microscopy. Positron techniques are both highly sensitive and can resolve the size of atomic vacancies at any depth in the sample. The solid black line outlines the range of interest for studies of fine lines used as electronic interconnects (from Howell *et al.* 1997).

microscope, it will be possible to switch between the electron beam of the SEM and the positron beam. Thus electrons can be used to seek out an interesting location for further study after which the positrons can do a defect depth scan down to a depth of several µm at that position. This will allow investigation of defects in actual industrial microelectronics devices. The first measurements planned for this facility will study microscale MOS (Metal-Oxide-Semiconductor) systems and electro-migration in microelectronic devices. Positron microprobes for depth profiling of defects are also planned/under construction at Lawrence Livermore National Laboratory, U.S.A. (Howell *et al.* 1997) and Technical University of Munich, Germany (Triftshäuser *et al.* 1997).

With the use of positron moderation to generate the beam, a transmission remoderation stage at the exit from the reactor and a three stage transmission remoderation right before the injection into the SEM, the efficiency attainable in moderation and remoderation will greatly influence the final positron flux. Thus a factor two increase in remoderation efficiency will result in an increase of the number of positrons present in the probe of more than an order of magnitude. Therefore we decided to investigate a number of materials and techniques that might potentially lead to more efficient moderation and remoderation of positrons.

The experiments performed at the University of Aarhus, Denmark, (chapter 3) were done as a part of an international collaboration to synthesize and characterize low energy atomic antihydrogen (Deutch *et al.* 1993, Merrison *et al.* 1997). Again the moderation efficiency is of great importance since a large positron flux will help counter the low cross-sections involved.

1.2. Basic positronic properties

1.2.1. Positrons

The positron is the antiparticle of the electron and its existence was first suggested by Dirac in 1930 as the negative energy solution to his relativistic wave equation. Dirac originally thought that the antiparticle of the electron was the proton, but in 1931 Weyl pointed out that the antielectron necessarily had to have the same mass as the electron. The positron was first observed by Anderson (1932a, 1932b, 1933) in cloud chamber experiments observing the energy loss of cosmic rays when passing through lead.

Being the antiparticle of the electron, the positron has the same mass ($\Delta m/m < 1.3 \times 10^{-7}$; Schwinberg, Van Dyck and Dehmelt 1981) and according to the CPT theorem they should have the same spin, but opposite charge and thus opposite magnetic moment. The positron is stable in vacuum ($\tau > 2 \times 10^{21}$ yrs.; Bellotti *et al.* 1983). It may, however, annihilate with its antiparticle, the electron.

This annihilation may occur in a number of ways denoted by the number of γ-photons involved, viz. non-photon, one-photon, two-photon, three-photon, etc. The two first annihilation modes are very rare because of energy and momentum conservation. Detailed calculations by Ore and Powell (1949) gives the 3γ to 2γ ratio as $1/371$, so the 3γ process, as well as any higher order processes can generally be ignored.

In 2γ annihilations where the positron-electron pair is at rest at the time of annihilation, conservation of energy and momentum requires that the two photons are emitted in opposite directions with an energy of $m_0c^2 = 511$ keV each, where m_0 is the electron rest mass. If, at the time of annihilation, the positron-electron pair has a momentum **p**, the two photons will be emitted at an angle slightly deviating from collinearity and with energies shifted slightly from 511
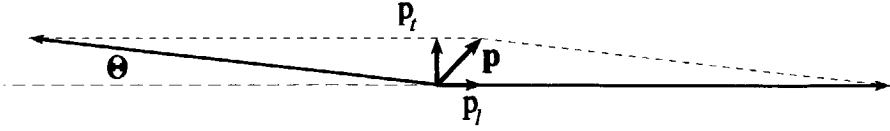
Fig. 1.2. Vector diagram for the momentum of the two photons from the annihilation process of an positron-electron pair with momentum **p**. Θ is the deviation from exact collinearity.

keV (Fig. 1.2). To the first order the angular deviation from collinearity is given by

$$\Theta = \frac{p_t}{m_0 c} \tag{1.1}$$

where p_t is the transverse component of the momentum. The energy shift, ΔE, from 511 keV can be derived from the longitudinal momentum component of the positron-electron pair

$$\Delta E = \frac{c p_l}{2} \tag{1.2}$$

Typical values of electron momentum using the free electron model yields angular deviations of up to 5 mrad and energy shifts in the order of 1 to 2 keV. The angular deviations are easily detected in modern angular correlation measurements and form the basis of the two dimensional angular correlation of annihilation radiation (2D-ACAR) technique. The energy shifts are also well within the experimental reach of modern solid state detectors and form the basis of Doppler broadening measurements (see chapter 2). Since the thermalization time for positrons in most solids is about two orders of magnitude shorter than the positron lifetime in solids, the positron's contribution to the total momentum of the positron-electron pair is negligible. Hence the 2D-ACAR and Doppler broadening techniques yield information about the electron momentum distribution in the solid.

The probability of a positron annihilating with an electron is determined by the overlap of

the electron and positron wavefunctions. The annihilation rate, Γ, is given by

$$\Gamma = \pi r_0 \int dr\, \rho_-(r)\, \rho_+(r) \qquad (1.3)$$

where $\rho_-(r)$ and $\rho_+(r)$ are the electron and positron probability densities at position r, respectively, and r_0 is the classical electron radius. The lifetime of the positron, τ, is the inverse of the decay rate, $\tau = \Gamma^{-1}$, so the lifetime is inversely proportional to the electron density. Therefore the positron annihilation lifetime spectroscopy (PALS) technique yields information about the electron density at the annihilation site. Typical lifetimes in metals are of the order of 150 ps, although it can vary considerably from one metal to another (Dupasquier 1981). It should be noted that although the lifetimes of positrons in solids seem short on a macroscopic scale, they are orders of magnitude larger than many other microscopical timescales of solids such as lattice relaxation times ($\sim 10^{-13}$ s) or electronic relaxation times ($\sim 10^{-16}$ s).

The usefulness of positron techniques in the study of vacancy-type and open-volume defects in materials is attributable to the positrons propensity to trap at such defects, which form an attractive positron potential in the host material. Being trapped at such a defect the positron experiences a very different electron density and electron momentum density than in the bulk and this can be observed in positron experiments.

1.2.2. Positronium

The existence of a bound state of a positron and an electron was first predicted classically by Mohorovicic (1934). In 1945 Ruark made the quantum mechanical prediction of its existence and calculated its spectrum. He suggested the name positronium for this entity and the abbreviation Ps. Positronium was first experimentally observed by Deutsch in 1951. Wheeler (1946) also showed that it is energetically possible to form bound states of $2e^+ + e^- = Ps^+$, $e^+ + 2e^- = Ps^-$ and $2e^+ + 2e^- = Ps_2$. Of these so far only Ps^- has been observed experimentally (Mills 1981).

Positronium has a hydrogen-like structure, but has approximately half the reduced mass and thus twice as large spatial dimensions. It therefore has a binding energy in vacuum of 6.8 eV, half that of hydrogen. In vacuum positronium is formed in two distinct spin ground states: para-positronium and ortho-positronium, with the formation ratio of 1:3. The former is a $^1S_0$ singlet

state and the latter a $^3S_1$ triplet state with vacuum lifetimes of 125 ps and 142 ns, respectively. Wolfenstein and Ravenhall (1952), using C invariance, showed that para-positronium predominantly decays under emission of 2γ rays of 511 keV each in a collinear mode. Ortho-positronium mostly decays via 3γ rays with a continuous distribution of energies below 511 keV. Due to the high electron densities in metals and semiconductors, positronium does not form in the bulk of these materials. In insulators and ionic solids positronium formation in the bulk has been observed. However, because of the size of positronium compared to lattice dimensions, the wavefunction of Ps formed in solids is very perturbed. Due to spin-exchange processes with the surrounding electrons, the ortho-positronium lifetime is much shorter than in vacuum. Therefore bulk positronium is usually referred to as quasi-positronium or q-Ps. The annihilation of para-Ps in the bulk can be observed in 2D-ACAR and Doppler broadening measurements as a narrow contribution due to the low intrinsic momentum in the Ps positron-electron pair.

In positron beam studies the formation of positronium on the surface of the solid is also of great importance. This is because it yields information about the diffusion of positrons implanted at some depth that make it back to the surface of entry. Furthermore it might in some cases yield information about the surface condition and surface potentials. Barring any spin-exchange processes with the electrons of the surface, the positronium formed here will be 1/4 para-positronium and 3/4 ortho-positronium. The continuous energy distribution below 511 keV of the photon energy from ortho-positronium annihilation allows determination of the Ps fraction by monitoring the photon energy distribution in the region below the annihilation peak.

1.3. Positron moderation and remoderation

1.3.1. The concept of positron moderation

Most positrons used in experiments originate from radioactive sources. The energy distribution of positrons coming from a radioactive source is very large, typically from 0 eV up to in the order of 1 MeV (Fig.1.3). In principle a beam of positrons could be made directly from the β^+ radioactive source energy distribution through energy selection. But as can be seen from Fig. 2.1 this would have a very small conversion efficiency unless the energy window is set very

wide. A more promising method is the one first suggested by Madanski and Rasetti (1950). This involves implanting the β^+ in a solid where they are stopped (thermalized) and a part of them diffuse back to the surface where they might be re-emitted with low energy. This method for getting low energy positrons is called positron moderation. It was first successfully demonstrated by Cherry (1959). It was not until the '70s, with the discovery of smoked MgO on Au as an efficient material for moderation (Canter *et al.* 1972) and the prediction of workfunction emission of positrons from metals (Tong 1972), that the first practical mono-energetic positron beamlines were built. The latter approach of workfunction emission from metallic surfaces has been the mainstay in positron moderation in the past 20 years.

Compared to energy selection moderation through stopping, diffusion to the surface and workfunction emission has a number of notable advantages. Because the positrons are emitted from the surface with a velocity perpendicular to the surface corresponding to $-\phi_+$, with ϕ_+ being
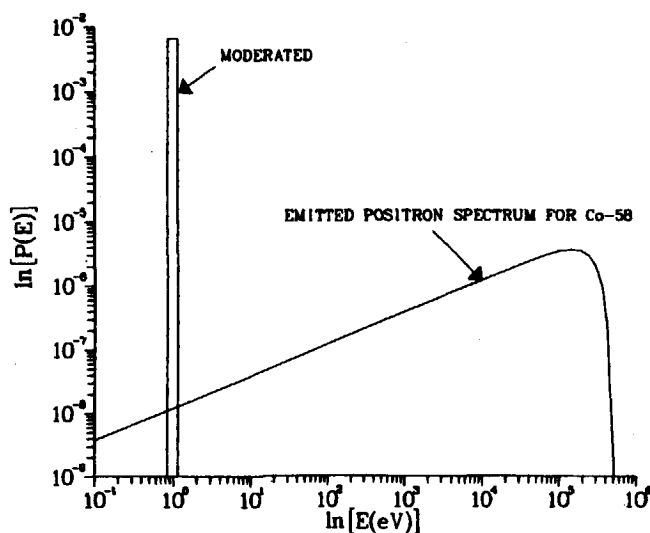

Fig. 1.3. Comparison of positron yield from a moderator with the original β^+ particle energy spectrum for ^{58}Co (normalized) (from Schultz and Lynn 1988).

the positron workfunction (negative for most metals), and with only thermal velocities parallel to the surface the angular spread of the emitted positrons is very small. The energy width of positrons emitted from a clean, mono-crystalline surface is also very narrow (typically < 0.1 eV), being limited primarily by the thermal energy of the positron in the lattice (Schultz and Lynn 1988). Thus it is possible to make very well defined beams of low energy positrons by moderation, but the main advantage of moderation over energy selection is that much higher efficiencies are attainable ($\sim 10^{-3}$ compared to $\sim 10^{-8}$). In the last 10 years the most used material for positron moderation has been W which exhibits a very good efficiency combined with good energy- and angular width characteristics.

1.3.2. Positron remoderation

Regardless of whether a magnetic or electrostatic guidance transport system is used, a central limitation to the quality of any beam is stated by Liouvilles theorem. This means that an assembly of charged particles under the influence of conservative forces occupies a constant volume in phase space:

$$\Omega\,E\,d^{2} = constant \tag{1.4}$$

where Ω is the solid angle, d is the beam diameter and E is the beam energy.

One of the most useful figures of merit for positron beams is the reduced brightness

$$B_r = \frac{I}{\frac{\pi}{4}\,\Omega\,E\,d^{2}} \tag{1.5}$$

where I is the beam current. Because of Liouvilles theorem, the reduced brightness is a conserved quantity for conservative fields. Thus the brightness will not change by acceleration, deceleration, (de)magnification or aperturing of the beam. It is determined by the source -moderator arrangement. The brightness of normal mono-energetic positron beams is low and certainly too low for many highly demanding applications such as our microprobe facility or, e.g., Low Energy Positron Diffraction (LEPD).
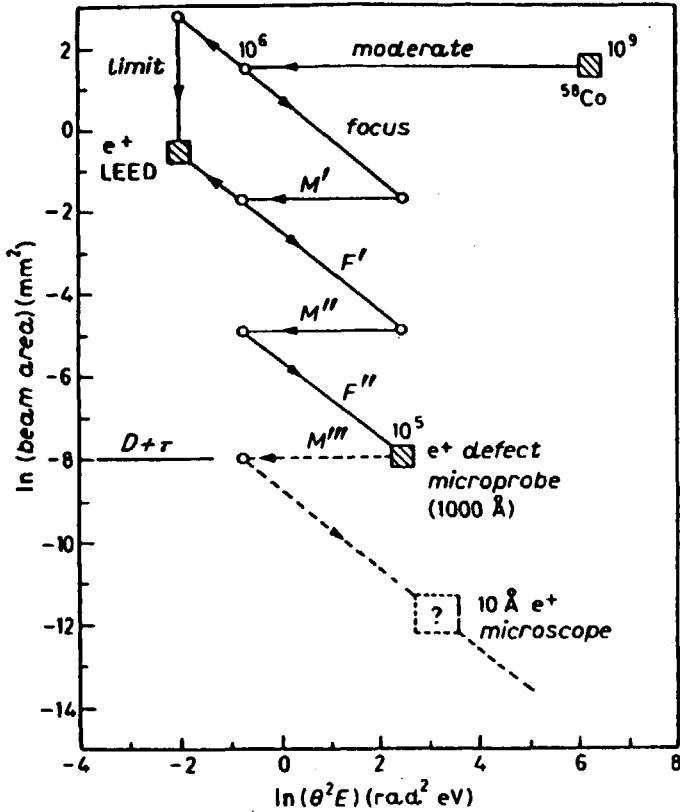
Fig. 1.4. The principle of remoderation (Mills 1981)

It was suggested by Mills (1980), that since the process of moderation is non-conservative, and is therefore not constrained by Liouvilles theorem, it could form the basis for making brighter positron beams. The process is called brightness enhancement and involves the repeated re-moderation of the positron beam (see Fig. 1.4). A beam of positrons focused down to a small spot size before implantation in a negative workfunction solid will be stopped in that solid and a significant fraction might diffuse back to the surface of entry or, in the case of transmission remoderation, to another surface, and there be re-emitted with a velocity perpendicular to the surface determined by the positron workfunction for that surface. By tuning

the energy of the focused incident beam the fraction of positrons reaching the desired exit surface can be maximized. Therefore remoderation efficiencies are much higher than for primary moderation. Since the emitting spot on the moderator is roughly the same size as the focussed entry spot (plus diffusion parallel to the surface) and the positrons are preferentially emitted in the direction perpendicular to the surface, the brightness of the remoderated beam has increased. Thus despite loss of current in the remoderation material the brightness can be increased by up to a factor of 1000. The remoderated beam can be focused and remoderated one more time. This can be repeated until either the desired brightness has been reached, one has run out of beam current or the diffusion limit has been reached. The diffusion limit is when the contribution to the exit spotsize is dominated by the positron diffusion parallel to the exit surface in the remoderator material.

For our reactor based beamline and microprobe facility it has been calculated (Seijbel 1995) that (1+3) times remoderation is necessary to achieve the desired spot size of 100 nm in the probe. As mentioned earlier, the first remoderation will take place at the exit from the reactor to produce a more easily transportable beam and the three other will take place immediately prior to injection in the SEM.

1.3.3. Positron interaction with solids and surfaces

In order to assess how the efficiency of positron moderation and remoderation might be improved, it is important to understand the interactions positrons undergo during moderation or remoderation. An overview of the various interactions occurring for a mono-energetic positron beam incident on a solid is shown in Fig. 1.5. A short description of the most important processes occurring after the positron has entered the solid will be given. For a more detailed description as well as an account of pre-entry phenomena such as diffraction of the positron beam, backscattering, secondary electron emission or post-entry processes such as channeling, the reader is referred to Schultz and Lynn (1988), Dupasquier and Mills (1995) and references therein.

The main energy loss mechanism for positrons with energies in the range from 100 keV down to 100 eV is electron interactions. In this region the energy loss rate, dE/dt, is proportional to $E^{-1/2}$, where E is the energy of the positron in the material (Nieminen and Oliva 1980). Below about 100 eV the energy loss rate varies with energy as $E^{5/2}$. Electron-hole excitations and
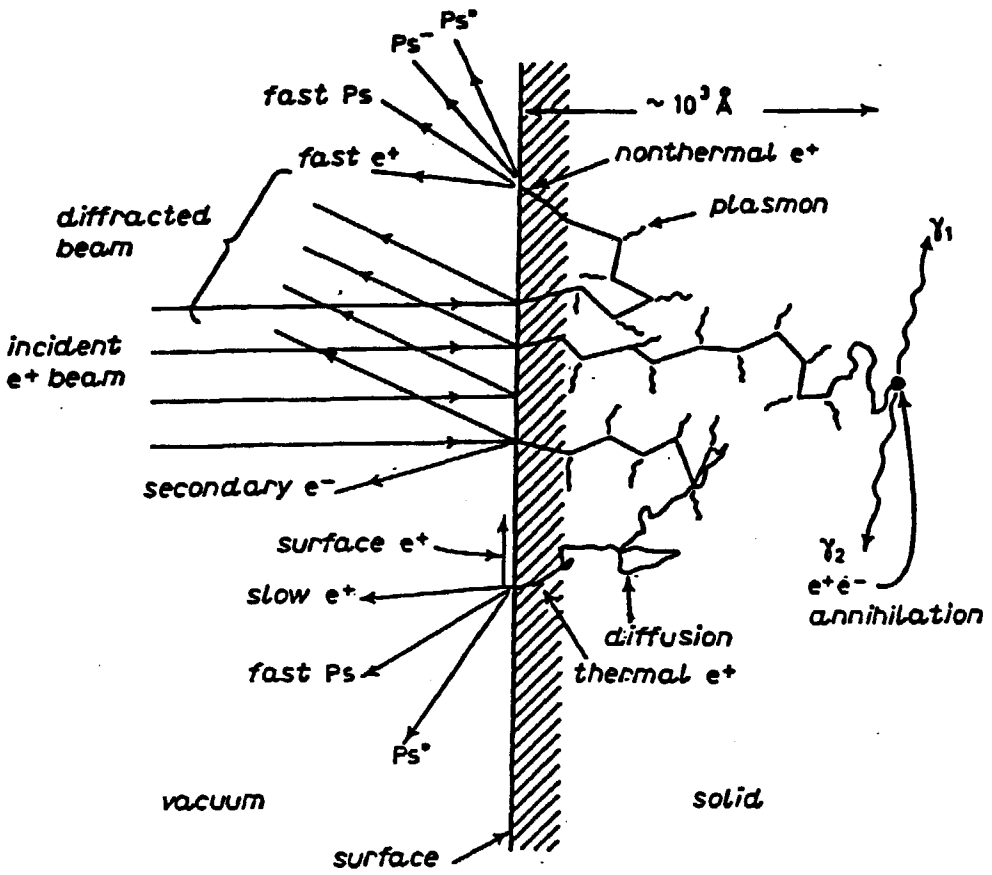
Fig. 1.5. Positron beam interaction with a solid and surface region (Mills 1983)

plasmon excitations continue to dominate the energy loss processes down to a near thermal energy, E_c, below which phonon interactions dominate. E_c is typically of the order of a tenth of an eV. The time it takes for a positron to slow down from its initial energy to E_c is about a picosecond.

Phonon interactions have a much lower energy transfer than electron excitations and the positron can even gain energy from the phonon field. Therefore the time a positron spends in the phonon dominated energy loss region before it is fully thermalized can be up to 10 ps.

The statistical profile of the depth at which implanted positrons reach thermal energies is called the implantation profile. Using the proper cross-sections for electron excitations, plasmon excitations, etc., this profile can be simulated in a Monte Carlo calculation. However, traditionally it has been found that the mathematically much simpler Makhovian profile constituted an adequately close representation of the real implantation profile. The Makhovian profile has the form

$$P(z,E) = \frac{m\,z^{\,m-1}}{z_0^{\,m}} \exp\left[-(z/z_0)^m\right] \tag{1.6}$$

where m is a shape parameter, $z_0 = \langle z \rangle / \Gamma[(1/m) + 1]$, $\langle z \rangle = (\alpha/\rho)E^n$ is the mean implantation depth for incident positron energy E in a material with density ρ and Γ is the gamma function. For a standard Makhovian implantation profile the values used for the two material independent constants α and n were 3.6 μg cm^{-2}keV^{-n} and 1.62, respectively. For implantation with monoenergetic positron a shape parameter of $m = 2$ is usually used. This reduces the Makhovian profile to the analytically simple case of a Gaussian derivative profile. For $m = 1$ the Makhovian profile becomes an exponential profile. This is traditionally used for calculating the implantation profile for positrons coming directly from a radioactive source. The precise shape of the implantation profile and the associated mean implantation depth is still a matter of some discussion. We have found many instances of poor agreement between the Makhovian profile and experimental data on thin foils and thin overlayers (see chapter 5) and in the case of the thin foils we have also shown poor agreement between experimental data and the full Monte Carlo simulation. However, for thick or semi-infinite samples the Makhovian profile seems to be a good approximation to the experimental data.

The average lifetime of a positron in a solid is of the order of 100 ps. Since the time needed to reach the critical energy, E_c, was only about 1 ps and only about 10 ps to reach full thermalization, the positron will spend most of its lifetime in the bulk diffusing around randomly. This can be modelled by the one dimensional steady state diffusion equation

$$D_+ \frac{d^2 c(z)}{dz^2} - \frac{d(v_d(z)c(z))}{dz} - (v_t n_t(z) + \lambda_b)c(z) + P(z) = 0 \qquad (1.7)$$

where

$c(z)$	=	the steady state positron distribution
D_+	=	the positron diffusion coefficient
v_d	=	$\mu_+ E(z)$ = the positron drift velocity, where
μ_+	=	$eD_+/k_B T$ = the positron mobility
$E(z)$	=	the electric field strength
v_t	=	the specific positron trapping rate for defects
$n_t(z)$	=	the defect concentration
λ_b	=	the bulk annihilation rate
$P(z)$	=	the energy dependant positron implantation profile

Even though the positron is delocalized in the bulk it is thus still possible to describe the positron motion as a random walk diffusion because the number of phonon scatterings and the angular deflection of the propagating delocalized positron wave is large. A diffusing positron typically probes 10^9 lattice sites before it annihilates. This makes positrons good probes of even minute quantities of defects in a crystal lattice.

1.3.4. Positron re-emission.

Thermalized positrons may encounter the surface during their random diffusion in the solid. The fraction of the positrons for which this happens depends on the implantation energy and thus on the implantation depth. If they do reach the surface they may undergo one of the following surface processes:

1. emission into vacuum as a free positron

2. emission into vacuum as positronium

3. trapping into a two-dimensional or defect localized positron surface state

4. quantum mechanical reflection by the positron surface potential

Emission as a free positron is only possible if the surface has a negative positron workfunction, ϕ_+. The positron workfunction is defined as the energy needed to remove a positron from the inside the solid to a position just outside the surface. It is given by

$$\phi_+ = -D - \mu_+ \qquad\qquad (1.8)$$

where D is the surface dipole barrier caused by the spill-over of electrons into the vacuum and μ_+ is the positron chemical potential of the solid. The chemical potential includes terms due to correlation with the conduction electrons (V_{corr}) and the repulsive interaction with the ion cores (V_0). It is the opposite sign for the dipole, D, that in many cases can lead to a negative positron workfunction like the one shown in Fig. 1.6.
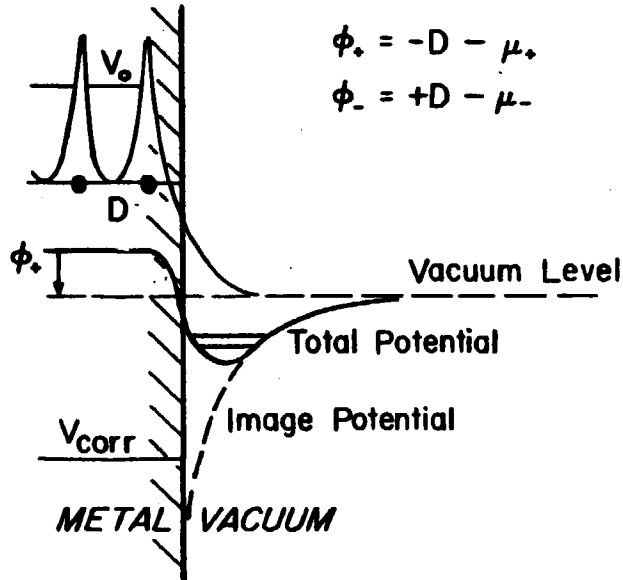

Fig. 1.6. Potential energy for a thermalized positron near a metallic surface.

Emission as Ps following pick up of a near surface electron is energetically possible if the sum of the positron workfunction, ϕ_+, and electron workfunction, ϕ_-, is less than the binding energy of the Ps atom. Fig. 1.6 shows a potential energy diagram for thermalized positrons near a metallic surface. It shows a surface potential well. The attractive nature of the potential outside the metal is caused by the image potential. It is this potential well that might trap some of the positrons arriving at the surface.

Quantum mechanical reflection at the positron surface potential when approaching the surface from inside the solid plays a minor role at room temperature (Britton *et al.* 1989). However, at lower energies it becomes important and theory predicts a total positron reflection for temperatures close to 0 K. Recent studies have shown that the large reflection at low temperature may be overcome by numerous encounters with the surface (Jacobsen and Lynn 1996).

1.3.5. Possible improvements to positron moderation and remoderation

With the knowledge of positron moderation and what processes a positron undergoes before it reaches the surface and is reemitted, some suggestions can be made of how it might be possible to increase the efficiency of positron moderators and remoderators. These fall in two categories: New materials and new techniques.

Presently the most widely used material for moderation and remoderation is W, though better efficiencies can be achieved by rare gas solid moderators. The reason the latter is less used is the necessity of maintaining the moderator at very low temperatures and depositing a new moderator at regular intervals. Compared to this a W moderator is very rugged and needs very little maintenance for up to several years. The rare gas solids lend their high efficiency to epithermal diffusion. They even have positive positron workfunctions and should otherwise not be able to emit free positrons. However, the extremely large bandgap leads to a very broad energy region where energy loss is only possible through phonon processes. For argon the inelastic threshold is about 10 eV. Below this energy only the very slow energy loss mechanism of phonon interaction is open to the positron. This leads to 'hot' positron diffusion and diffusion lengths of the order of 1 μm. It also causes the emitted positrons to have a rather wide energy distribution.

It might be interesting if the qualities of W and the rare gas solids could be combined. That
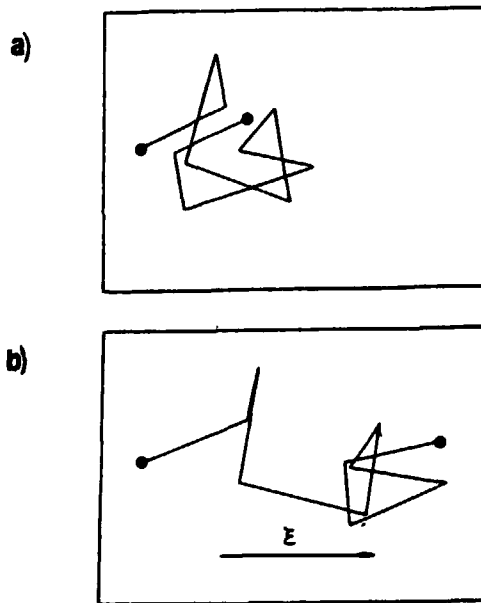
Fig. 1.7. Schematic of the motion of a diffusing positron a) without and b) with an applied electric field.

is if both 'hot' positron diffusion and good emission characteristics for thermalized positrons could both be present in the same material. Such a material would have a wide bandgap and still exhibit a negative workfunction. If such a material could be found in a very good, almost defect free quality, it should have a long positron diffusion length. If the surface branching ratio (see chapter 2) to free positrons is also sufficiently large, the material would be a prime candidate for a new moderator material. Investigation of a number of such materials is the subject of chapter 4.

One of the most promising techniques for increasing the moderation efficiency is field assisted moderation. The penetration of an electric field through a solid will influence the diffusion of any charged particles such as positrons by causing the charged particles to drift through the solid. This will make the drift term in the diffusion equation (1.7) non-zero. Thus an average drift

velocity is superimposed on the random diffusion motion (Fig. 1.7). If the electric field is aligned correctly it will increase the likelihood of the positron reaching the exit surface. The idea of enhancing the emission of positrons from a moderator by applying an electric field was first suggested by Madey (1969). The effect was recently demonstrated in surface charged rare gas solids (Merrison *et al.* 1992). The study of electric field effects in surface charged argon will be the subject of chapter 3. However, field assisted moderation has thus far not been experimentally viable in semiconductors. This is because of the vacancy-type defects at the interface between the semiconductor and the metal gate used to apply the electric field. These defects act as efficient positron traps and lead to no emission of positrons from the surface of the material. Work is ongoing around the world to try to solve this problem by finding other methods for applying the electric field. Therefore it is still of interest to study the possible characteristic emission properties of new semiconductor materials when under the influence of an electric field. The new materials investigated in chapter 4 will thus also be evaluated for their potential for field assisted moderation since wide bandgap materials should hold good promise for this application.

If it is possible to alter the positron diffusion to make the positron diffuse preferentially in one direction by applying an external electric field, maybe something similar can be done by making internal potential barriers to the positron. This could be done by utilising the differences in positron affinities between different materials. It would work much the same way as a diode works for electrons by allowing thermal positrons to diffuse in one direction, while in the other direction they could diffuse only as far as the nearest potential barrier before being repelled. However, in the case of positrons, unlike for electrons, these rectifiers could be made entirely from metal. The different layers would, however, have to be very well matched to avoid vacancy-type positron traps at the interface between the different layers. Further investigation of this idea for increasing the efficiency of thin foil moderators and re-moderators is the subject of chapter 5.

Finally, it has been shown in rare gas solids that the geometry of the moderator can lead to an improvement in the moderator efficiency of up to a factor of 5 (Khatri *et al.* 1990). Maybe something similar is possible for metal moderators such as W. One effect that could make such geometrical enhancements possible is low energy positron reflection. In this case the reflection is of positrons approaching the surface from the outside with energy less than the absolute value of the negative positron workfunction of the material. The positron thus does not have enough

energy to enter the solid but may still annihilate with electrons from the surface of the solid or become trapped in the surface potential well. This effect is the subject of chapter 6.

1.4. Outline

The rest of this thesis falls into three parts. In chapter 2 the experimental setup and techniques used for the experiments described in the rest of the thesis is presented. In chapters 3, 4, 5 and 6 the experimental results are presented and discussed. Chapter 7 describes the present status of the reactor based beamline and the microprobe facility. It also describes the construction and testing of a new electrostatic beamline and the use of this beamline to test the remoderation section for the microprobe facility. There will be an introduction at the beginning of each of the following chapters where some of the concepts specific to the subject of that chapter will be discussed in more depth.

CHAPTER 2

EXPERIMENTS WITH POSITRON MODERATION AND REMODERATION

2.1. Introduction

The aim of this chapter is to give some of the relevant background information concerning the positron beamline and experimental techniques used to perform most of the experiments described in this thesis. However, the experiments described in chapter 3, using the magnetic beamline at the University of Aarhus, Denmark, form an exception and here the experimental details are included in that chapter. In section 2.2 the present status of the Variable Energy Positron beamline (VEP) is given and in the following sections each of the experimental techniques used in this thesis is presented together with some of their background.

2.2. The VEP beamline

2.2.1   Basics

All the experiments described in chapters 4, 5 and 6 were performed using the Variable Energy Positron Beam (VEP) at Delft. This beam, based on a 20 mCi ^{22}Na source, delivered about 2×10^4 positrons per second at the target with a spot diameter of 7 mm. In April 1996 a new 95 mCi ^{22}Na source was installed and the beam now delivers about 1×10^5 positrons per second with the same spot size as before. The energy of the magnetically guided monoenergetic positrons could be varied in the range from 0-30 keV. The experiments were done with a base pressure in the target chamber of 1×10^{-8} Torr. The annihilation signal was recorded using a high purity Ge γ-counter placed perpendicular to the beam axis at a distance of about 45 mm from the center of the samples. The samples were placed on a linear motion drive with room for up to 6 samples at a time, depending on their size. A grid was placed 1.15 m up the beamline from the foils. This grid could be used to retard low energy positrons back to the sample. Next to this grid in the direction towards the source was a set of parallel plates constituting an E×B filter that was set at a low bias. The purpose of this first E×B filter was to deflect low energy re-emitted positrons coming from the sample away from the center of the beamline. Since the filter was farther away from the sample than the grid this was only done for positrons that had not been retarded by the grid. This was necessary as they would otherwise reflect off the potentials of the accelerator stage and return to the sample. The fact that these positrons would otherwise return
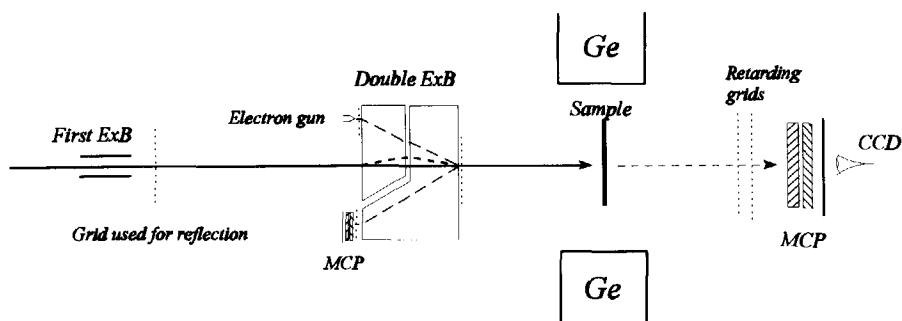

Fig. 2.1. The instrumentation on the VEP beamline. Recently the MCP-CCD system has been replaced by a channeltron detector.

to the sample indicates that the beams magnetic transport Helmholtz configuration was well tuned. The bias on the grid was low so as not to interfere with the primary beam. For more details about the beamline, see A. van Veen (1990) and H. Schut (1990).

2.2.2. New instrumentation

During the course of the work presented in this thesis several new instruments were fitted to the beamline. An extra high purity germanium γ-counter was installed opposite the original detector at the same distance from the sample. This detector has been used in the two detector Doppler broadening measurements mentioned below.

A Galileo Chevron-type Micro Channel Plate (MCP) detector was fitted to the end of the beamline. This detector was used to measure transmission through thin foils (see below). The MCP was fitted with a phosphorous screen, allowing a Charge Coupled Device (CCD) camera outside the vacuum chamber to monitor the beam during counting of MCP pulses. The MCP in conjunction with the CCD camera was also used to help position the samples optimally. This was of particular importance when measuring on very small samples, i.e. samples only slightly larger than the beam diameter. For the thin foil experiments described in chapter 5 positioning was of particular importance since the foils in that case were positioned on frames with an inner diameter smaller than the beam diameter. When measuring the full beam on a normal sized sample (10 × 10 mm or larger) the countrate registered by the Ge counter does not vary with incident energy, even for the highest energies. However, when measuring the beam through a dummy sample of diameter 5.2 mm during the thin foil measurements, the beam exhibited oscillations at higher energies. This was interpreted as caused by changes in the beam profile as the energy was changed. This was verified with the MCP-CCD system. The beam was spiraling and this led to more of the beam being cut off at some energies than at others. The effect was not seen below 8 keV and above that energy the amplitude and wavelength of the oscillations was increasing with the beam energy. This should not influence the measured transmitted fractions provided that the dummy sample could be placed exactly like the actual foil. Therefore the MCP-CCD system was crucial in getting the optimum positioning of the samples. Obviously, despite the precautions taken, this introduced an extra source of error in the measurements, particularly at high energies.

Lately this MCP-CCD setup has been moved to the new E-beam beamline (see chapter

7) to help diagnose this beamline. Meanwhile a Galileo Channeltron 4821B detector has been placed at the end of the VEP beamline. This detector was used for the most recent transmission measurements described in the last part of chapter 5. This is mounted with a three grid retarder in front of it on a flange which also had a viewport, allowing visual inspection of the samples in situ as well as temperature measurements using a pyrometer from the outside.

Recently a double E × B filter has also been added to the beamline about 25 cm in front of the sample (see Fig. 2.1). A filament was mounted on the E × B filter, allowing the sample to be irradiated with low energy electrons in situ. This filament could also be used to heat the samples by electron bombardment. On the other side of the double E × B filter a channelplate was situated. This channelplate was fitted with two grids in front of it and allowed for direct measurement of re-emitted positrons and their energy spectrum. This new setup has not been used in any of the experiments described in this thesis, but might be very useful in a number of possible follow-up experiments (see e.g. section 4.3.4).

2.3. Doppler Broadening and the VEPFIT fitting and modeling program

The use of positrons as a non-destructive probe to study defects in materials have been shown to be a useful tool (Asoka-Kumar *et al.* 1994, Hautojärvi 1995). The technique is based on the propensity of positrons to be trapped at defects such as vacancies and voids (Puska and Nieminen 1994) making them a sensitive probe for studying these kinds of defects. After being trapped the positron will annihilate with an electron from the near vicinity of the defect emitting two 511 keV γ-photons. These two photons carry with them information on the electron momentum density of the annihilation site. Measuring the Doppler broadening of the annihilation γ-photons yields information about the electron momentum distribution in the direction of the detector. Furthermore, if a beam of mono-energetic positrons is used, the measurements will also yield information on the depth distribution of the defects. This is the basis of Doppler broadening defect profiling.

Traditionally in Doppler broadening measurements the lineshape parameter, S, is measured as a function of incident positron energy. The S parameter measures the integrated area in the
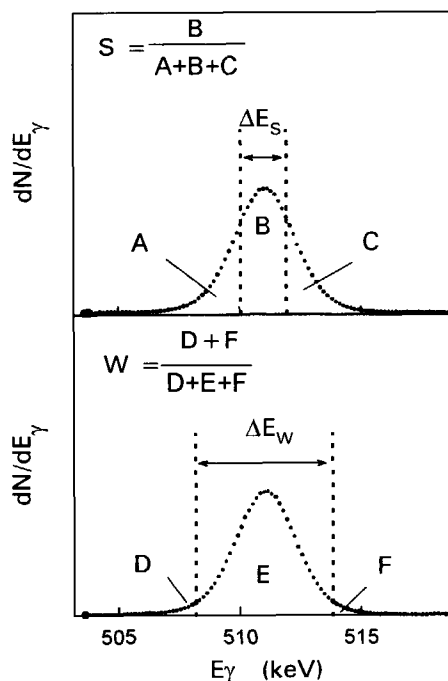
Fig. 2.2. Definition of the *S*- and *W*- parameters of Doppler broadening measurements.

central region of the peak compared to the total area of the peak (Fig. 2.2). Since this corresponds to annihilations with low-momentum electrons this parameter is especially sensitive to the density of valence electrons. Another lineshape parameter that has become increasingly more used in recent years is the *W* or wing parameter (Clement *et al.* 1996). This measures changes in the far wings of the annihilation peak and thus monitors annihilations with high momentum, i.e. core electrons.

The Doppler broadening data were analyzed using the VEPFIT fitting and modelling program (A. van Veen *et al.* 1990 and 1995). The program models and fits the data using a layered structure model. The implantation is modeled using a standard Makhovian implantation profile,

$$P(z,E) = \frac{m\,z^{m-1}}{z_0^{m}} \exp\left[-(z/z_0)^m\right]$$

(2.1)

where m is a shape parameter, most commonly set to 2, making the profile a Gaussian derivative profile, $z_0 = <z>/\Gamma[(1/m) + 1]$, $<z>=(\alpha/\rho)E^n$ is the mean implantation depth for incident positron energy E in a material with density ρ and Γ is the gamma function. For a standard Makhovian implantation profile the values used for the two material independent constants α and n were 3.6 $\mu g\ cm^{-2}keV^{-n}$ and 1.62, respectively.

The VEPFIT program then describes the system in terms of a stack of different positron trapping layers, taking inter-layer diffusion into account. Each layer is ascribed an S-value, where S is the Doppler lineshape parameter. The S-value for a given energy E is then given by

$$S(E) = \sum_{i-1}^{n} f_i(E)S_i + f_{surface}(E)S_{surface}$$

(2.2)

where $f_i(E)$ is the fraction of positrons implanted at energy E which after thermalization and diffusion annihilate in layer i. A similar equation can be set up for W and by fitting the two sets of experimental data information about the layer specific S and W values, the positron diffusion length in the layers and the layer thicknesses can be obtained. In combination the two lineshape parameters can therefore yield a good characterization of the involved materials and their defects. By plotting the measured S and W data as a trajectory in the $S - W$ plane, using the implantation energy as the running parameter, a direct interpretation of the experimental data in terms of positron trapping layers with distinct S and W values can be obtained (Clement *et al.* 1996). Since absolute S and W values can vary with the specific experimental setup while relative values are reproducible, all reported S and W values are relative to the value for bulk Si, except for the values concerning GaN-SI which is given relative to the bulk value for that material.

In a conventional Doppler broadening measurement the sensitivity to annihilations with core electrons is hampered by the background at high momenta. Based on the ideas of Lynn *et al.* (1977) we have recently used a two detector coincidence setup to reduce this background (Kruseman *et al.* 1997, Jørgensen *et al.* 1997). For these measurements a second high purity Ge γ-counter was placed directly opposite to the other Ge detector and at the same distance to the

samples. By using both timing coincidence and energy conservation considerations in a manner similar to that described by Asoka-Kumar *et al.* (1996) we were able to improve the peak to background ratio by a factor of almost 1000 compared to a single detector system. At the same time, by using this setup, the resolution of the system was improved from 1.3 keV (FWHM) at the 511 keV photopeak for a single detector to 0.93 keV with the two detector system. This increased sensitivity to core electrons comes at the price of much lower count rates.

2.4. Surface branching ratio measurements

It is often of interest to know the surface branching ratios of a given material, i.e. the ratio of thermalized positrons arriving at the surface branching into each of the different channels open to them. There are three channels open to such positrons: (1) they can form positronium, (2) they can get trapped in the surface potential well, or (3) they can be emitted as free positrons. A method for experimentally determining these branching ratios has been developed by Schut *et al.* (1986) (See also Schut 1990).

The method is based on the fact that by reversing the electric field in front of the sample only the (charged) reemitted positrons are influenced. Thus, with a negative bias on the grid in front of the sample all positrons are removed, and with a positive bias all positrons are forced back to the sample where they can only branch into the surface state or form positronium. By monitoring the number of counts in the 'peak' (P) and 'total' (T) region of the spectrum and the Doppler lineshape parameter S for both negative and positive bias, sufficient information is available to determine the fractions of interest. Here the 'peak' region designates a region in the annihilation spectrum centered around the 511 keV annihilation line and the 'total' region is the region below 511 keV in the spectrum. This last region is especially sensitive to three photon annihilation events.

For every incident positron energy it is thus recorded what fraction of the positrons are re-emitted as free positrons, as positronium, trapped at the surface potential well or trapped in the bulk. Obviously most of the incident positrons will be trapped in the bulk at higher implantation energies and only very few will reach the surface of entry again. This will mean that the measured fractions of such positrons that, e.g., are emitted from the surface as free positrons will be

exceedingly small. However, since the branching ratios are for thermalized positrons reaching the surface, they should be independent of the incident energy of the positrons. It should be noted, however, that because the fraction of thermalized positrons reaching the surface gets smaller as the implantation energy gets higher, the surface branching ratios determined from the measurements will have a considerably larger statistical uncertainty or scattering at such energies. Therefore the most reliable surface branching ratios are those measured at energies where the fraction of positrons returning to the surface is still statistically sound.

Another phenomenon that might cause the branching ratios to vary with energy is the effect of epithermal positrons. Like thermalized positrons, epithermals might also reach the surface and they might well have different branching ratios than thermalized positrons. However, epithermal positrons reaching the surface should mainly be a problem at shallow implantation energies. Therefore it should be relatively easy to discern such effects. In all, branching ratios measured in the energy region from 0.5 keV to 2.5 keV will most often be the most reliable.

2.5. Retarding field measurements

The energy distribution of re-emitted positrons is a vital positronic characteristic of any material, not least a potential material for positron moderation. By measuring the energy distribution of re-emitted positrons the positron workfunction for the surface studied can be determined and epithermal contributions can be determined. In many cases the presence of contaminants on the surface of the material can also be derived from the energy spread of the re-emitted positrons.

A simple method to measure the energy distribution of the re-emitted positrons is a retarding field measurement. Here a grid at some distance away from the surface in question is used to retard the reemitted positrons back to the surface. By slowly varying the bias on the grid while monitoring the annihilation countrate observed by the Ge γ-counter, the countrate will be seen to increase as the bias is increased and gradually more and more positrons are returned to the surface. The energy distribution of the re-emitted positrons is then given by the derivative of this retarding field spectrum. Since we generally used the Ge counter viewing the sample a grid not in view of the detector was used. We used the grid about 1 m in front of the sample position.

The energy scale in retarding field measurements is given by $E_1 = e(V_{grid}) + (\phi_-^{grid} - \phi_-^{A})$ where ϕ_- is the electron workfunction of the grid material (molybdenum) and surface in question (A) respectively. The value of $\Delta\phi_- = (\phi_-^{grid} - \phi_-^{A})$ can be derived from the retarding field measurement in the form of the grid voltage needed to repel positrons just escaping from the sample, i.e. positrons with nearly zero energy. Thus an off-set caused by the difference in electron workfunction between the grid material and the surface under investigation can be observed in most retarding field measurements. Therefore such measurements can also be used to determine the electron workfunction of a surface if the electron workfunction of the grid material is known. However, there are other more precise methods to determine the electron workfunction of a surface.

To get a high energy resolution in retarding field measurements small net holes in the grids are preferable in order to avoid field penetration. Small net holes in the grids would, however, also lead to low transmission grids. This could lead to a low count rate in the experiment. A suitable compromise must be found that will fit the individual experiment. Generally a three grid retarder is also preferable. In that case the two outer grids will remain grounded and the middle grid is used for the actual retarding. In that way the presence of stray electric fields that could influence the experiment at very low energies is avoided. In the first series of experiments where we only had two grids between the sample and the detector, the grid farthest away from the samples was used to retard the positrons and the other grid then shielded the positrons from seeing the retarding potential until they were only millimeters away from the retarding grid.

2.6. Transmission measurements

When studying the positron transmission through thin foils, we used a particle counter on the far side of the foils to detect the arrival of transmitted positrons. In the first set of experiments described in chapter 5 a Micro Channel Plate (MCP) was used as the particle counter. In the more recent experiments described in chapter 5 a Channeltron was used. In the first case there were two grids in between the sample and the detector and in the latter there were three grids. These grids were used to separate low energy transmitted positrons from positrons which passed through the foil without being thermalized. Thus for every incident energy there were two measurements: one

with + 50 V retarding to measure only the high energy component and one with - 50 V to measure the full transmission. The low energy transmission was then found as the difference between these two measurements. By also measuring on dummy samples without foils the full beam flux incident on the foil was measured and transmitted fractions could be calculated. Since the detection efficiency of the detectors used varied with the impact energy of the incident positrons, calibration measurements determining the relative efficiency of the detectors as a function of impact energy were performed and the transmitted fractions were corrected for this.

2.7. The E-beam and remoderation

The preceding sections have described the VEP beamline and the techniques used in the experiments performed on that beamline. The experiments performed to diagnose the new electrostatic beamline (E-beam) described in chapter 7 were done using the MCP-CCD setup previously used at the VEP beamline. Thus it was possible to study the beam profile for different lens settings and optimize the beam to the smallest possible spotsize and divergence in a very direct manner. The MCP was fitted with a retarding grid in front of it to make measurement of the energy profile of the beam possible. The MCP has now been moved to the second beamport to be able to monitor the beam quality while testing the remoderation section. The first test of the three stage transmission remoderation stage will be done using a channeltron fitted with a three grid retarder. This will be placed right after the 1 mm exit of the μ-metal chamber, that houses the remoderation section (see chapter 7).

CHAPTER 3

POSITRON DYNAMICS OF FIELD ASSISTED SOLID RARE GAS MODERATORS

3.1. Introduction

The study of positron dynamics within solids and at their surfaces is not only of interest in its own right, but has been the focus of much research over the past 20 years in the development of more efficient β^+ moderators for the production of low energy positron beams (Schultz and Lynn 1988). Much of this research has involved the use of metals within which positron thermalization is generally rapid and precedes diffusion and possible emission into vacuum from a negative work function surface. The rare gas solids (RGS), despite having positive work functions, were discovered to have good positron reemission properties and to be efficient β^+ moderators (Gullikson and Mills 1986, Mills and Gullikson 1986). Here the dynamics were described in terms of epithermal diffusion and emission of positrons as a result of inefficient cooling below the positronium formation threshold, which is the inelastic threshold in these wide band gap insulators. The highest quoted moderation efficiencies for a flat geometry (0.30 ± 0.02 %) were obtained using solid neon films (Khatri *et al.* 1990). Enhancements in this efficiency have been obtained using different source/moderator geometries with a cup yielding 0.70 ± 0.02 %

(Mills and Gullikson 1986) and a conical design 1.4 ± 0.2 % (Khatri *et al.* 1990).

In recent years rare gas solid primary moderators have been installed on many beamlines around the world with good result. The Brandeis high-brightness beam using a plane geometry Kr moderator as primary moderator has achieved a working efficiency of 4×10^{-4} (Vasumathi *et al.* 1995). The Helsinki group has used both Ar and Kr in a cone geometry and achieved efficiencies of 9.5×10^{-4} and 1.2×10^{-3} for Ar and Kr, respectively (Jääskeläinen *et al.* 1997). The Aarhus magnetic beamline achieves a standard operating efficiency of 1×10^{-3} using a Kr moderator (Merrison *et al.* 1997). In a study of the role of annealing and impurities in the efficiency of rare gas solid moderators (Ar, Kr and Xe) Petkov *et al.* (1997) found surface impurities to be the main factor limiting the endurance over long times of this type of moderators.

One method of improving moderation efficiencies which does not rely solely on the random diffusion of positrons to an exit surface was originally discussed by Madey (1969) and utilizes a bulk electric field in order to drift implanted positrons to the surface of a semiconductor or insulator. The first attempt to construct such a device was made by Lynn and McKee (1979) who used a silicon wafer and applied the electric field using a thin gold contact. This and other later attempts have not been successful, probably due to trapping of the positrons at the metal-semiconductor interface (Beling *et al.* 1987, Simpson *et al.* 1989). More recently Shan *et al.* (1994) have reported, from a positron lifetime type investigation, that ~10 % of β^+ implanted into GaAs could be drifted to a metal contact and suggested how it might be possible to design a field assisted moderator using this technique.

A field induced enhancement in moderation efficiency was recently observed by Merrison *et al.* (1992, 1993) as a result of applying an electric field to solid Ar and Kr films. The method involved a novel technique in which the RGS surface was charged by capture of low energy electrons on adsorbed O_2 (Sanche and Deschenes 1988, Marsolais and Sanche 1988). The work reported here has been carried out as an extension of the latter investigation in order to better understand the positron dynamics in such surface charged RGS by using beam implantation and observing the subsequent low energy positron reemission.

Very recently the first preliminary results of field assisted positron moderation using diamond were reported (Brandes *et al.* 1997). Here the interface trapping problem was circumvented by having a 41 nm B-doped epilayer on one side of the diamond and having a Ti/Au contact deposited around the perimeter of the B-doped epilayer. Further experiments underway

should reveal whether this approach does indeed work.

3.2. Experimental setup and procedure

The experiments described in this chapter were performed in 1993 using the magnetically guided positron beam at the University of Aarhus, Denmark. The beamline was fitted with a ~75MBq ^{22}Na radioactive source and a W mesh moderator producing a beam of 2×10^4 slow positrons per second. This beam was passed through a trochoidal charged-particle velocity filter at an energy of 100 eV before being accelerated to energies in the range of 1 - 10 keV. The acceleration was performed by having the entire source end floating at a positive potential equal to the desired beam energy minus 100 V. The beam had an energy spread of ~4 eV full width at
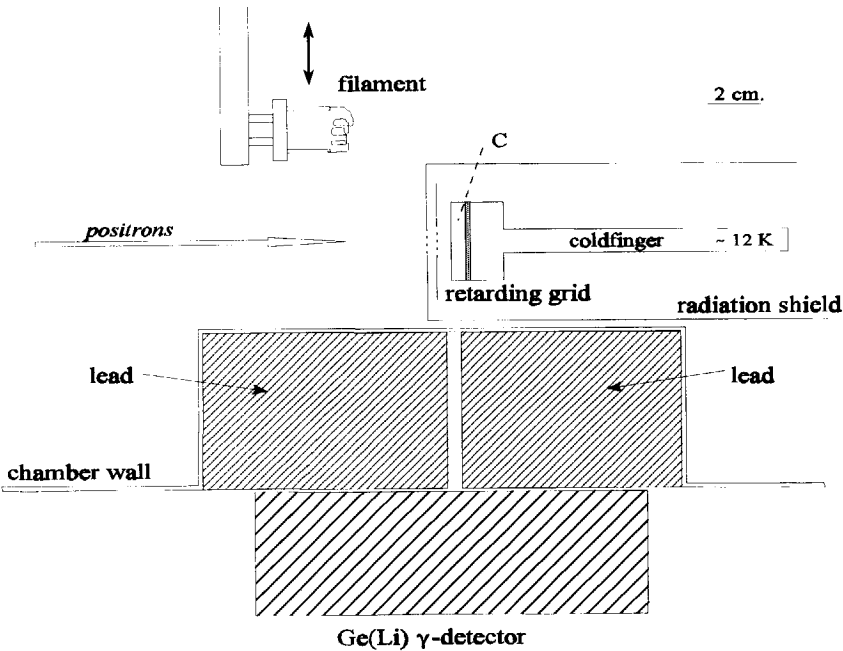

Fig. 3.1. The experimental setup near the sample. The sample copper backing C is electrically isolated from the cold finger.

half maximum and a diameter of roughly 5 mm as measured using a ceratron (ceramic channeltron) lowered into the beam axis immediately in front of the target. In the experiment, implantation energies of 1, 2, 4, 6, 8 and 10 keV were used.

The target consisted of a copper plate mounted on, but electrically isolated from, the coldfinger of an APD Cryogenics model H2 cryopump (Fig. 3.1). The coldfinger was surrounded by a grounded copper radiation shield and cooled to ~12 K. A retarding grid inserted to analyze the reemitted beam was placed at a distance of 4.8 mm from the target.

The argon samples were frozen directly onto the copper substrate by letting gas into the chamber at a pressure of 2×10^{-4} Torr for various lengths of time to obtain layers of different thickness. The gas had a stated purity of 99.998% with the major impurities being N_2 (<10ppmv) and H_2O (<3ppmv) and was used without further treatment. The base pressure of the vacuum chamber was ~2×10^{-9} Torr. Film thicknesses were calibrated by depositing a relatively thick layer of argon (depositing time ~6 hours) and measuring the increase in the target voltage required to prevent implantation of 100 - 450 eV beams of positrons as a result of the argon surface becoming closer to the earthed retarding grid. Through simple capacitance considerations this shift in retarding potential is given by $\Delta V = (d / \epsilon_r(D-d))E_{e+}$, where d is the sample thickness, ϵ_r is the relative dielectric constant for argon, D is the distance between the copper substrate and the earthed retarding grid and E_{e+} is the positron energy in eV. The measured ΔV was of the order of 5 % of E_{e+}. Assuming linearity with depositing time and gas pressure it was then possible to calculate the thickness of the other samples. The thicknesses used in the experiment were thus determined to be 4, 8, 16, 24 and 40 μm with an error of around 20 % in all cases, which combines uncertainties from the depth calibration experiment and in the pressure during deposition. This method was also used to estimate the thickness of the oxygen overlayer which was applied to the sample by letting in this gas at a pressure of 2×10^{-7} Torr, typically for 60 seconds and thus obtaining a coating of 15±3Å.

The surface coated RGS was subsequently irradiated by low energy electrons from a tungsten filament lowered into the beam axis roughly 2.5 cm in front of the target. The filament was biased at -1 V giving an electron current of 50 nA impinging on the target. During irradiation the target potential was slowly ramped positively over several minutes, at a rate of ~ 0.5 Vs^{-1}, until the desired surface potential was reached, as measured using a 100 eV positron beam by determining the target bias required to prevent implantation. Exposure of the surface to the

impinging slow positron beam caused some decay of the surface potential at a rate of roughly 5 Vhr^{-1}, whereas no decay was observed with the beam off. Recharging was performed simply by repeating the process outlined above.

The low energy reemitted positron fraction was measured by alternately biasing the target ± 45 V with respect to the surface potential while monitoring the positron annihilation rate in the argon using a Ge(Li) γ-ray detector which observed the sample through a lead-slit system. The purpose of the slit arrangement was to reduce the background due to annihilations on the 86 % transmission copper retarding grid by preferentially viewing the argon film. Data acquisition times of 300 - 800s per point were used to obtain good statistics with increasing accumulation time at
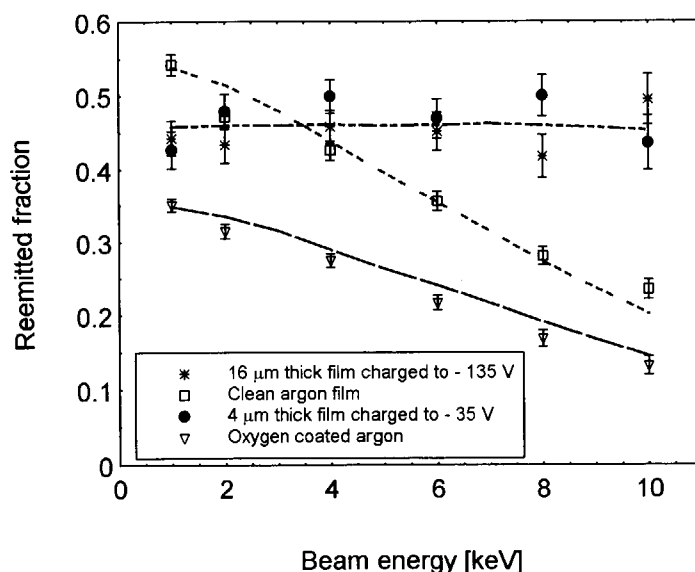

Fig. 3.2. Reemission yield versus implantation energy for Ar samples subjected to various surface conditions. Note that despite differences in surface potential and thickness the reemission of the two charged samples, which both have electric fields of around 8.5 kVmm^{-1} is much alike. The lines are plots of the simulation discussed in section 3.5.

the higher energies due to reduced beam intensity.

3.3. Experimental results

For a clean uncoated argon sample the reemission was observed to decrease linearly with increasing implantation energy (Fig. 3.2) in reasonable agreement with previous studies (Mills and Gullikson 1986). The reemitted fraction included only positrons which left the surface of the sample with an energy of less than 45 eV. It did not include backscattered positrons or those emitted as positronium. The backscattered fraction should constitute a little over 10 % for solid argon when interpolating the results of Mäkinen *et al.*(1992) and Coleman *et al.*(1992) to Z = 18. Figure 3.2 also shows a decrease in reemission yield after treatment with oxygen, most notably for the lower implantation energies. After irradiating with electrons to produce a negative surface potential a marked increase in the reemitted fraction was observed at higher implantation energies with the yield at 10 keV increasing by a factor of ~3. The reemission after charging was observed to be roughly constant over the entire energy range.

As shown in figure 3.3, the positron reemission was observed to increase with surface potential (and thus with bulk electric field) up to a maximum at about 7 kVmm^{-1} for all film thicknesses. For electric fields above this maximum and up to a sudden cut-off, described later, a gradual reduction in the enhancement was observed which was dependent upon implantation energy, with those implanted at lower energies suffering less reduction in reemission yield.

In addition to the effects described above another distinct process was apparent which is illustrated most clearly in figure 3.3. When a specific value of the surface potential was reached, for a given sample thickness, a rapid decrease in the reemitted fraction was observed for all implantation energies. This cut-off was also observed for positrons implanted at 100 eV. The reemitted yield decreased below the level of the uncharged sample resulting in a value close to zero. The surface potential at which this occurred varied weakly with thickness from around -95 V for the thinnest sample (4 μm) to -215 V for the thickest sample (40 μm)(Fig. 3.4). For the thicker samples this decrease appeared before the maximum reemission enhancement had been achieved.
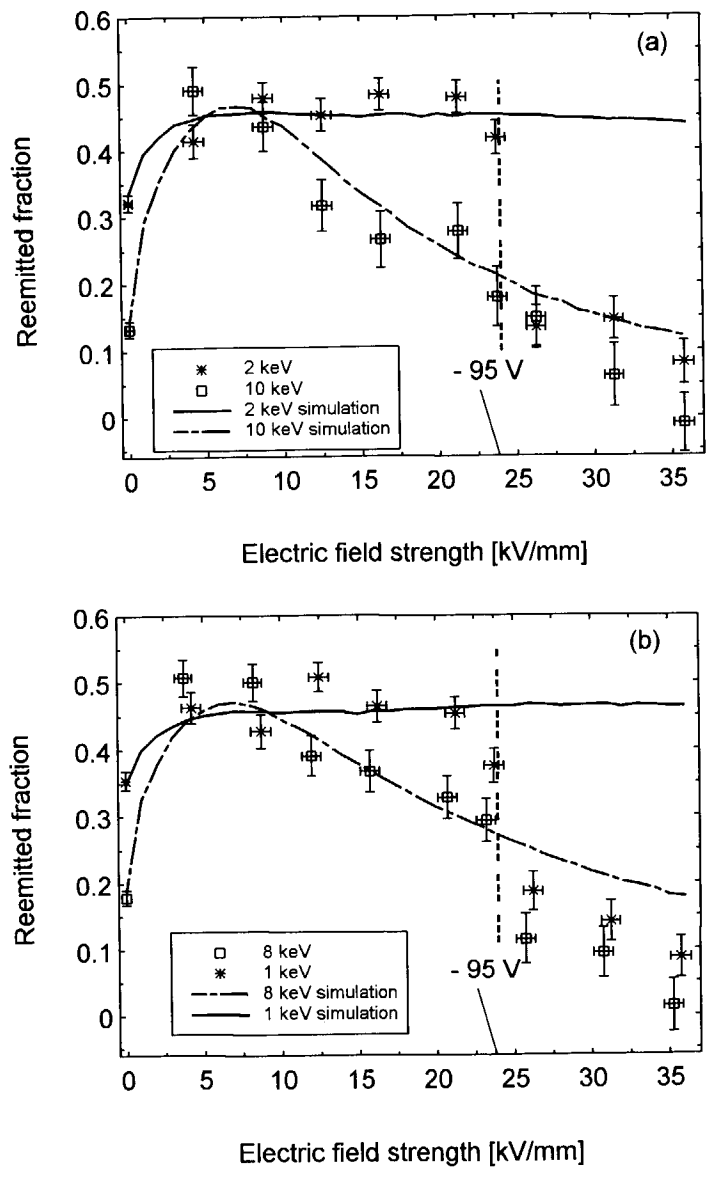
Fig. 3.3. Reemission yield versus electric field strength for a charged 4 μm thick O_2 coated Ar sample for implantation energies of (a) 2 and 10 keV and (b) 1 and 8 keV. The lines are plots of the simulation discussed in section 2.5. The vertical dashed line indicates the approximate onset of the cut-off.
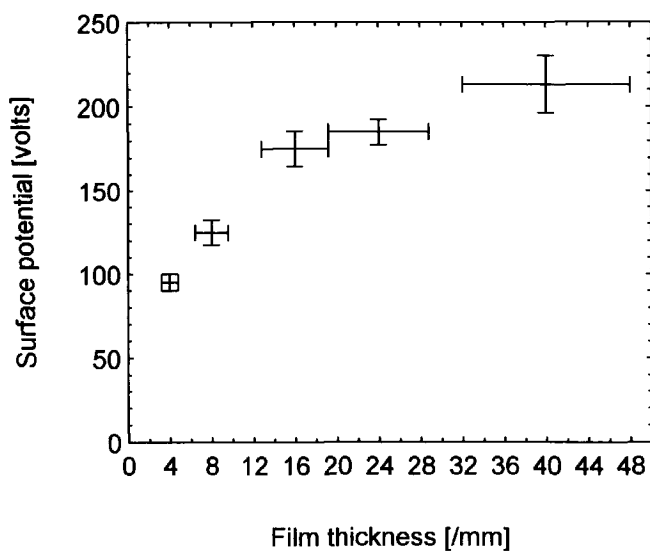
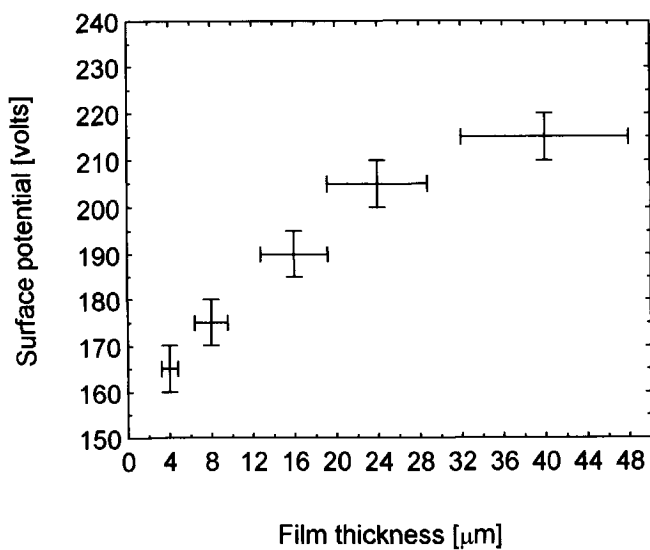Fig. 3.4. The cut-off potential as a function of film thickness.

Fig. 3.5. The maximum surface potential that could be applied to the different films as a function of their thickness.

It is interesting to note that a maximum surface potential was observed above which it was not possible to further charge the sample. This maximum seemed to depend weakly on film thickness, increasing from - 170 V for the thinnest films to - 220 V for the thickest samples (Fig. 3.5).

3.4. Computer simulation

A computer simulation was carried out in an attempt to model the experimental results. It was not possible to perform a true Monte Carlo calculation as has been done for various metal substrates (Baker *et al.* 1991a and 1991b) since this requires knowledge of scattering cross sections for all energy loss processes encountered following implantation and these are presently unknown for the RGS. A Makhovian implantation profile with a shape parameter $m = 1.9$ was therefore used to describe the positron implantation profile. This was taken to mean slowing to below the bulk inelastic (positronium formation) threshold E_{Ps}^{BAr}. The positrons then proceed on a random walk from discrete depths with an energy chosen randomly (below E_{Ps}^{BAr}) and in random directions. After traversing a scattering length (l_s) the positrons were isotropically scattered and lost an average energy (dE) due to a phonon interaction. The specific parameters and assumptions used in the simulation are given below:

1.   The Makhovian implantation profile is given by

$$P\ (z)\ =\ \frac{1.9\,z^{0.9}}{z_0^{1.9}}\ \exp\left[-(z/z_0)^{1.9}\right] \tag{3.1}$$

where z_0 is related to the mean implantation depth $<z>$ by $z_0 = <z> / \Gamma[\ (1/1.9) + 1\ ]$ where Γ is the gamma function (Vehanen *et al.* 1987, Velkealahti and Nieminen 1984). An integration over the Makhovian profile was performed using an ensemble of typically 10^5 positrons.

2.   The Ps formation fraction on slowing down was 10 % (Schrader *et al.* 1982)

3.   The bulk positronium threshold for argon, E_{Ps}^{BAr}, was 10 eV (Gullikson and Mills 1986). Positrons gaining energy in excess of this were assumed to form Ps and annihilate in the

bulk. The effective Ps thresholds at the surface of O_2 coated Ar, E_{Ps}^{O2}, and contaminated Ar, E_{Ps}^{cAr}, were 5.9($\pm$0.4) eV and 8.1($\pm$0.4)eV respectively.

4.   The average energy loss per collision, dE, was 1.1(+0.4,-0.5)meV. This was used as a fitting parameter to reproduce the experimentally observed reemitted fraction. This value can be compared to the Debye energy of 7.4 meV, corresponding to $\Theta_D = 85$ K, which is a measure of the maximum phonon energy.

5.   The scattering length, l_s, was also a fitting parameter and was taken to be 250(+150, -20)Å, in agreement with other work (Gullikson *et al.* 1988).

6.   The value used for the positron workfunction, ϕ_+, was +1.5 eV (Schrader *et al.* 1982). Positrons reaching the surface with perpendicular energy below this value were reflected.

7.   The positron lifetime in argon was 430 ps (Liu and Roberts 1963).

8.   The positron mass was assumed to be m_e, identical to its vacuum value.

9.   The effect of the electric field, ϵ which is assumed to act throughout the bulk of the film, was to add a small drift distance in the direction toward the exit surface of the film

$$\Delta z_i = \frac{1}{2} \frac{e\,\epsilon}{m_e} \tau_i^2 \tag{3.2}$$

and to give the positron an average extra velocity in this direction (and thus to increase the energy)

$$\Delta v_i = \frac{1}{2} \frac{e\,\epsilon}{m_e} \tau_i \tag{3.3}$$

where τ_i is the time between collisions for the ith step and m_e is the electron mass.

It should be noted that this is a rather crude model. It is reasonable to expect that the energy loss per collision is a function of positron energy. The value of dE used in the simulation should therefore be viewed as an average value. Similar arguments hold for the scattering length, l_s. Uncertainties quoted on the values of dE, E_{Ps}^{O2}, E_{Ps}^{BAr} and l_s were estimated by independently varying each parameter while requiring a reasonable fit to the e^+ re-emission observed from the Ar samples when clean, O_2 coated and with applied electric field. In addition to the fraction of reemitted slow positrons the simulation also calculated the fraction of implanted positrons

reaching energies below 2kT and the fraction forming positronium.

Unfortunately the positronic properties of solid oxygen are virtually unknown. There was thus no theoretical foundation to describe the effect of the solid oxygen overlayer. The presence of the oxygen (approx. 10 monolayers) was taken to lower the positronium threshold energy, $E_{P_s}^{O2}$, at the surface. A reasonable fit to the experimental data was found giving a value of $E_{P_s}^{O2}$ = 5.9 (±0.4) eV. The corresponding threshold in the gaseous phase is at 5.3 eV. Given the base pressure ($\sim 10^{-9}$ Torr) and data accumulation time for the 'clean' argon results a surface contamination of at least one monolayer must be anticipated. A modification of the effective Ps threshold at the surface was therefore assumed. A reasonable fit to the data was obtained using a value of $E_{P_s}^{cAr} = 8.1(\pm 0.4)$eV.

3.5. Discussion

Generally good agreement was obtained between experiment and the results of the computer simulation, despite the crudeness of the latter (see figures 3.2 and 3.3). Using the values of dE and the scattering length (l_s) given earlier an estimate of the diffusion length may be obtained: $L = (E_{P_s}^{BAr}/2dE)^{1/2} l_s = 1.7(+2.0,-0.4)\mu$m. An estimate may also be made of the positron mobility $\mu = e\tau_{sc}/m$ where τ_{sc} is the average time between collisions. A value for τ_{sc} can be obtained by calculating the mean velocity during thermalization $v_{th} = (E_{P_s}/2m)^{1/2}$, yielding τ_{sc} = l_s/v_{th} = 2.7(+1.6,-0.2) × 10^{-14} s and thus a mobility of μ = 4.7(+2.9,-0.4) × 10^{-3} m^{2}V^{-1}s^{-1}. It should be noted that the value for dE (1.1(+0.4,-0.5)meV) is not in agreement with that obtained previously of 6(±2)meV (Gullikson and Mills 1986) and therefore the derived value for the diffusion length is also different. The value for the scattering length (l_s = 250(+150,-20)Å) is in agreement with a previous determination (230±90Å) (Gullikson *et al.* 1988).

The model suggested that the lower positron reemission yield after coating the Ar film with molecular oxygen (Fig. 3.2) was the result of positrons with energies larger than $E_{P_s}^{O2}$ forming Ps at the surface, similar to the effect of the contaminants on the clean argon film. Shallowly implanted positrons (lower incident energy) generally have higher energies on returning to the surface and thus a larger fraction are subsequently lost due to lowering of the Ps formation threshold by the O_2 on the surface.

The observed increase in reemission following charging of the oxygen overlayer and the successful modelling of this is consistent with an efficient field induced drift of positrons to the surface. After applying an electric field of 7-8 kVmm^{-1} (by surface charging) roughly constant positron reemission was observed for all implantation energies (Fig. 3.2) indicating that even the most deeply implanted positrons were drifted back to the exit surface. Thus they had a similar reemission probability as those implanted at lower energies. The experimental data are not consistent with a surface effect which would have had a greater effect on the more shallowly implanted lower energy positrons since more of these are able to diffuse back to the surface.

A related field-induced phenomenon was observed by Gullikson and Henke (1989) in X-ray induced secondary electron emission, where enhancement was observed resulting from positive charging of solid xenon films. This was attributed to the electrons being drifted toward the surface by the electric field. A similar effect occurs here for the implanted positrons.

The effect of the electric field on the energy of the diffusing positrons (ie 'heating' of the positron distribution) could be investigated using this model. This was observed as a reduction in the thermalised fraction and was significant at the field strengths used in this study. At high fields (> 23 kVmm^{-1}) the fraction thermalizing was less than 1 % at all implantation energies. Despite the heating of the positrons, which had the effect of increasing the probability of emission once at the surface, drift in the electric field was still responsible for the e^{+} reaching the surface. A reversal of the applied electric field (i.e. + 8 kVmm^{-1}) resulted in a reduction of the predicted reemission at 10 keV implantation to approx. 4 %. This was in qualitative agreement with previous β^{+} moderation efficiency measurements (Merrison *et al.* 1992) where an almost total reduction in positron emission was observed when the field was reversed after positive charging of the surface by bombardment with positive ions.

The gradual reduction in reemission yield observed above a maximum of about 7 kVmm^{-1} and up to the cutoff (Fig.3.3) was also modelled by the simulation and shown to result from heating of the positrons above the positronium formation threshold and into the so-called Ore gap (Brandt 1982). This was reflected by an increase in the positronium formation fraction yielded by the computer simulation which at the highest electric fields became the dominant positron annihilation process for all implantation energies. Such heating effects have also been observed in gaseous argon at comparable density-normalized electric fields (Marder *et al.* 1956; Charlton *et al.* 1992). The observed maximum enhancement occurs at 7 kVmm^{-1} corresponding to a density

normalized electric field of ~3.9×10^3 Vm^{2}kg^{-1}, which is similar to the those fields which cause the positronium fraction to rise in dense gases (Charlton *et al.* 1992). This behavior is also in good quantitative agreement with previous observations using surface charged solid argon β^+ moderators (Merrison *et al.* 1993).

After this gradual decrease a very rapid decrease in the reemitted fraction was observed. For the sample thickness shown in figure 3.3 this occurred at a field strength of approximately 23 kVmm^{-1}. The results deviate at this point from the computer simulation which could not account for this decrease. This effect did not appear to depend on either electric field strength or surface charge density, both of which should vary approximately inversely with film thickness. The fact that it did not vary with surface charge density suggested that it was not entirely due to trapping at anion sites on the surface of the film. The exact nature of this process is not clear at this stage.

By modification of the computer simulation it was possible to model the process of β^+ moderation in a (transmission mode) solid Ar film. It could then be used to fit the data obtained in a previous experimental study of Ar moderation under the influence of various surface potentials (applied electric fields) (Merrison *et al.* 1992). In this case the implantation profile becomes exponential in form thus replacing assumption 1 given earlier with:

$$P(z) = \alpha \exp(-\alpha z) \tag{3.4}$$

where $\alpha = 29\ \rho\ \text{cm}^2\,\text{g}^{-1}$ and ρ is the density of the target, in this case argon (Brandt and Paulin 1977). All other parameters in the simulation remain the same, although of course the positrons are now emitted from the opposite side to that of entry. The number of β^+ entering the film was taken as half of those created in the source plus those backscattered from the source mount. In the experiment this source mount was copper which has an approximate backscattering coefficient of 30 % (MacKenzie *et al.* 1973). Positrons diffusing back to the source mount are assumed to annihilate. The depth of the film (d) was taken as the only fitting parameter in order to model the experimental data since this parameter was poorly determined in the earlier work (Merrison *et al.* 1992). All other parameters were the ones used or determined in the previous simulation. The experimental and predicted moderation efficiency are shown in figure 3.6 as a function of surface potential (and thus electric field) for a film depth $d = 1.3$ μm. As can be seen the zero field and
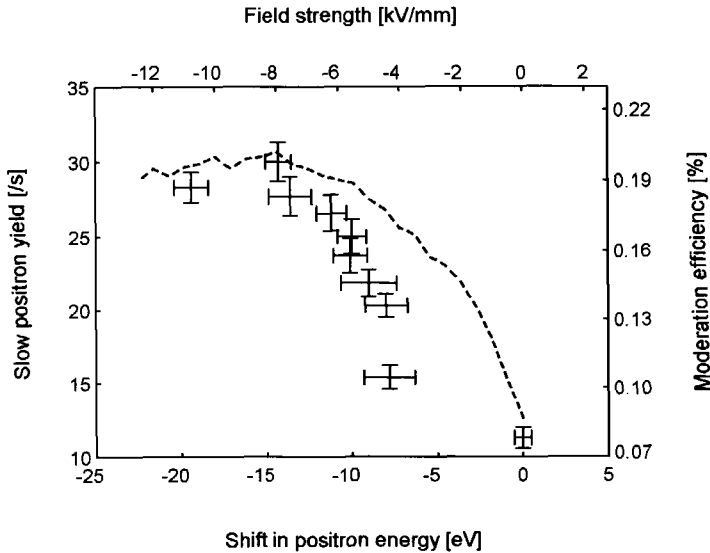
Fig. 3.6. Moderation efficiency for a solid argon β⁺moderator as a function of surface potential. The curve drawn is the result of the computer simulation mentioned in the text. For experimental details see Merrison *et al.* (1992).

high field values are in good agreement although those measured at low field fall below theory. The reason for this discrepancy was probably surface contamination (Petkov *et al.* 1997). The field dependence was obtained experimentally by allowing the surface potential to decay before measuring the positron yield at various times after charging. The low field measurements were therefore taken at relatively long times after deposition. The last data point, which deviates most from that predicted, was taken over 3 hours after deposition. Taking the reported base pressure of 4×10^{-9} Torr and using the same depth dependence of pressure and time as that for the Ar film this would correspond to an ~50 Å thick overlayer of contaminants. This would undoubtedly have had a serious detrimental effect upon the positron emission efficiency.

3.6. Conclusion

In summary we have measured positron reemission properties of surface charged solid argon for different thicknesses and different surface potentials and have obtained good agreement a with a computer simulation from which a diffusion length of $1.7(+2.0,-0.4)\mu m$ and a mobility of $4.7(+2.9,-0.4) \times 10^{-3} \ m^2 \ V^{-1}s^{-1}$ have been derived. The value for the diffusion length is in disagreement with earlier studies, mainly due to a difference in the average energy loss per collision determined here to be $1.1(+0.4,-0.5)meV$. The Monte Carlo simulation was also found to be in reasonable agreement with our previous studies of surface charged Ar moderators. The results are consistent with a field induced drift of the positrons in the bulk. A maximum enhancement in reemission was reached at an electric field strength of roughly $7 \ kVmm^{-1}$. By increasing electric fields above $7 \ kVmm^{-1}$ a slow decrease in the enhancement was observed; this was shown to result from heating of the positron energy distribution above the inelastic positronium threshold. Furthermore a rapid and almost total reduction of the reemitted fraction occurred for surface potentials above a thickness dependent value in the range of -95 to -215 V. Further work is necessary in order to explain this latter effect.

CHAPTER 4

POSITRON MODERATION CHARACTERISTICS OF WIDE BANDGAP SEMICONDUCTORS

4.1. Introduction

Wide bandgap semiconductors have been a rapidly growing field of research in the last years. The reason for this interest are the new uses envisioned for such materials which cannot be met by conventional Si based semiconductors. Among the most prominent of these are high power and high temperature applications and light emitting diodes and lasers operating in the blue and ultraviolet region. In recent years most of the interest has focused around SiC and the III-V nitrides. SiC with its high thermal conductivity, high breakdown voltage and high electron saturation velocity has proven useful for high power and temperature applications and despite the indirect bandgap blue light LEDs based on SiC are commercially available. However, for bright blue and UV LEDs and lasers the III-V nitrides particularly GaN and its AlN and InN alloys have shown very great promise and already very bright blue LEDs based on these materials are commercially available and continuous wave lasers operating in the blue and UV region at room temperature have been demonstrated in the laboratory (see e.g. Morkoç *et al.* 1994, Nakamura
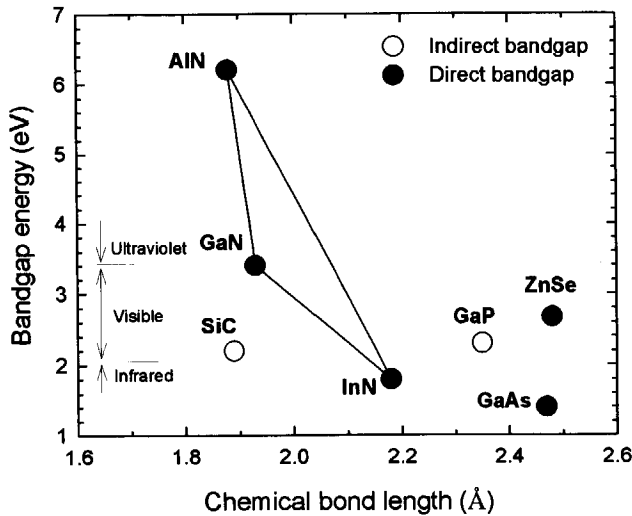
Fig.4.1. Chemical bond length versus bandgap energy for some wide bandgap compound semiconductors. The lines drawn between the three nitrides indicate the span in bandgap and chemical bondlength of GaN based alloys.

1997, Ponce and Bour 1997))(Fig. 4.1).

        With the increased interest in these materials the quality of available samples has steadily gone up and high quality samples of particularly 6H-SiC, the hexagonal polytype of SiC, are now readily available commercially and it is also possible to obtain 3C- or β-SiC, the cubic polytype of SiC. We therefore decided that it now merited having a closer look at the positron emission properties of these materials with a particular view to their suitability as materials for positron moderation and field assisted positron moderation. The wide bandgap could be very useful for field assisted moderation as it might, in the presence of an electric field, cause part of the positron distribution to get 'heated' to epithermal energies and thus, if the materials also exhibit negative workfunctions, afford both the advantages of rare gas solids ('hot' positron diffusion) and those of traditional metal moderators (workfunction emission).

        This chapter is divided into three main sections. In the first part measurements on β-SiC will be presented. The second section deals with our measurements on semi-insulating GaN and

TABLE 4.1. Some characteristics of SiC and GaN

	3C-SiC	6H-SiC	GaN
Lattice structure	cubic	hexagonal	wurtzite
Bandgap (eV)	2.2	2.9	3.39
Direct/Indirect bandgap	indirect	indirect	direct
Therm. cond. (W/cm)	5	5	1.3
Breakdown voltage (10^6V/cm)	4	4	5
Physical stability	excellent	excellent	good

finally the last section will deal with measurements on other III-V nitrides, mainly BN.

4.2. β-SiC

Positron beam experiments have been performed to establish the diffusion behavior and surface branching of positrons implanted with energies varying from 0-25 keV into an epitaxially grown layer of β-SiC on a silicon substrate. The energy distribution of the re-emitted positrons was also measured. With this data an assessment of the materials potential as a positron moderator could be made. The use of this wide band gap material for field assisted positron moderation is discussed.

4.2.1. Introduction

A few years ago it was found by Brandes *et al.*(1992) that synthetic diamond showed good re-emission properties for implanted positrons. It was also shown that diamond layers obtained by chemical vapor deposition emitted positrons (Xiong *et al.* 1997, Uedeno *et al.* 1990). However, in the latter case the layer was composed of small diamond crystallites and therefore the angular distribution of the emitted positrons was expected to spread over a wide angle. Large area synthetic diamonds are difficult to obtain and therefore our interest went to other wide band gap materials related to diamond. The compound semiconductor material SiC can now be

deposited in thin epitaxial layers and is commercially available (for a general review of some of these wide band gap semiconductors see Morkoç *et al.*(1994) and refs. therein). Therefore we initiated the search for suitable remoderation materials with this material. We have chosen to study the cubic polytype of SiC, β-SiC or 3C-SiC, because of its similarity with diamond. Recently results for positron reemisson obtained for the hexagonal polytype 6H-SiC were published by Störmer *et al.* (1996). Further results on the positron characteristics of both 3C-SiC and 6H-SiC have been published by Brauer *et al.* (1996, 1997).

An extra reason for the interest in wide band gap materials as positron moderators is their possible use as field assisted moderators (Madey 1969, Lynn and McKee 1979, Beling *et al.* 1987), where an external electric field is used to drift the thermalized positrons toward the exit surface. Recently, the first such device was demonstrated using solid argon (Chapter 3, Merrison *et al.* 1992, Jørgensen *et al.* 1995). However, despite the mechanical simplicity afforded by using semiconductors, all attempts at making field assisted moderators using these materials have so far failed due to trapping of the positrons at the interface between the semiconductor and the gate material. Research directed at overcoming this obstacle is continuing (Shan *et al.* 1994)

4.2.2. Experimental

The experiments described in this chapter were performed using (100) orientated β-SiC from CREE Research, Inc.. The β-SiC was grown on a n-type Si wafer with a wafer doping level of 0.01 Ωcm. On top of this wafer a layer of β-SiC was deposited with a quoted thickness of 1.2 μm and a doping level of 4×10^{16} cm^{-3} of an n-type dopant (Sample A). A similar sample grown on a p-type Si wafer with an n-type β-SiC doping level of 1.3×10^{16} cm^{-3} was also studied (Sample B).

The samples were placed on a molybdenum base plate with a heating filament behind it. This allowed the sample to be heated for annealing purposes. A thermocouple was attached to the front of the sample. A molybdenum grid was positioned at a distance of 1.15 meters in front of the sample. This grid was used to alternately remove low energy reemitted positrons and hold them back for determining the positron surface branching ratios (see chapter 2). Retarding field energy distribution measurements were performed by varying the grid potential from 0 to 12 V. The high purity Ge γ-detector positioned perpendicular to the beam axis at a distance of about

45 mm from the center of the samples was used for data collection.

4.2.3. Results and discussion

The data presented here fall in three categories that will be treated separately. These are the measurements of the Doppler broadening, the surface branching ratios and the energy spectrum of positrons reemitted from the surface of the β-SiC.

Results of Doppler broadening measurements are shown in fig.4.2. S- and W- parameters, which are sensitive to valence- and core-electron annihilations respectively, are measured for varying positron implantation energy (for a more detailed description of the technique, see Asoka-Kumar *et al.* 1994 and Clement *et al.* 1995). It is observed that the value of S decreases with energy from its initial value for low energies, i.e., its surface value, to the value of the SiC layer, where it persists for energies up to about 10 keV. This energy range corresponds approximately to the expected thickness of the layer. At higher energies the S-value increases and approaches the saturation value of bulk-Si at about 25 keV. Similar effects are observed for the W-parameter, although here they are mirrored since a low S-value generally corresponds to a high W-value and vice-versa. An exception to this is formed by the surface values (low energies) where both the S- and W-value are seen to increase. A full analysis using the VEPFIT fitting program (see chapter 2) was performed. Both the measured S- and W-values were fitted independently. This yielded a value for the positron diffusion length in β-SiC of 42nm ± 5nm. The characteristic set of (S,W)-values for β-SiC were found to be (0.90,1.37) relative to the bulk values for Si. The fitting consistently yielded a value for the thickness of the SiC overlayer which was roughly 250 nm lower than the value quoted by the manufacturer. The reason for this discrepancy is not clear at this time. However, we have lately noted several instances where the Makhovian implantation profile with shape parameter 2 (Gaussian derivative profile), traditionally used in fitting, has lead to underestimation of the thickness of thin overlayers. However, these overlayers have mostly been about an order of magnitude thinner than the present one. The lines in figure 4.2 are all results of the fitting. In Fig. 4.2(b) the S- and W-values from Fig. 4.2(a) are plotted in a so-called (S,W)-plot. The plot shows clearly that for increasing energy of the positrons first the surface state is probed, then the SiC layer and finally the Si substrate. Little difference was observed between the Doppler broadening measurements performed on samples A and B though the
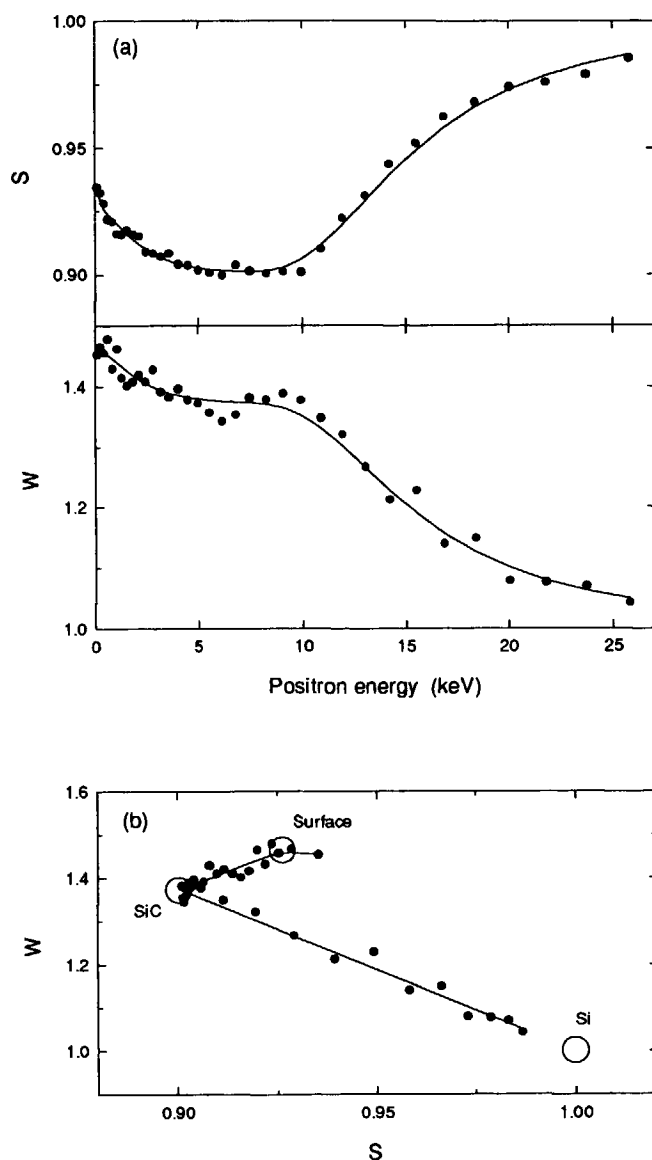
Fig.4.2. Doppler broadening *S*- and *W*-parameter data for sample A. The lines are the results of fitting using the VEPFIT fitting program. All *S*- and *W*-values are relative to the bulk value for Si. (a) shows the lineshape parameters as a function of incident positron energy, i.e. depth. (b) *W* versus *S* plot of the data shown in (a). With increasing energy the positrons first probe the surface state, then the SiC layer and finally the Si substrate. The open circles are the characteristic (*S,W*) values for each layer as derived from VEPFIT.

characteristic S-value for the SiC layer in the case of sample B was slightly lower than for sample A.

The results of surface branching ratio measurements are shown in figure 4.3. For the samples which had no special treatment after insertion into the vacuum a positron reemission yield of 30% was found. This is rather close to what has been measured before for molybdenum and tungsten foils and bodes well for the potential of β-SiC as a positron moderator material. A branching of about 40 % to the bound surface state was observed for both samples with the remaining ~ 30 % being emitted as positronium. Note that the values are virtually independent
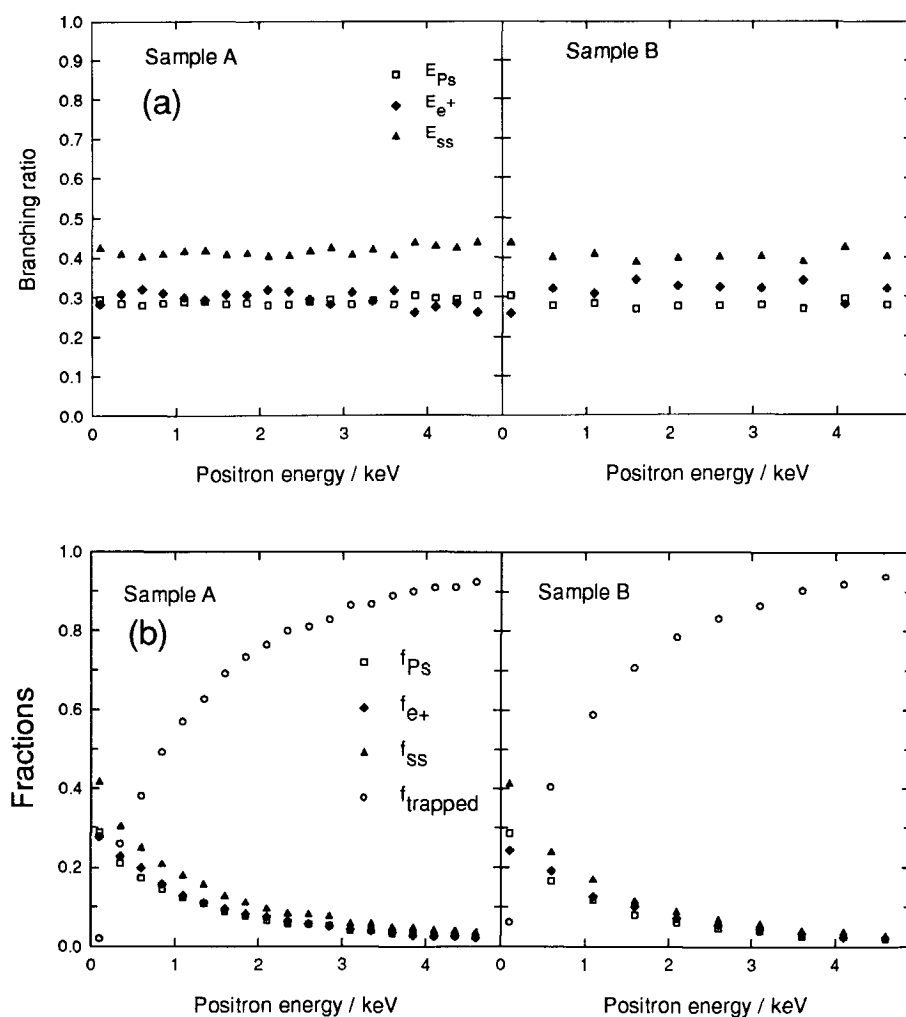
Fig.4.3. Surface branching ratio measurements for the two SiC samples.

of the depth of implantation of the positrons. This indicates that either few epithermal positrons are present or that epithermal positrons have about the same branching ratios.

With knowledge of the diffusion length and the surface branching ratio, the fraction of implanted positrons that are re-emitted from the surface as slow positrons can be calculated. The fraction of the incoming beam being reemitted as slow positrons, F_{e+}, is given by $F_{e+}(E) = (1-\eta)F_s(E)\epsilon_{e+}$, where η is the backscattering fraction, $F_s(E)$ is the fraction of implanted positron that make it back to the surface and ϵ_{e+} is the surface branching ratio to free positrons. The fraction of positrons being backscattered, η, is typically of the order of 0.25-0.3 (Coleman *et al.*, 1992). $F_s(E)$ can be calculated from the diffusion length and the energy specific implantation profile. The fraction of implanted positrons being reemitted as free positrons, $f_{e+} = F_s(E)\epsilon_{e+}$, is measured during surface branching ratio measurements and can be seen in fig. 4.3(b) together with the other relevant fractions.

A retarding field measurement of the energy distribution of the reemitted positrons is shown in fig. 4.4. Figure 4.4(a) shows the result of a retarding field measurement observed with 0.5 keV incident positron energy. The annihilation peak count rate is plotted as a function of the positive bias on the grid. Figure 4.4(b) shows the energy distribution of the reemitted low energy positrons, obtained by taking the smoothed derivative of the retarding field measurement. The energy scale is given by $E_+ = e(V_{grid}) + (\phi^-_{grid} - \phi^-_{\beta-SiC})$ where ϕ^- is the workfunction of the grid material (molybdenum) and β-SiC respectively. The value of the off-set, $\Delta\phi_- = (\phi^-_{grid} - \phi^-_{\beta-SiC})$, can be derived from the retarding field measurement (see chapter 2). This cut-off, situated at ~ 0.3 eV, is indicated in Fig.4.4(a) by the dashed line. The reemitted positron energy distribution in Fig.4.4(b) is observed to consist of a narrow contribution centered around 0.5 eV and a wider contribution up to just below 3 eV, in reasonable agreement with the value for the positron workfunction quoted by Brauer *et al.* (1997) for 3C-SiC and the value quoted by Störmer *et al.*(1996) for 6H-SiC. Contributions at higher energies are not significant in view of the statistical accuracy, as can be seen by comparing figs. 4.4(a) and (b). One may speculate about the reason for the two energy distributions observed. The surface of the sample would invariably be contaminated due to the vacuum conditions of our set-up. Such surface contamination may play a role in degrading the energy of the emitted positrons. But then the energy distribution centered around 0.5 eV would not have been narrow. An alternative explanation might be that the surface composition is not uniform. It is not unlikely that a part of the surface is terminated

by Si atoms and another part by C atoms. Then, different positron characteristics are expected for positrons emitted from the different surface areas. A third explanation might be that the surface is not smooth and exhibits facets in specific directions. Because we measure only the energy associated with the axial component of the velocity this might lead to two contributions in the retarding field spectrum.
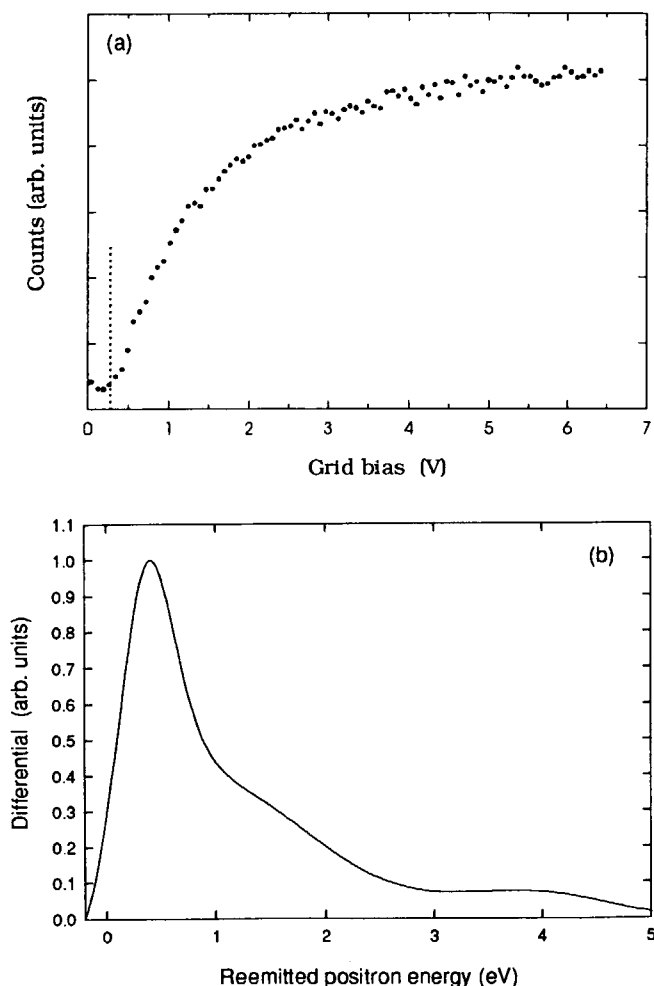

Fig. 4.4. (a) Retarding field measurement of re-emitted positrons for sample A obtained as the annihilation peak count rate at the sample as a function of the positive bias on a retarding grid in front of it. The dashed line indicates the zero cut-off bias. (b) Energy spectrum of the re-emitted positrons obtained by taking the derivative of the smoothed retarding field measurement shown in (a).

4.2.4. Conclusion and final remarks for β-SiC

The wide band gap semiconductor β-SiC shows promising positron reemission characteristics which, together with its ruggedness, might make it a candidate for positron moderation as well as a useful material for field assisted moderation purposes. In the future, efforts on the surface characterization and defect analysis are required to improve the quality of the layers.

4.3. GaN - SI

The positron diffusion length, the surface branching ratios for positrons, and the positron workfunction for SI-GaN has been measured using a mono-energetic positron beam with incident energies from 0 to 25 keV. The materials feasibility for positron moderation and its possible use in field assisted moderation is discussed.

4.3.1. Introduction

GaN has attracted much attention in the last years due to its physical and electronic properties and above all its recently demonstrated qualities as a high efficiency material for optical devices operating in the blue and ultraviolet (UV) regions of the optical spectrum (Nakamura *et al.* 1997, Nakamura 1997, Ponce and Bour 1997). This increased interest has lead to much improvement in the growth and quality of samples though there are still problems with intrinsic defects in GaN. As-grown samples of GaN are typically heavily auto-doped n-type with carrier concentrations as high as 10^{20} cm^{-3}. Much research has been done to better understand the nature of this intrinsic donor and lately positron techniques have also been brought to bear on this problem for the first time. Quite unexpectedly, the study showed the presence of Ga vacancies in n-type samples (Jørgensen *et al.* 1997). Very recently positron annihilation studies have also been instrumental in solving the mystery of the origin of a broad band yellow luminescence in

GaN. It was shown to be correlated with the amount of Ga vacancies present in the sample (Saarinen *et al.* 1997). Lately the native defects have been attributed partly to an oxygen donor either alone on substitutional N-sites or in a vacancy-impurity complex with a gallium vacancy, partly to possible unintentional Si incorporation during growth. In the latter case the Si will occupy substitutional Ga sites (see e.g. van de Walle and Neugebauer 1997). In order to obtain semi-insulating samples it has therefore become customary in the last years to dope the sample with Mg which is an acceptor and compensates for the intrinsic donors.

As the interest in GaN has grown over the last years and more has been learned about the growth of GaN samples it has now become possible to obtain good quality semi-insulating samples. In terms of positron moderation, GaN is of interest because of its wide bandgap which might lead to longer average diffusion lengths due to epithermal ('hot') positron diffusion. Furthermore GaN would be well suited as a material for field assisted moderation. To find out if and how GaN works or would work as a positron moderator / field assisted moderator it is necessary to know some fundamental positron properties of the materials, such as the positron workfunction, diffusion length, surface branching ratios, etc.

4.3.2. Experimental

The measurements were performed on a semi-insulating (SI) sample of GaN grown by Dr. M. Fanciulli in the group of prof. Moustakas at Boston University. The sample was grown by the ECR-MBE method on sapphire substrates (Moustakas and Molnar 1993). The sample had a thickness of 1.38 μm with a buffer layer of about 30 nm grown at 600 °C. The rest of the film was grown at 900 °C. The sample was grown at a slight N_2 overpressure.

The experiments were performed using the variable energy positron beamline (VEP) at Delft. The annihilation radiation was measured using a high purity Ge γ-counter placed perpendicular to the beam axis at a distance of about 45 mm from the center of the samples. A grid some distance in front of the sample was used to alternately remove low energy positrons from in front of the sample or retard them back to the sample. This grid was used for the surface branching ratio measurements and the retarding field measurements.

4.3.3. Results and discussion

The data presented here fall in three categories that will be treated separately. These are the measurements of the Doppler broadening, the surface branching ratios, and the energy spectrum of positrons reemitted from the surface of the GaN-SI.

The results of the Doppler broadening measurements are shown in fig.4.5. S- and W-parameters, which are sensitive to valence- and core-electron annihilations respectively, are measured for varying positron implantation energy (Asoka-Kumar *et al.* 1994 and Clement *et al.* 1995). The data is given relative to the bulk value of GaN-SI. At the same time as the Doppler broadening measurements of this SI sample were performed, two other samples were investigated, an *n*-type and a *p*-type sample. Results of these measurements can be found in Jørgensen *et al.* (1997).
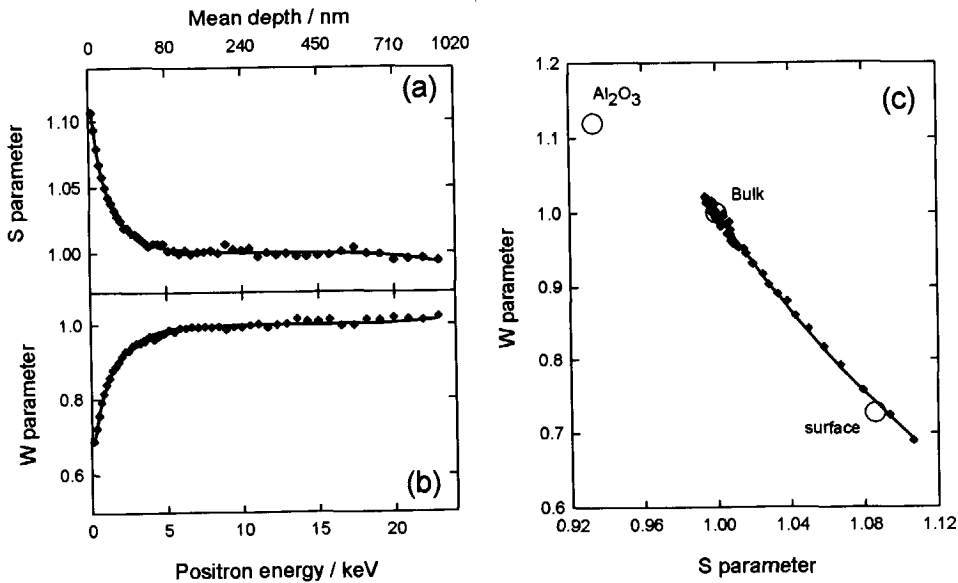
Fig. 4.5.(a) and (b) S and W parameters as a function of incident positron energy for the GaN - SI sample studied. (c) S-W plot of the data indicating the probing of the different layers. All lines in the figures are fitted values obtained from the VEPFIT fitting program. The S and W value are relative to the bulk value for GaN-SI.

The data was analyzed using the VEPFIT fitting and modelling program (see chapter 2). The lines in Figure 4.5 are VEPFIT fits to the data. The S parameter and W parameter measurements (Fig.4.5(a) and (b)) are nearly symmetric in that a high S value corresponds to a low W value. Due to the thickness of the sample and the good counting statistics the bulk S- and W-value could be determined with good accuracy. The high S-value for the surface and similar low surface W-value made an accurate determination of the positron diffusion length in the GaN-SI layer possible. A value of 19.3 nm ($\pm$ 1.4 nm) was found. Fig. 4.5(c) shows an S versus W plot of the same data shown in Fig. 4.5(a) and (b) but using the incident positron energy as a running parameter. The big open circles mark the fitted values for the surface, bulk and substrate, respectively. These all lie more or less on a straight line in this case and therefore the data pretty much follows a straight line as the positrons with increasing energy probe first the surface, then the bulk and finally heads off slightly in the direction of the substrate. That it never reached the substrate value, i.e. that the major part of the annihilation signal never originates from the
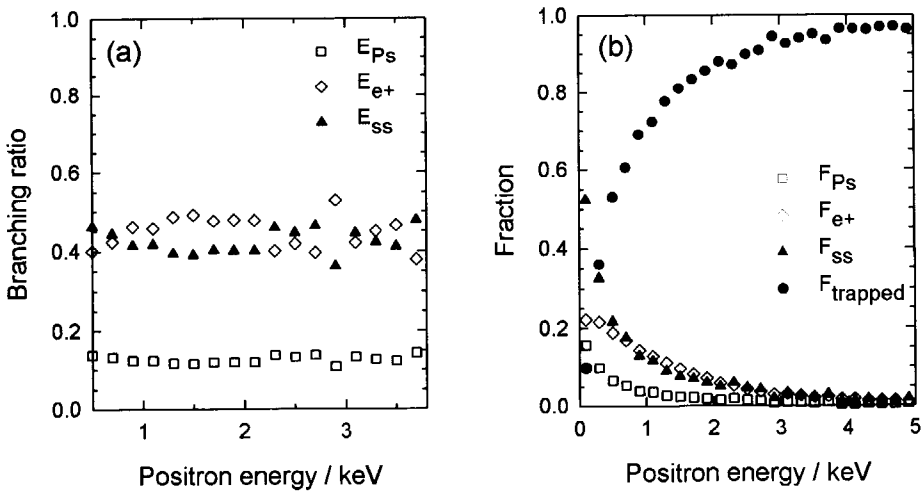

Fig. 4.6. (a) Surface branching ratios for the GaN-SI samples. (b) The actual fractions measured.

substrate, is because of the thickness of the sample and is illustrated by the mean depth scale shown atop Fig.4.5(b). That it is beginning to reach the substrate at the very highest energies can be seen from the slight decrease in S value seen for those energies and the corresponding slight increase in the W value.

The results of the surface branching ratio measurements are shown in Fig. 4.6. In Fig. 4.6(a) is shown the actual measured branching ratios while Fig. 4.6(b) shows the fractions used to derive the branching ratios (see chapter 2). As mentioned in chapter 2 the branching ratios are only reliable for relatively low energies since the involved fractions get very small for higher energies leading to large statistical scattering in the data. This is because at higher energies most positrons get trapped in the bulk (see fig. 4.6(b)) Also at very low energies epithermal effects can play a large role leading to unreliable branching ratios for thermal positrons. From the fractions it is evident that for low energies there is indeed an epithermal effect present in the case of GaN-SI. This can be seen from the dip in the free positron fraction at very low energies. Therefore the most reliable branching ratio data here is from the energy region from 1 to 2.5 keV and from those data points values of the branching ratios to free positrons, the surface state, and positronium are found to be 0.48, 0.40 and 0.12, respectively, all with an error of ± 0.02. The branching ratio to free positrons is very high here. In most materials used for positron moderation, like, e.g., tungsten, it lies somewhere around 0.30 and it is considerably lower for many materials. This very high value bodes well for the use of GaN as a moderator material.

Figure 4.7 shows the results of retarding field measurements on low energy positrons reemitted from the GaN-SI sample. In the first experiment (Fig. 4.7(a)) a 4 keV positron beam was directed at the sample. At such high energy implantation only a minor fraction of the incident positrons will return to the surface and according to the surface branching ratio measurements only 48% of those returning to the surface will be reemitted. One can see how small this fraction is by observing the fraction of incident positrons with an energy of 4 keV that are being reemitted as free positrons in Fig. 4.6(b). Therefore this will lead to larger statistical errors unless long counting times are used. In our case the counting time was 6 minutes per point. A first measurement of the energy distribution of reemitted positrons when using a 1 keV incident energy is shown in Fig. 4.7(b). This series are incomplete due to computer and vacuum problems. This energy should, however, be ideal for observing the energy distribution of thermalized positrons since at this energy the epithermal contribution is negligible (Fig. 4.6). From the two sets of data
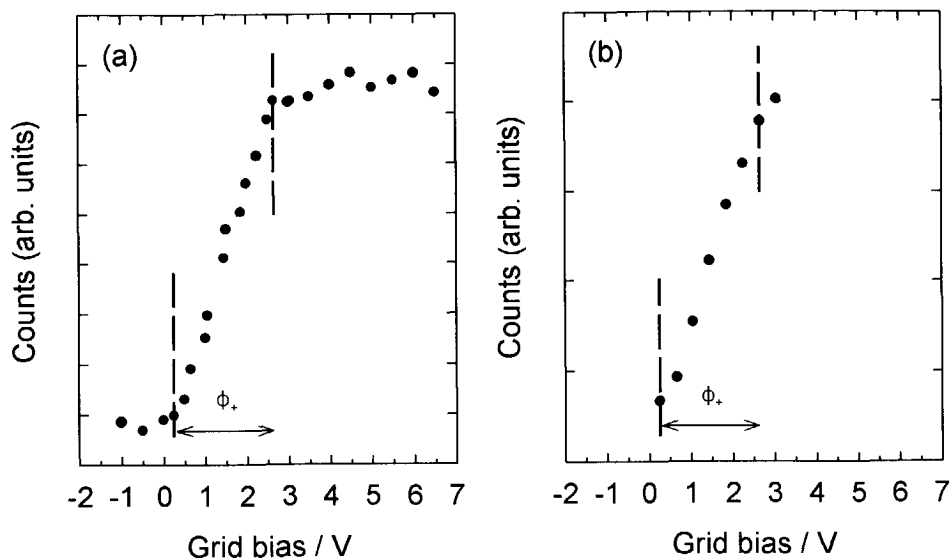
Fig. 4.7. Retarding field measurements for GaN-SI. (a) 4 keV incident positron energy. (b) 1 keV incident positron energy.

a value for the positron workfunction, ϕ_+, for GaN of -2.4 eV ($\pm$ 0.3 eV) was found. However, the 1 keV measurement, which was also done using a counting time of 6 minutes and thus superior statistics due to more positrons being emitted at this energy, could possibly have yielded a slightly larger value for ϕ_+ had it been completed. It would be interesting to measure the reemission for a wide variety of different incident energies now that the new E×B filter has been installed (see chapter 2). The channelplate and grids attached to it should make more sensitive measurements possible with far less background than with the Ge counter, which is somewhat crude for this kind of experiments. Measurements at lower incident energies would be useful for mapping the energy distribution of the epithermal contribution.

4.3.4. Conclusion and final remark for GaN - SI

Measurements of some of the positron characteristics of GaN have been performed. These have yielded values for the diffusion length, surface branching ratio to free positrons and positron workfunction of 19.3 nm, 0.48 and -2.4 eV, respectively. The large branching ratio and negative workfunction makes GaN a very promising material for positron moderation and field assisted moderation purposes. As the rapid development in the knowledge about GaN growth techniques continues, it should be possible to obtain semi-insulating GaN samples with less intentional and unintentional impurities incorporated which should hold promises of increasing the positron diffusion length in the material.

4.4. Pyrolytic BN and other III-V nitrides

4.4.1. Introduction

Beyond GaN, the other III-V nitrides also exhibit wide bandgap semiconductor or even insulator characteristics (see e.g. fig.4.1). Yet while they all might be interesting for positron moderation purposes, it is still difficult to obtain good quality samples of these materials. However, with the interest in AlN and InN growing as a consequence of the unique characteristics of their alloys with GaN it might be possible to obtain samples of sufficient quality in the near future. Meanwhile it is possible to commercially obtain pyrolytic BN samples of good quality. We therefore decided to investigate the positron characteristics of this material in closer detail with a view to its possible use as a moderator material.

BN has a hexagonal crystal structure and a number of interesting characteristics that has proven valuable commercially. Electrically it is an insulator with a very broad bandgap but thermally its properties are like those of a metal. It is lubricating like graphite (even after 8 days in water it has been shown to absorb no moisture), has a high sublimation temperature of about 3000 °C, is easily machinable and has a negligible outgassing, oxidation and gas permeability. All of these characteristics make it very interesting for a number of industrial applications.

4.4.2. Experimental

The measurements were performed on two samples of CVD grown pyrolytic BN obtained from CVD Products Inc. The samples were installed without any further treatment and positron Doppler broadening and surface branching ratio measurements were performed using the VEP mono-energetic positron beam line at Delft. The experiments followed the recipe used for β-SiC and GaN-SI (see also chapter 2 for details), though in this case no retarding field measurements were performed for reasons that will become evident in the next subsection.
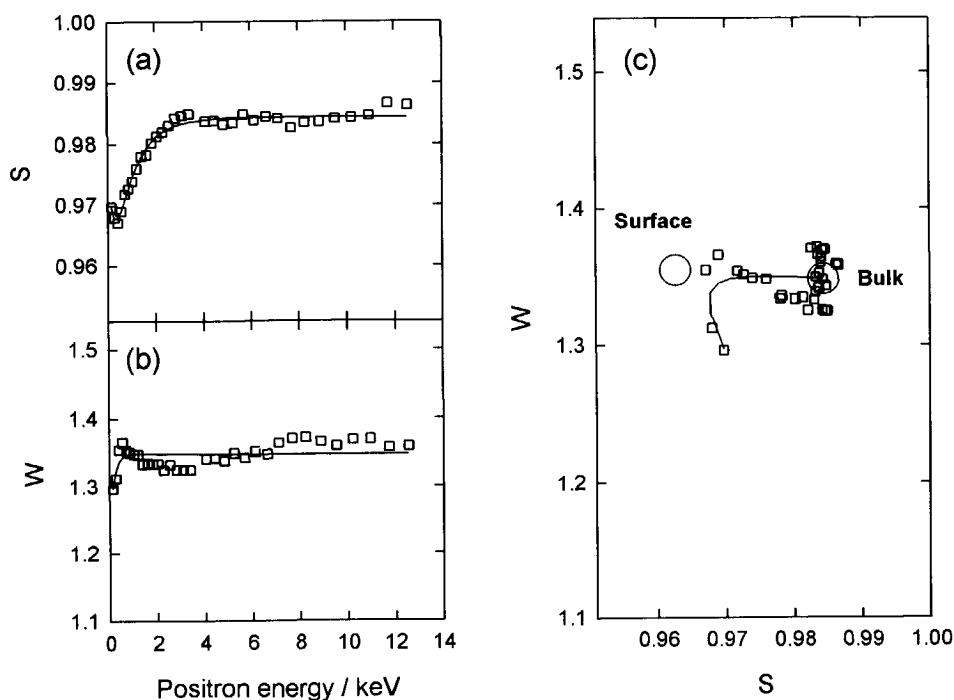
Fig. 4.8.(a) and (b) S and W parameters as a function of incident positron energy for the pyrolytic BN sample studied. (c) S-W plot of the data indicating the probing of the different layers. All lines in the figures are fitted values obtained from the VEPFIT fitting program and all S and W value are relative to the values for bulk Si.

4.4.3. Results and discussion

Figure 4.8 shows the results of the Doppler broadening experiment. The S and W values are shown relative to the bulk values for Si. The data was fitted using the VEPFIT fitting and modelling program (see chapter 2) and assuming one BN layer. The fit, and in particular the fit to the measured W values is not very good. The value for the diffusion length obtained from the fitting was 19 nm ($\pm$ 6 nm). The date seem to suggest that the sample consists of two layers. This can be seen very clearly in the (S,W) plot (Fig.4.8(c)) where it is evident that the bulk data points are spread out in W and can only be fitted if one uses two different W values for the bulk. As we had found no reason why there should be two different layers to the bulk it was fitted assuming only one bulk layer and therefore the fit is not as good as the other fits presented in this thesis. As described in chapter 2 the S parameter is associated with annihilations with valence electrons and the W parameter is associated with annihilations with core electrons. Therefore two layers observed in the W data most likely represent a difference in stoichiometry or crystal structure between the two regions. Since the difference is predominantly seen in the W data and hardly at all in the S data, we conclude that it must be due to a slight difference in elemental composition and not in defect type or concentration since that would have revealed itself more in the S data than in the W data.

After the positron measurements were completed one of the samples was measured using x-ray diffraction. The results of this measurement indicated the presence of two phases in that sample. The observed difference was consistent with two different values of interlayer distances in the c direction. The two values found were 6.6 Å and 6.8 Å, respectively. This difference could possibly explain the results in Fig.4.8(b) if the high interlayer distance correspond to a region at shallow depths and the lower value corresponds to larger depths. It should be noted that the theoretical value for the layer separation is $c = 6.661$ Å.

Branching ratio measurements were performed on the samples and the result is shown in figure 4.9. The observed branching ratio to free positrons for pyrolytic BN is 0.00 (± 0.02). Thus no free positrons are observed leaving the surface of pyrolytic BN. This is most likely caused by an positive positron workfunction. The other branching ratios were found to be 0.39 and 0.61 to positronium and to the surface state, respectively, both with an uncertainty of ± 0.02. It is interesting to observe in Fig. 4.9(b) that very few positrons seem to reach the surface. Already at an implantation energy of 1 keV the fraction of positrons trapped in the bulk is nearly unity.
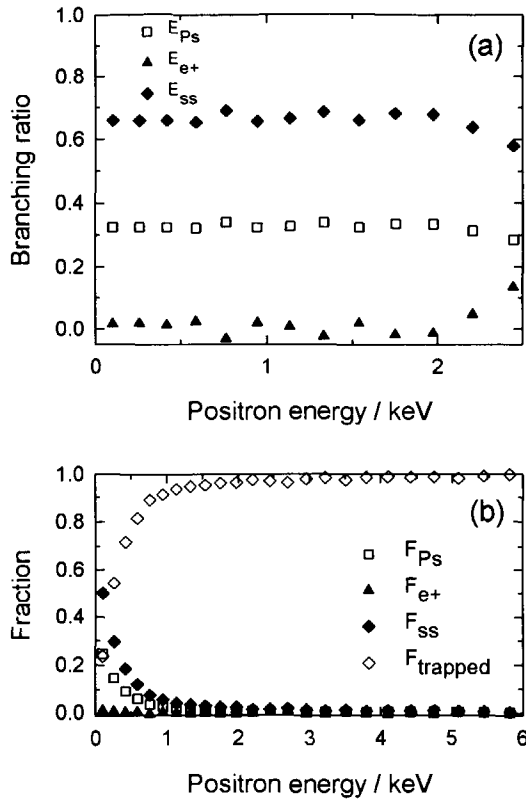
Fig. 4.9. (a) Surface branching ratios for pyrolytic BN. (b) The fractions derived from the measurement.

This could be caused by the relatively short diffusion length, large concentrations of positron traps, or perhaps the positive workfunction. The last of these will lead to a reflective potential barrier at the surface region that will return most of the positrons to the bulk. As a consequence of the non-existing surface branching to free positrons no retarding field measurements were performed on these samples.

4.4.4. Other III-V nitrides

Doppler broadening measurements and surface branching measurements were also performed on pressed powder AlN samples. We were able to discern radiation damage in one of

the samples by means of Doppler broadening. However the nature of the sample made it difficult to get any accurate data on the positronic properties of AlN. However, the samples did emit low energy positrons from the surface as observed in the surface branching ratio measurement. This would indicate that the positron workfunction for the material is negative. Thus it would very be interesting to study an epitaxially grown layer of AlN to better assess its positronic properties.

4.4.5. Conclusion for BN and other nitrides

We have performed Doppler broadening and surface branching measurements on CVD grown pyrolytic BN. Our results show that this material is not suitable for use as a positron moderator. Similar experiments on pressed powder samples of AlN have indicated that this material show good promise for moderation and possibly also for field assisted moderation of positrons.

4.5. Conclusion and final remarks

Some of the new wide bandgap semiconductors have been investigated to assess their suitability as positron moderator materials with a particular view to field assisted moderation. The investigation has centered around β-SiC and the III-V nitrides and GaN in particular. β-SiC was shown to exhibit excellent properties for positron moderation. GaN exhibited properties that, except for a rather short diffusion length, were even superior to those of β-SiC. Indeed, newer samples with better impurity control could do much to alleviate this problem and might make GaN the material of choice in future field assisted moderation applications. However, for this material to reach that level more work is needed, e.g. in mapping the epithermal contribution and in observing its properties under the influence of an electric field.

It might also be possible to use SiC and GaN as transmission moderators or remoderators by etching the substrate away to make the sample semi self-supporting. A frame and possibly a supporting grid could be left unetched, keeping the sample sturdy. An attempt in this direction is

presently under deliberation. If this experiment falls out well, transmission field assisted moderators might be possible.

Measurements on pyrolytic BN indicated that this material might have a positive positron workfunction and thus not emit free low energy positrons from the surface. Therefore this material is not suitable for positron moderation purposes. Measurements on pressed powder AlN samples showed this material to hold some promise but more work needs to be done on better epitaxially grown samples of this material to properly ascertain its positronic properties.

CHAPTER 5

BIMETALLIC POSITRON RECTIFIERS

5.1. Introduction

The development of bigger and brighter positron beams has made steady progress over the last 20 years, thus making positrons applicable to new fields of research (Schultz and Lynn 1988, Mills 1995). An important tool to achieve the kind of brightness necessary in, e.g., positron microscopes is the method of brightness enhancement first proposed by Mills (1980) (see chapter 1). This method utilizes the fact that forces acting on a positron during stopping and thermalization in a solid are generally non-conservative and the process can therefore be used to breach Liouvilles theorem, provided that the positrons can be reemitted from the solid after thermalization. Since most of the materials with a negative positron workfunction need in situ annealing and/or surface treatment to function efficiently as positron moderators the design of most of the early positron beams employed, for heating and mechanical purposes, the easier backwards reemission geometry for primary moderation. However, this setup constitutes a far more difficult optical system than the, in this respect, much simpler transmission geometry now employed by most beams for primary positron moderation. For remoderation, most systems still

use the backwards reemission geometry (Canter *et al.* 1987, Uhlmann *et al.* 1995) though a system employing transmission geometry remoderation is currently under construction at Delft (van Veen *et al.* 1994).

For transmission geometry remoderation, foils of single crystal W are most often used because of the high efficiency attainable with this material due to its large negative positron workfunction (Schultz and Lynn 1988, Gullikson *et al.* 1988, Puska and Nieminen 1994). With such systems the thickness of the W foil can be matched to the optimal implantation energy to maximize the transmission efficiency. However, even under optimum conditions, with the usual foil thicknesses of the order of 100 - 200 nm, the fraction of the implanted positrons that will be reemitted from the back of the foil is of the same order or larger than the transmitted fraction. From the point of view of transmission remoderation these positrons are lost. Our starting point for the experiments described here was the idea of trying to promote preferential emission in the forward direction by introducing an internal potential barrier which would block thermalised positrons from being reemitted through the entrance surface and thus possibly increase the efficiency of transmission remoderators.

When two metals are brought into contact their electron Fermi levels are equalized by means of charge transfer across the junction and a dipole potential step is introduced at the interface. The size of the dipole step is given by the difference between the electron chemical potentials of the two metals, $\Delta = \mu_-^A - \mu_-^B$. The dipole together with the difference in positron chemical potentials of the two metals results in a difference between the ground state positron energy in metal A and B on either side of the interface of

$$\Delta E_+^{A,B} = \Delta + \mu_+^A - \mu_+^B = \mu_-^A + \mu_+^A - (\mu_-^B + \mu_+^B) = A_+^A - A_+^B \qquad (5.1)$$

where $A_+ = \mu_- + \mu_+ = -(\phi_- + \phi_+)$ is the positron affinity (Puska and Nieminen 1994, Puska *et al.* 1989). The energy difference between the lowest positron states in the two metals is thus given by the difference between their respective positron affinities. Furthermore the following relations exist between the electron and positron workfunctions on both sides of the foil and the above mentioned internal potential step, $\Delta E_+^{A,B}$, where the workfunctions of Mo and W have been

$$\phi_-^{Mo} - \phi_-^W + \phi_+^{Mo} - \phi_+^W = -\Delta E_+^{W,Mo} \qquad (5.2)$$

marked to indicate that they might differ from the workfunctions of pure W(100) and Mo(100) faces by surface adsorption of impurity gas atoms, notably oxygen. The relation between ϕ^* and ϕ is given by $\phi_-^{*\,Mo,\,W} = \phi_-^{Mo,\,W} + \delta_{Mo,\,w}$ and $\phi_+^{*\,Mo,W} = \phi_+^{Mo,\,W} - \delta_{Mo,\,w}$ with δ being the change in the dipole barrier caused by the adsorption. The observables in an experiment are $\phi_-^{*\,Mo} - \phi_-^{*\,W}$, i.e. the contact potential difference, $\phi_+^{*\,Mo}$ and $\phi_+^{*\,W}$. Note that $\Delta E_+^{W,Mo}$ is not affected by the value of δ_{Mo} or δ_W. For the two metals used in our layered foils, tungsten and molybdenum, the potential step, $\Delta E_+^{W,Mo}$, at the interface has a theoretical value of 0.61 eV (Puska and Nieminen 1994, Puska *et al.* 1989) and an experimental value of 0.64 eV (Gidley and Frieze 1988). Therefore the positrons gain this energy when they enter the Mo from the W and they are subject to nearly total reflection when approaching the interface from the Mo side after thermalization in that medium. Furthermore, W has a positron workfunction, ϕ_+, of - 3.0 eV for the (100) surface (Chen *et al.* 1985) whereas ϕ_+ for Mo(100) is -1.7 eV (Nielsen *et al.* 1985).

However, any such two-layer system would be very sensitive to defects at the interface between the two layers and consequently to positron trapping at the interface. To try to avoid this pitfall we chose to use W and Mo as the two materials because of the good match between their crystal lattices. Both have a bcc crystal structure, W with a lattice constant of 3.1647 Å and Mo with 3.1473 Å , measured at 300 K (Wyckoff 1965), making the lattice misfit between the two layers only 0.55%. The low misfit gives a critical thickness for relaxation of 6.5 nm, though it has been suggested that this thickness could be slightly larger (Matthews 1975). A sufficiently thin overlayer would therefore cause no relaxation of the added layer, thus further decreasing the possibility of positron trapping at the interface.

Another combination of materials that might work even better than W-Mo is Re-W. Re is predicted to have an even more negative workfunction for positrons than W. Therefore this should be an even more efficient system for emitting slow positrons in transmission mode, since the positron emission scales with the absolute size of the negative workfunction. Also Re is predicted to have a higher positron affinity than W. The value for the potential step, $\Delta E_+^{Re,W}$, should thus be 0.34 eV. However in this case the mismatch is much larger, because Re has a hexagonal crystal structure with a lattice constants $a = 2.76$ Å and $c = 4.46$ Å. By growing the Re epitaxially on the (110) surface of W the mismatch is smallest possible, but still much larger than for the W-Mo system.

5.2. Experimental

The experiments described in this chapter fall in two series, performed about one year apart. Since the experimental setup differed between the two series a careful description of both setups and the differences between them will be given.

For the first series the layered foils used consisted of 10 nm W(100) epitaxially grown on 100 nm Mo(100). For comparison with previous studies 100 nm W(100) foils were also installed. The foils were mounted on W poly-crystalline carrier foils with a thickness of 50 μm and a 5.2 mm diameter hole at the center. Prior to installation the foils in their frames were annealed at 1200 °C in a separate vacuum vessel. The two foils, together with a dummy sample with a 5.2 mm hole, were mounted on a linear drive attached to the experimental setup.

The foils used in the second set of experiments were, like in the first series, 10 nm W(100) epitaxially grown on 100 nm Mo(100) and 100 nm W(100), but this time there were two foils more: 10 nm Re epitaxially grown on 100 nm W(110) and a thick WMo foil (10 nm W(100) grown on 1000 nm Mo(100)). The foils were mounted on thin (7 μm) carrier foils with a 5 mm hole in the center. The carrier foils had a total width of about 10 mm and were clamped on a ceramic plate with electrodes attached to either end of the foils. This setup was the same as the one that is to be used in the new remoderation stage for our microbeam (see chapter 7) and allows for in situ heating. A dummy sample with no thin foils mounted over the center hole of the carrier foil was also installed.

The experiments were done using the Variable Energy Positron Beam (VEP) at Delft. Since the time between the two sets of experiments coincided with the installation of the new source, the beam strengths differ by a factor five between the two sets. Please note that the beam spot size of 7 mm diameter is larger than the hole in the carrier foils. To monitor the primary and transmitted positron beam, a microchannel plate (MCP) was positioned on the transmission side of the foils for the first set of experiments. Two 90 % transmission retarding grids were situated between the foils and the MCP (see Fig. 5.1). The MCP was fitted with a phosphorus screen, allowing a CCD camera outside the vacuum system to monitor the beam during counting of MCP pulses. A third retarding grid was positioned in front of the foils. For the transmission measurements, the front of the MCP was kept at a bias of -1.75 kV to obtain optimum detection efficiency for the low energy positrons. The sample was kept grounded and the grid B1 between
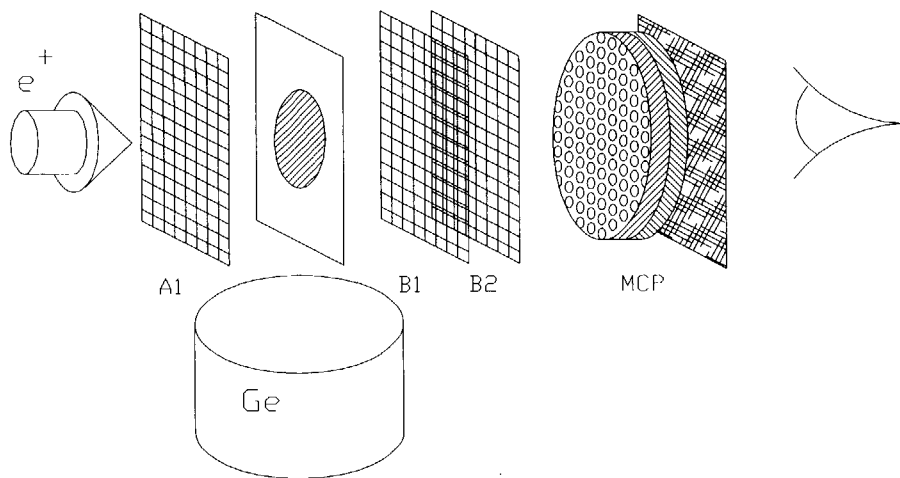
Fig.5.1. Schematic diagram of the experimental setup.

the sample and the MCP was used as a retarding grid to determine the fraction of positrons being emitted from the transmission side of the foils as low-energy positrons. This fraction was derived from the difference between the total transmission and the high-energy transmission, obtained by switching grid B1 from -50V to 50 V. The count rate through the 5.2 mm hole of the dummy sample was measured and corrected for the MCP detection efficiency as a function of the impact energy of positrons hitting the MCP. The ratio between low-energy transmission and the corrected count rate through the dummy sample constituted the fraction of transmitted low-energy positrons. Grid B1 was also used to obtain a retarding energy spectrum of the transmitted low energy positrons.

For the second set of experiments a Channeltron (see chapter 2) had replaced the MCP. This Channeltron had three grids in front of it which were used to retard the slow positrons being reemitted from the foils in the same manner as for the MCP. The front of the Channeltron was kept at -2.0 kV and the back at ground potential. Again the count rate through the dummy sample was measured and corrected for the detection efficiency of the Channeltron.

Directly next to the foils, perpendicularly to the beam axis, a high-purity Ge γ-detector
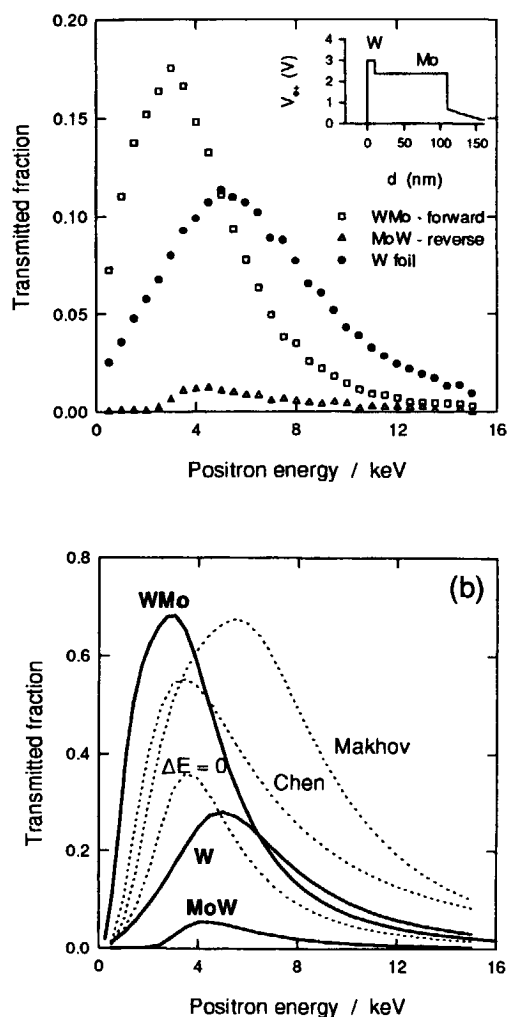
Fig.5.2. Positron transmission results. (a) Measured transmission through a foil consisting of 10 nm W on 100 nm Mo as a function of incident positron energy in the rectifying direction (WMo - positrons incident on W side) and in opposite direction (MoW - positrons incident on Mo side). Also shown is transmission data for a 100 nm W foil. The insert illustrates the potentials involved as experienced by positrons. (b) Calculated transmission using the model and Makhovian profile parameters described in this text for the three cases shown in fig.2(a) (solid lines). Also shown are calculated transmissions for the WMo case using the same model and profile parameters but with no internal potential barrier ($\Delta E=0$) as well as calculations for the WMo case using a standard Makhovian implantation profile (Makhov) and a Makhovian profile using the parameters derived by Chen et al.[11] (Chen).

was situated at a distance of 45 mm from the center of the foils. This detector was used to obtain Doppler broadened lineshape spectra of the foils to study the quality of the interface. It was also used in conjunction with the grids to obtain surface branching ratios for the foils using the method described in chapter 2.

5.3. Results and discussion

5.3.1. The first series of experiments

The results of the measurements of low-energy positron transmission for the W on Mo foil (WMo) are shown in Fig.5.2a. Also shown in Fig.5.2a is the result of a measurement with the same layered foil turned around 180° (MoW). Thus the positrons in this case impinge on the Mo side of the foil and the transmission out through the W layer is measured. The data show a striking difference between these two measurements with about a factor of 10 difference between the maximum yield in the two cases. The result of the measurement from the MoW setup is consistent with emission of only those positrons which after implantation have thermalized in the 10 nm W layer. This clearly demonstrates the rectifying effect of the potential barrier at the W-Mo interface. For comparison, Fig.5.2a also shows the results obtained for a W foil.

In order to model the experimental transmission data calculations using the VEPFIT modelling and fitting program were performed. The model employed was, in forward mode (WMo), a sandwich of 5 layers:

1)   10 nm W

2)   A 1 nm thin layer with an electric field pointing towards the Mo.

3)   100 nm Mo

4)   3 nm absorbing layer to calculate arrival of reemitted positrons.

5)   Vacuum

In backward mode (MoW) layers 1, 2 and 3 appeared in the opposite order. The yield was found by counting the fraction of positrons that arrived by diffusion into layer 4. For the W layer and the interface layer positron diffusion lengths significantly larger than the layer thickness were used.

The calculation showed little sensitivity to the exact values of these two parameters provided they were larger than the layer widths. For the Mo layer a diffusion length of about half the layer width was used. The values used for the positron diffusion length in the calculation were 80 nm, 15 nm and 147 nm for the W layer, the interface and the Mo layer, respectively. The obtained calculated values (full drawn lines in Fig. 5.2b) are in good qualitative agreement with the experimental data. The difference in the absolute fraction between the calculation and the experiment is due to the assumption of a surface penetration probability of unity as well as a branching ratio into free positrons at the surface of unity used in the calculation. This approximation, used only to simplify calculations, is clearly in error.

Traditionally, a Makhovian implantation profile of the form

$$P(z) = \frac{m z^{m-1}}{z_0^m} \exp\left[-(z/z_0)^m\right] \tag{5.3}$$

has been used to model experimental data. Here m is a shape parameter, usually taken to be 2 for beam implantation experiments, and $z_0 = <z>/\Gamma[(1/m)+1]$, where Γ is the gamma function and $<z>$ is the mean positron implantation depth given by $<z> = (\alpha/\rho) E^n$, where ρ is the density in g/cm^3 and E is the positron energy in keV. The parameters α and n are fitting parameters that are assumed to be material independent with standard values of $n = 1.62$ and $\alpha = 3.6$ µg cm^{-2} keV^{-n} (Vehanen *et al.* 1987). The profile obtained using these parameters proved to be a poor fit to our transmission data, as it has been for a number of thin film positron transmission measurements (see e.g. Chen *et al.* 1985, Poulsen *et al.* 1991). The standard parameters yield a transmission curve with the maximum yield at about twice the positron energy of the experimental maximum yield. A possible reason for this could be that positrons during slow-down in a semi-infinite solid also can be scattered back from a deeper layer and this is not the case for thin foils. A similar problem arises when working with very thin overlayers and these inadequacies of the standard implantation profiles have led to a number of theoretical studies and Monte Carlo simulations (Ghosh *et al.* 1995, Jensen *et al.* 1990). However, some of the earlier works on thin foils have attempted to fit their data with Makhovian profiles with a shape parameter m other than the standard value of 2 and values of n and α other than the standard values (Chen *et al.* 1985, Poulsen *et al.* 1991). In the case of Poulsen *et al.* an attempt was also made to model the data

using a Monte Carlo calculation but with limited success (Poulsen *et al.* 1992). We attempted to fit our data using a Makhovian profile and found good agreement between model and data with the parameters $m = 2$, $n = 1.5$ and $\alpha = 11$ μg cm^{-2} keV^{-n}. Note that this is a profile with the same shape as the standard Makhov profile but with a deeper mean implantation depth. It is this profile that has been used in the calculations shown in Fig.5.2b. Figure 5.2b also shows the results of the modelling if a standard Makhov profile or a Makhov profile using the parameters quoted by Chen *et al.* (1985) is used instead of our fitted profile.

The adopted Makhovian parameters thus lend additional credence to the fact that traditional Makhovian profiles with $m = 2$, $n = 1.6$ and $\alpha = 3.6$ fail completely to give a reasonable approximation to positron implantation in thin films. We also attempted to fit the data using a Katz-Penfold function to calculate the mean implantation depth using the method and values for the fitting parameters described by Aers *et al.* (1995) but this proved to be only slightly
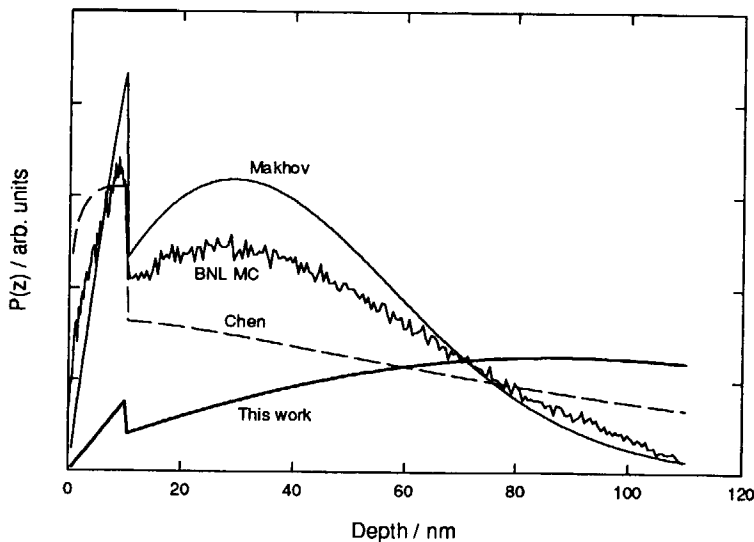
Fig.5.3. Calculated implantation profiles for a 5 keV positron beam incident on WMo, i.e. 10 nm W on 100 nm Mo. See text for details. At an incident positron energy of 5 keV the measured transmission yield through the rectifier foil has decreased from its maximum (see fig. 2) due to an increased number of positrons passing through the foil before they are thermalized as observed by the high energy transmission.

better than a standard Makhovian. Finally, we calculated the implantation profile using the BNL Monte Carlo code (Ghosh *et al.* 1995), which takes the finite thickness of the foil into account, but this attempt also failed to reproduce the experimental data. Fig. 5.3 shows some of the different calculated implantation profiles for a positron energy of 5 keV. The discontinuity at a depth of 10 nm is caused by the difference in density between W and Mo. Note the strikingly large difference between the different implantation profiles, even though they are all calculated for the same implantation energy. Monte Carlo calculations using the BNL code were also performed for a much thicker Mo layer to observe any effect of the foil thickness, i.e. that it was not semi-infinite, but this also yielded no significant improvement. It is interesting to note that the implantation profile parameters used to fit data for transmission through thin foils always lead to much higher mean implantation depth than either the standard Makhov profile, a Katz-Penfold profile or the results of a BNL Monte Carlo calculation, with the latter performed for a thin foil. The difference between our fitted profile and the standard Makhov profile is thus exclusively in the mean implantation depth.

The higher transmission fractions for the calculated data shown in Fig. 5.2(b) compared to the experimental data shown in Fig. 5.2(a) are ascribed to the assumptions concerning the branching ratios used in the calculation. Thus realistic branching ratios for free positron emission have to be introduced. However, since surface branching ratios are for thermalized positrons arriving at the surface, they should not vary with implantation energy and should thus not influence the shape of the calculated transmission curves but merely lead to a scaling in the yield. The surface branching ratios will be dependent on the surface conditions and can lead to different scaling factors for the different foils. Since the W-Mo foil was attached to the frame on the W side and the frame was grounded, the alignment of electron Fermi levels will lead to a shift in the potentials experienced by the positrons at the Mo surface as indicated in the insert in Fig. 5.2(a).

In addition to the transmission experiments, measurements were performed to determine the surface branching ratios for the transmission side of the rectifier foil. The measurements, following the method described in chapter 2, involve observing the change in the annihilation peak count rate and the amount of positronium formed at the surface while applying plus or minus 15 V to a grid situated some distance from the surface being studied. This allows a determination of the ratios of thermalised positrons reaching the surface being emitted as low energy positrons, as positronium or being trapped in the surface potential well. Since the Ge detector did not

preferentially view either of the two sides of the foil, an energy range of 1 - 4 keV for the primary positron beam was chosen, which corresponds with the energy range with the highest transmission of low energy positrons. Furthermore, we relied on the fact that hardly any positrons were emitted from the front side of the rectifier foil at those incident energies. A branching ratio of 22 % to free positrons is found, though a measurement following an accidental contamination of the Mo surface showed a branching ratio of only 10 %, indicating the dependence of the transmission yield on the specific surface conditions. The shift in the positron potential at the Mo surface mentioned earlier would not influence the surface branching ratio measurements since it may be considered small compared to the 15 V applied to the grid.

To further study the quality of the interface between the two layers, a positron annihilation Doppler Broadening measurement was performed on the foils . The method is highly sensitive to vacancy type defects and should thus reveal whether any such defects were present at the
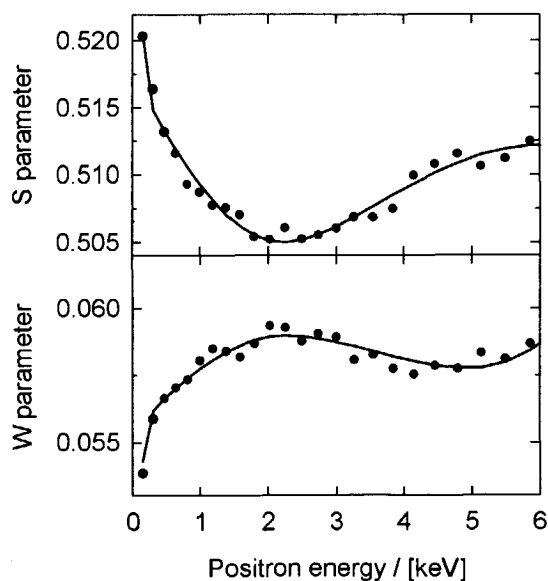
Fig.5.4. Doppler broadening measurement showing the lineshape parameters S, corresponding to annihilation with valence electrons, and W, corresponding to annihilation with core electrons, as a function of incident positron energy. The drawn lines are results of fits using the VEPFIT program.
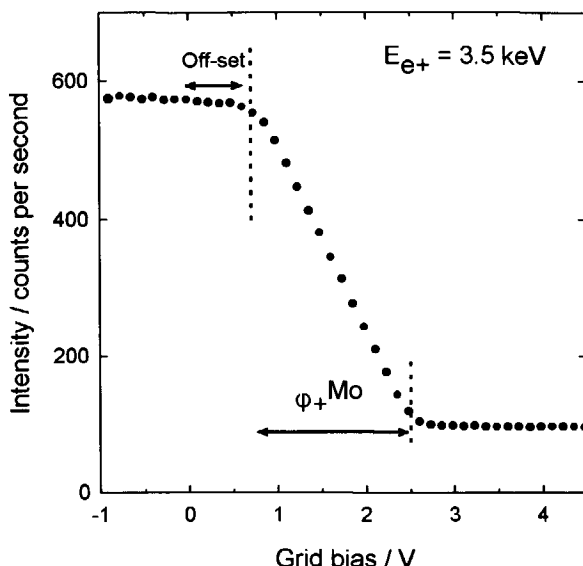
Fig.5.5. Retarding field measurement of positrons being emitted from the transmission (Mo) side of the rectifying foil. The upper dotted line indicates the off-set described in the text and the gridbias difference between the two dotted lines corresponds with the Mo positron workfunction , $\phi_{Mo}^{+} = 1.7$ eV.

interface. The measurement (Fig. 5.4) shows no evidence of a vacancy defect layer at the interface and thus confirms the excellent interface match between the two materials. The interface, which should be most visible at around 2.5 keV, should show an increase in S-parameter value and a decrease in W if vacancies above the level of a few ppm were present. The match between the two layers is therefore concluded to be very good and a crucial contributing factor in making the potential barrier a good positron rectifier.

Finally a retarding field measurement of the reemitted positrons on the transmission side was performed using the grid between the sample and the micro-channel-plate. The result is shown in Fig.5.5 and this clearly shows the off-set due to the shift in the positron potential at the surface of Mo as well as the Mo positron workfunction, $\phi_{Mo}^{+} = 1.7$ eV. It should be noted that the off-set cannot be explained by the difference in electron workfunctions between the Mo and the material of the grid, in this case Cu, since that only gives a shift of 0.06 eV.

We would like to point out that the fraction of transmitted low energy positrons of 17 % we measured should not be seen as an absolute maximum. Most likely surface conditions can be

improved. The only treatment we could give the foils in these experiments was the pre-measurement annealing at 1200 °C. It is expected that a yield of 40 % can be achieved by improving the surface. However, annealing of multilayer foils such as these is not as straightforward as for single layer foils since high temperatures will lead to interdiffusion in layered foils. As a rule of thumb such systems should not be heated to temperatures higher than half the melting temperature of the material with the lowest melting point. In our case that material is Mo, which also constitutes the surface that needs cleaning.

5.3.2. The second series of experiments

Figure 5.6 shows the result of the measurements on the Re-W foil. There is no indication of a rectifying effect in the results. This can be seen from the fact that the two directions give a transmission yield that has the same shape as a function of incident energy. The change should have been especially visible for low incident energies, as can be seen in Fig. 5.2. The implantation profile should vary very little for the two directions in this case since Re has a density of 21 g/cm^3, which is much closer to the value for W (19.3 g/cm^3) than Mo was (10.2 g/cm^3). The close similarity of the two transmission profiles also leads to the conclusion that the trapping rate for
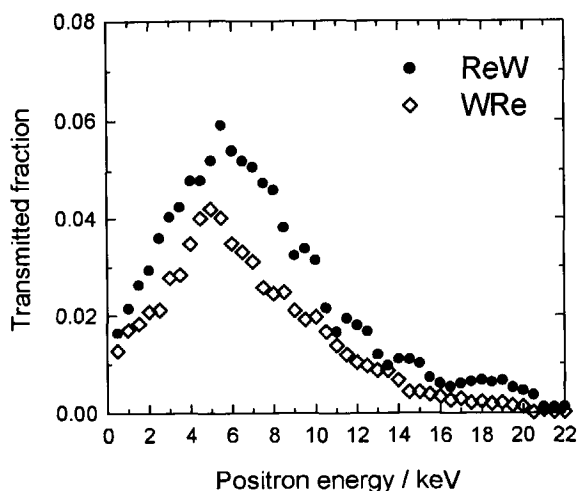
Fig. 5.6. Results of the measurement of low energy positron transmission through a foil consisting of 10 nm Re grown on 100 nm W(110). The forward direction (ReW) refers to the orientation of the foil where the positrons enter at the Re side and exit at the W side.

traps at the interface between the layers cannot be very big. Otherwise much less transmission should have been seen for the WRe direction, where the interface is close to the emitting surface, compared to the forward direction. The difference in transmission ratios for the two directions can be explained by surface conditions. Thus different branching ratios should be expected for the two surfaces. It was expected that either a rectifying effect would be observed or the foil would show signs of interface trapping. That neither is seen in our experiments is not well understood. However, there are several possible explanations. The values for the positron workfunction and affinity for Re, on which we based our choice of this material, is purely theoretical. No experimental data exists for Re. Error in these values could obviously explain the lack of a rectifying effect. Another possible explanation is the large mismatch between the two materials caused by the different crystal structure. The thin overlayer of Re may be poly-crystaline because of this mismatch. This might lead to defects along the grain boundaries, but there could be additional defects caused by strain relaxation. This should, however, be observable from the defect trapping it would cause and has not been observed.

The measurements on the thick WMo sample are shown in Fig. 5.7(a). In Fig. 5.7(b) the results of model calculations using the model described earlier are shown. Here the model was modified to make the Mo layer 1000 nm thick. A Doppler broadening measurement was also made of this sample. From this measurement a diffusion length of 70 nm in the Mo was derived. This value was used in the modeling of the transmission data. The calculation was performed using a standard Makhovian profile and using the Makhovian with a deeper implantation profile found from fitting the data in the earlier measurements. It should be noted that the bumps in the experimental data (Fig. (5.7(a)) are probably an artifact of the experiment. Because the center hole in the carrier foils was smaller than the beam diameter, the count rate through the dummy sample is sensitive to the exact positioning of that sample. This was especially true for higher incident energies as the beam would precess ('spiral') increasingly more in the guiding magnetic field with higher energies. For the thin foils this was a minor problem as the 'spiraling' was only seen above about 10 keV. Also the thin foils could be positioned very precisely by monitoring the count rate at a number of set incident energies. For the thick foil this was not possible and the only way of verifying the position was by using a vernier caliper. The raw data before dividing by the count rate through the dummy sample showed no bump halfway up and leveled off for the highest energies.
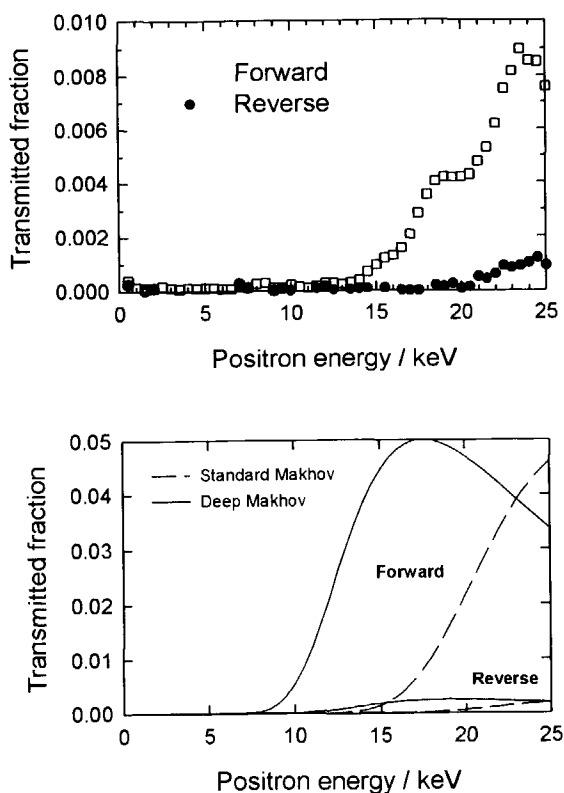
Fig. 5.7. (a) The experimental results of low energy positron transmission through a thick sample of WMo consisting of 10 nm W(100) grown on 1000 nm Mo(100). The forward direction refers to the orientation of the foil where the positrons enter at the W side and exit at the Mo side of the foil. (b) Calculated transmission for the two cases shown in (a) using the model described in the text. The standard Makhov refers to a Makhovian implantation profile with standard parameters and deep Makhov refers to a Makhovian profile with the parameters derived from the earlier measurements on thin WMo foils.

As can be seen from Fig. 5.7(b), the standard Makhovian fits the data far better in this case. However, the data lie somewhere between the two calculations, but closer to the standard Makhovian. This again illustrates that the problem with the Makhovian implantation profile is only for thin foils and thin overlayers. For thick layers such as this the problem is much less severe. One possible explanation why the problem is only seen for such thin layers is the assumption implicit in the Makhovian profile and also in the Monte Carlo calculations performed to model positron implantation in solids (Ghosh *et al.* 1995, Jensen *et al.* 1990). In these calculations the

solid is assumed to be amorphous. Crystalline materials could have channeling effects even at low energies. It need not be channeling in the standard sense, but more a sort channeling-dechanneling effect where the positrons travel some distance in the channel before being scattered out of the channel. It could perhaps even scatter back to the channel. At these low energies the opening angle for entering the channels should be larger than for traditional channeling. One should perhaps more think of it as a partial channeling that simply guide some of the positrons to larger depths than they would have been able to achieve in an amorphous solid. At large depth, these effects are less dominant and treating the solid as an amorphus structure becomes a good approximation. It should be clear from this that Monte Carlo simulations that take the crystal structure of the solid into account would be very useful.

The thin WMo foils and the W foil measured before heating confirmed our earlier results. The heating was performed by passing a current through the foil for 10 min. with a 10 min. cooling time. After each heating step a transmission measurement for incident energies from 0.5 to 10 keV was performed. Fig. 5.8 shows the count rate as a function of the current passed through the foil, measured for a 3.5 keV incident positron beam. The countrate is for low energy positrons. For these currents no glowing of the foil was observed, indicating that the foil did not
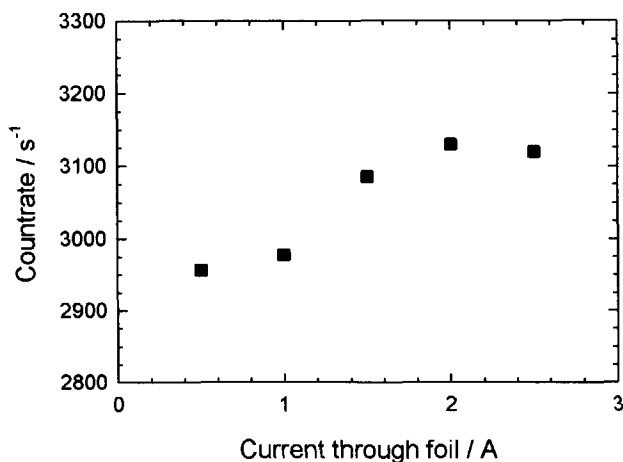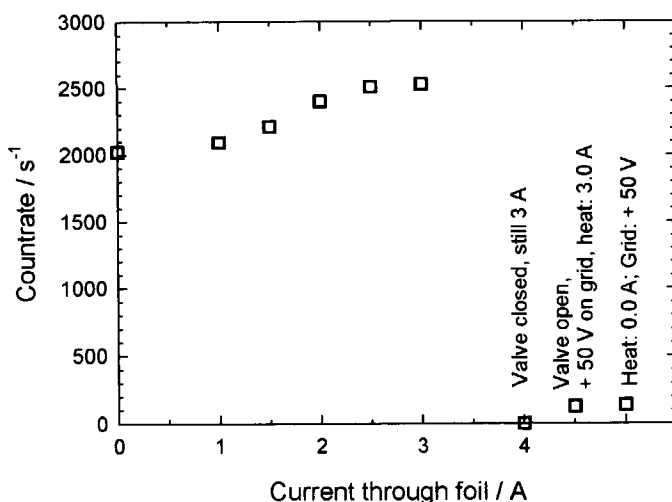

Fig. 5.8. The count rate through a 10 nm W(100) on 100 nm Mo(100) foil as a function of heating current for an incident positron energy of 3.5 keV measured ten minutes after the current was turned off.

become hotter than a few hundred degrees Celsius. The increase observed in Fig. 5.8 is thus most likely due to desorption of water from the surface of the sample. The count rate after heating to 2.5 A corresponds to a transmitted fraction of 0.22 at 3.5 keV incident energy, up from the 0.18 measured without heating in the first series.

After the measurements shown in Fig. 5.8 the sample was raised about 5 cm so that it was visible from the outside via a viewport. Current was again passed through the sample while it was monitored using a pyrometer. At about 4 A the carrier foil would begin to glow, but at no point was the thin foil itself observed to glow. At about 5 A the contacts on the wires leading to the foils began to heat up and the carrier foils would stop glowing. This also led to contamination of the foil and a subsequent lower countrate.

As a method for cleaning the foils the resistive heating did not live up to our expectations. We had expected the thin rectifier foils to conduct the current just as well as the carrier foil. The fact that only the carrier foil glowed while passing current through the foils must be due to poor electical contact between the two types of foils. Perhaps it would work better if the only connection between the two electrodes was through the rectifier foil. However, the installation of the foils would be much more difficult if the thin foils were not supported. Another idea that might be tried is to cut off the side support of the carrier foils after mounting. Unfortunately this would also cut off some of the rectifier foil, causing it to break even easier. Another obvious means of cleaning the foils (primarily the Mo side, since as emitting surface that is the most sensitive to impurities) would be heating by electron bombardment. However, this could not be used in the actual remoderations stage, since there simply isn't enough room. We therefore did not attempt this though it might be worth trying just to observe the cleaning effect it has on the foils. A disadvantage of electron irradiation is the poor control. The rectifier foils are only 110 nm thick in total and one could very easily burn a hole through them by accident. Further work is needed for these foils to reach their full potential.

While doing the heating for the measurements described above the Channeltron was left on a couple of times. An increased countrate during heating was observed. It was therefore decided to do a series of measurements with the sample at elevated temperatures. The result of these measurements is shown in Fig. 5.9 for a 3.5 keV incident positron beam. Passing large currents through the sample which was placed at a distance of about 3 cm from the detector could seriously influence the measurements. The Helmholtz coils guiding the beam in this region had

a current of about 10 A running through them. Fortunately the region on either side of the hole at the center of the carrier foils were about the same size and the resulting magnetic fields should cancel each other out. However, at larger distances there could still be serious effects. The heating of the foils could also liberate ions from the foils. These would also be observed by the detector. Therefore to validate the results three additional measurements were performed (last three points in fig. 5.9). In one of these test experiments the heating was left on at the maximum and the pneumatic valve in the beamline was closed. This shuts off the positron beam and the experiment confirmed that what was detected earlier was positrons and not ions (the front of the detector was kept at -2 kV, so it could not be electrons). After reopening the valve a bias of + 50 V was applied to the retarder grid confirming that the observed extra positrons were low energy positrons. Finally the heat was turned off while the bias on the retarder was retained. This showed that the heating did not cause extra high energy counts. Also the detector was shown to still function with the same efficiency as before and had thus not been damaged by the heat. The conclusion must therefore be that we have observed thermally desorbed free positrons from the surface potential. This is the first time that such desorption has been observed. Generally thermal activation of positronium is a more energetically favorable process. To see how free positron

Fig. 5.9. The count rate through a 10 nm W(100) on 100 nm Mo(100) foil as a function of heating current for an incident positron energy of 3.5 keV measured while the current was on. Also shown is three test experiments. See text for more details.

activation might be possible it is useful to look at the energetics of thermal positron and positronium emission. For thermal activation of positronium the following energy relation holds:

$$E_a = E_b + \phi_- - 6.8\, eV \qquad\qquad (5.4)$$

where E_a is the activation energy for positronium, E_b is the binding energy of the positron to the surface potential well, ϕ_- is the electron workfunction for the material and 6.8 eV is the binding energy of positronium. If $E_a > E_b \approx$ 0-0.3 eV thermal emission of positrons could occur. This is not the case for a clean Mo surface where emission of thermally activated positronium has been observed. However, in our case the surface is probably contaminated. The base pressure in the vacuum chamber was 1×10^{-8} Torr. With a sticking coefficient of one this should lead to a monolayer of dirt building every 10 sec. and while the heating probably gets rid of the water, there is most likely still contaminant on the surface. The presence of such contaminants on the surface will affect the energetics of the surface. Thus an increase in the electron workfunction for the surface, combined with a lowering of the binding energy for positron to the surface potential well could make thermal activation of free positrons possible. That the observed increase was not simply due to a cleaning of the surface could be seen by the fact that the count rate dropped immediately when the current was turned off. A recontamination of the surface would be expected to take longer. It is interesting to note that the after-heating measurements in Fig. 5.8 resulted in an increase in countrate of only about 10 % while the thermal activation process showed an increase in countrate of 25 % for the same temperatures (currents). A more in-depth investigation of this thermal activation effect would be useful and might provide new insights into the details of the surface potential and how it can be influenced by adsorbates.

5.3.3. The POSH experiment

A 10 nm W(100) on 100 nm Mo(100) was installed in the POSH beamline (see chapter 7) during the test experiment run in September 1997. The purpose was to test the WMo foil as the first remoderation foil under realistic conditions. In this experiment the sample was kept at +50 V and a grid after the foil was switched between + 100 V and - 100 V. The count rate was monitored by a Ge γ-counter with a grid in front of it kept at - 1 kV. Fig. 5.10(a) shows the count
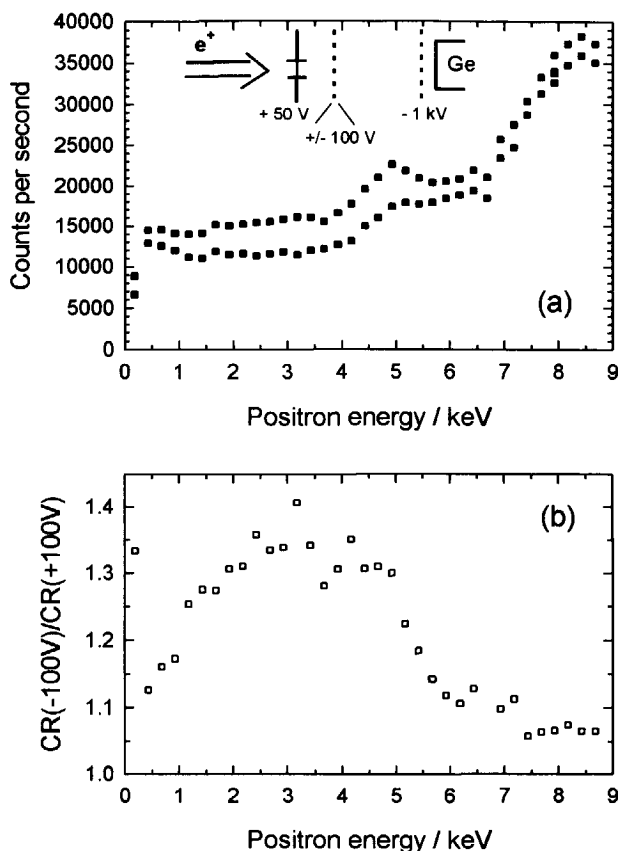
Fig.5.10. Results of POSH measurements on a WMo foil (10 nm/100 nm). (a) The count rate with + 100 V and - 100 V on the retarding grid as a function of incident positron energy. Insert shows a schematic of the experimental setup. (b) The ratio between the count rate with - 100 V on the retarding grid (full beam) and + 100 V on grid (only high energy positrons). This ratio is a measure of the low energy transmission.

rate as a function of incident positron energy for + and - 100 V on the grid. Also shown in Fig. 5.10(a) is a schematic of the experimental setup. Note the large background in the data caused by the detector-grid-sample configuration. Fig. 5.10(b) shows the ratio between the countrates with - 100 V and + 100 V on the grid as a function of incident energy. This is a measure of the transmitted fraction. Note how the shape is similar to that of Fig. 5.2.

A retarding field experiment was also performed on this foil. The result of this measurement is shown in Fig. 5.11. Note how the data is in agreement with the positron
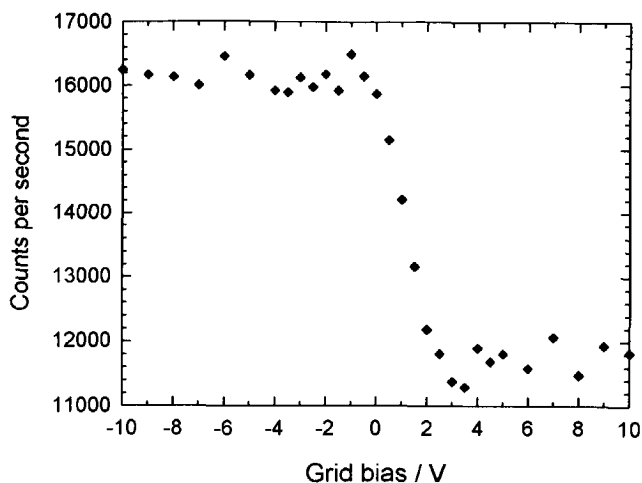
Fig. 5.11. POSH beam retarding field measurement.

workfunction for Mo of 1.7 eV. However, again the scattering in the data is rather large due to

the large background.

5.4. Conclusion and final remarks

We have measured the positron transmission through a layered foil consisting of an epitaxially grown 10 nm W (100) layer on top of 100 nm Mo (100). A rectifying effect, caused by the difference in positron affinity between these two well matched materials, is observed. This effect is observed as a marked increase in transmission yield, making such foils ideal for positron remoderation purposes. Transmission through a layered foil of 10 nm Re on 100 nm W(110) did not exhibit any rectifying effect. The results showed large discrepancies for the positron implantation profiles for thin films and overlayers but better agreement for thicker layers. Heating up to a few hundred degrees Celsius resulted in an increase of about 10 % in the transmitted fraction. Observations consistent with thermal activation of free positrons from a contaminated Mo surface were made. This effect led to an increase of about 25 % in the transmission yield.

Further experiments to characterize the surface and study the effects of different surface conditions on the transmission yield would be useful. The first measurements using a W-Mo foil as remoderation foil for POSH beamline were presented. The results of these experiments were consistent with the earlier results from the VEP beamline.

An additional effect that will help to improve the overall transmission efficiency of moderated positrons for layered foils compared to backwards remoderation is that most of the backscattered positrons will be returned to the foil by the electric field configuration used to focus the positrons onto the foil in an electrostatic transmission remoderation set-up. Thus, transmission remoderation using rectifying foils might prove to be superior to remoderation in backward geometries. For practical purposes foils thicker than ours may be preferable since optically it is easier to get a small spot size using a 5 keV beam than using a 3 keV beam. Such thicker foils, however, might have a detrimental influence on the overall transmission efficiency.

CHAPTER 6

VERY LOW ENERGY
POSITRON REFLECTION

6.1. Introduction

When positrons encounter a metal-vacuum interface part of the positrons may undergo reflection and be repelled away from the interface. The quantum mechanical reflection of positrons approaching the surface of a metal from within the solid is caused by the rapidly changing potentials near the surface and has been the subject of numerous studies and experiments (Nieminen and Oliva 1980, Lynn *et al.* 1981, Schultz and Lynn 1982, Brown *et al.* 1986, Fischer *et al.* 1986, Britton *et al.* 1989, Jacobsen and Lynn 1996). Most of these studies have dealt with the positron emission yield as a function of temperature since this type of reflection increases with lower temperature. The aim of these studies was to get a better understanding of the details of the surface potential as well as to investigate the possibilities of making brighter monoenergetic positron beams by reducing the thermal component of energy and angular spread of the positrons.

Most metals, and particularly those of interest as moderator materials, exhibit a negative positron workfunction, ϕ_+ (Schultz and Lynn 1988). Those positrons that approach such surfaces from the bulk side and are not quantum mechanically reflected will be emitted from the surface

with a perpendicular velocity corresponding to a kinetic energy of -ϕ_+ and thermal velocities parallel to the surface. Since the absolute value of the workfunction for many materials is several orders of magnitude larger than the thermal energy of a few tens of meV, the positrons are essentially emitted perpendicular to the surface of the metal. This forms the basis of most moderator systems. However, when positrons approach the surface of such negative workfunction materials from the vacuum side with an energy smaller than the absolute value of the positron workfunction for the material, a reflection off the surface potential might occur, as depicted in Fig.6.1. However, as the positron encounters the surface potential well it may get trapped there and eventually annihilate there. A fast annihilation event from a pick-off process might also occur if the positron wavefunction overlaps momentarily with the that of one of the electrons making up the surface dipole. Finally the positron may bind to an electron and form positronium.

Very little research has been done to investigate this phenomenon. This is mostly due to the difficulty in producing a good positron beam with these very low energies. Wilson (1983) using a low energy incident beam and slowly raising the bias on his samples of W(111), Cr(100) and Al(100) measured the emission and possible reflection of slow positrons but found no evidence of elastic reflection of very low energy incident positrons.
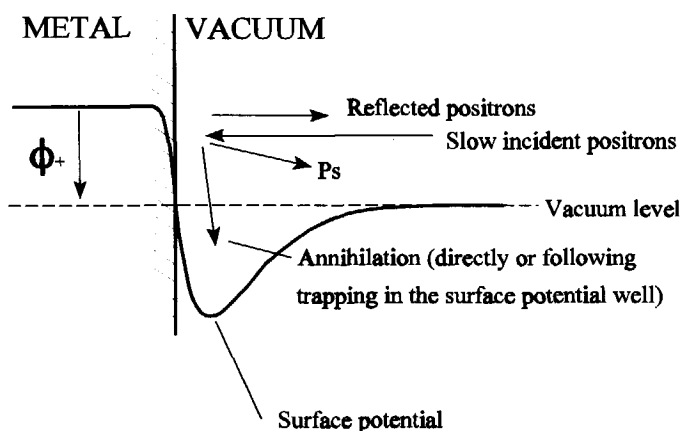
Fig.6.1. Potential energy diagram for slow positrons approaching a metallic surface. Also shown are the branching options open to such positrons.

Walker *et al.* (1992) in a series of calculations of positron surface sticking rates, i.e. trapping at the surface potential well, found for Al(100) that the probability for trapping at the surface as a function of incident positron energy peaked around the workfunction energy at a value for Al(100) of about 0.25 eV. Such relatively large trapping rates would obviously be a strong competing channel to reflection and limit the maximum attainable reflection probability.

Our interest in very low energy positron reflection from surfaces was stirred by some unexpected results from test experiments on the reactor based positron beamline, POSH, currently under construction at our institute (van Veen *et al.* 1997). The tests included studying the voltage needed to extract workfunction positrons emitted from the inside surface of tungsten foil cylinders. The tungsten foils were 7 µm thick and placed inside copper cylinders of length 12 mm and a diameter of 9.5 mm. Grids were placed at the end of the cylinders and bias was applied to these grids to extract the positrons from inside the cylinders. On the basis of simulations it was expected that an extraction bias of at least 30 V would be needed to get any significant amount of positrons out. However, even with no bias applied to the grids, copious amounts of slow positrons emerged from the cylinders. With a grid potential of 0 V about 60% of the eventual total positron yield was observed. Furthermore, retarding field measurements showed that a grid bias of +2.5 V was needed to stop these positrons. Further simulations indicated that these results could only be explained by low energy positrons being reflected by the opposite cylinder wall with a reflection coefficient in excess of 0.5. The experiments presented here were done to study this phenomenon of low energy positron reflection in more detail.

6.2. Experimental

The experiments were performed using the variable energy positron beamline (VEP) at Delft. This magnetically guided beamline delivers 2×10^4 positrons per second in a 7 mm spot (see chapter 2). The energy of the positrons is tunable in the range from 0 to 30 keV with an energy resolution of 1.7 eV FWHM. A grid placed 1.15 m in front of the sample was used to either remove low energy positrons from the sample region or return them to the sample. The experiments fell in two parts, both of which used a sample consisting of a 7 µm thick tungsten foil similar to the ones used for the POSH. The foil was baked to 1250 °C in a separate vacuum vessel

for several hours prior to installation in the UHV sample chamber. This mimicked the procedure for the foils used in the POSH setup. We did not have any means of monitoring the suface conditions of the sample after installation.

<u>1 keV incident energy experiment:</u>   The first set of experiments attempted to study the build-up of the count-rate when re-emitted positrons were sent back to the sample again. The idea was that the build-up would take infinitely long time when the reflection is unity and very short time for zero reflection. The large distance to the grid was intended to make any reflection more easily discernable. In this first experiment a 1 keV positron beam was directed at the sample. The energy was chosen to maximize the number of re-emitted thermalized positrons as opposed to
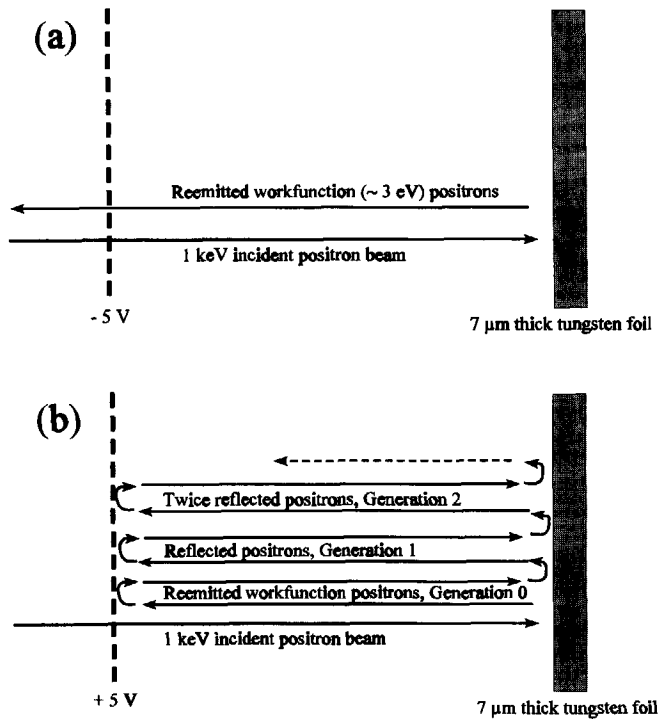
Fig.6.2. Schematic of the experiment for 1 keV incident energy positrons with a bias on the grid in front of the sample of (a) - 5 V and (b) + 5 V, respectively.

epithermals, i.e. positrons emitted before thermalization, typically with energies up to about 10 eV. The grid was switched between + 5 V and - 5 V. The positrons, being re-emitted with workfunction energy, could then either be returned to the sample by applying + 5 V to the grid (Fig.6.2.(b)) or dumped away from view of the detector by applying - 5 V (see Fig.6.2.(a)). The aim of the experiment was then to study the time evolution of the count-rate as the grid was switched from -5 V to +5 V over a period of tens of microseconds.

A Philips PM 5134 Function Generator (FG) was used to generate a duty-cycle-skewed
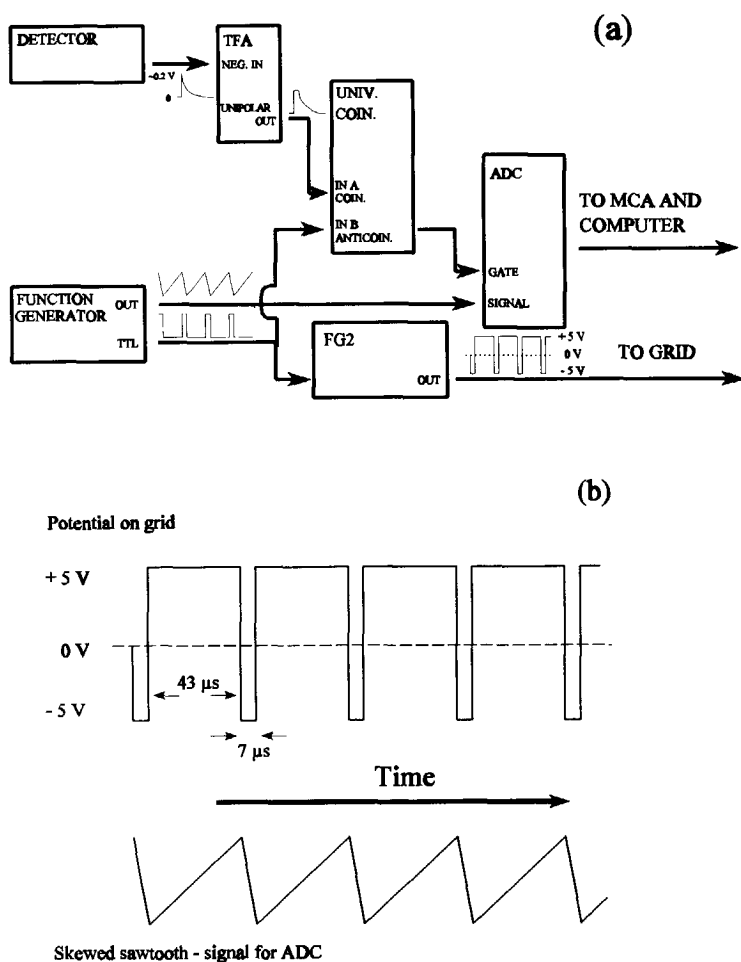
Fig.6.3. (a) Schematic of the electronic setup for the 1 keV incident energy experiment. (b) Detail of the time structure of the signals to the grid and computer.

saw-tooth signal as a time ramp. The FG was set to a frequency of 20 kHz (= 50 µs total duration of one cycle) and the duty cycle set so that the positive slope part of the saw-tooth signal had a duration of 43 µs and the negative slope part a duration of 7 µs. The TTL sync. output of the function generator was used to both switch the grid and provide a coincidence signal. The signal from the ORTEC Germanium γ-counter was fed into an ORTEC 454 Timing Filter Amplifier (TFA). The signal from the TFA was sent directly to an ORTEC 418A Universal Coincidence Unit where it was set to be in anticoincidence with the TTL signal from the FG (See Fig.6.3.(a)). The coincidence unit needs a signal of more than +2 V for at least 50 ns to trigger. The output of the coincidence unit was used as a gate in the ADC with the saw-tooth signal from the FG as the ADC signal. Since the TTL signal from the FG was only 2.8 V, it could not feed the grid directly. Instead it was used to trigger a second function generator (FG2) which sent a rectangular signal of ± 5 V to the grid. Fig.6.3.(b) shows the time structure of the bias to the grid and the skewed saw-tooth signal in more detail. Data was accumulated when the bias was positive. An annihilation event in the gamma counter was used as a gate in the ADC if it happened while the grid was positive. This gate would trigger the ADC to record the pulse-height of the saw- tooth signal at that time. This height corresponded to the time elapsed since the grid was switched positive.

Each series of measurements consisted of four experiments : (1) The actual coincidence measurement, (2) a measurement with +5 V static on the grid, (3) with -5 V static on the grid, and (4) a measurement where the polarity of the signal to the grid was switched. The polarity switched measurement worked as a kind of anticoincidence measurement where only counts accumulated when the grid bias was negative, were collected. Only the bias on the grid was changed between each of the above measurements. All the settings of the electronics stayed the same.

20 eV incident energy experiment: The other set of experiments was done with a primary positron energy of 20 eV and switching the grid between -5 V and +25 V (Fig.6.4). This was done to try to avoid the large background due to the primary positron beam. In this case we would thus try to observe the decrease in the number of annihilation events in the field of view of the detector as a function of time over a period of tens of µs. The grid bias was supplied by setting the second function generator (FG2) to its maximum output of ± 15 V, giving it a DC offset of +1 V (maximum offset was ± 5 V) and adding a 9 V battery.
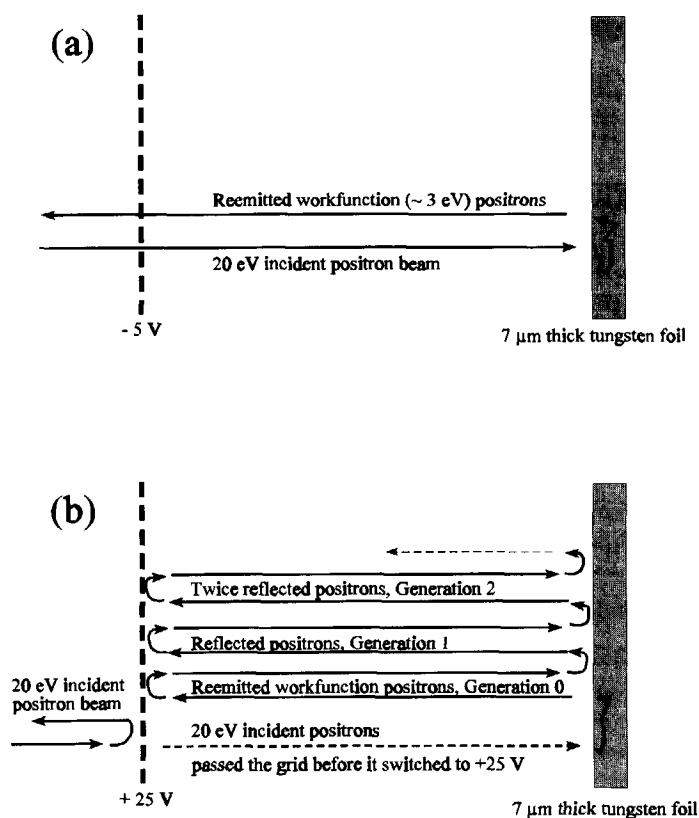
Fig.6.4. Schematic of the experiment for 20 eV incident energy positrons with a bias on the grid in front of the sample of (a) - 5 V and (b) + 25 V, respectively.

6.3. Results and discussion

The results of the 1 keV incident positron energy experiment are shown in Fig.6.5. The background obtained by having -5 V static on the grid has been subtracted from the data. Shown in Fig.6.5 is also the result of a fit to the data using the function
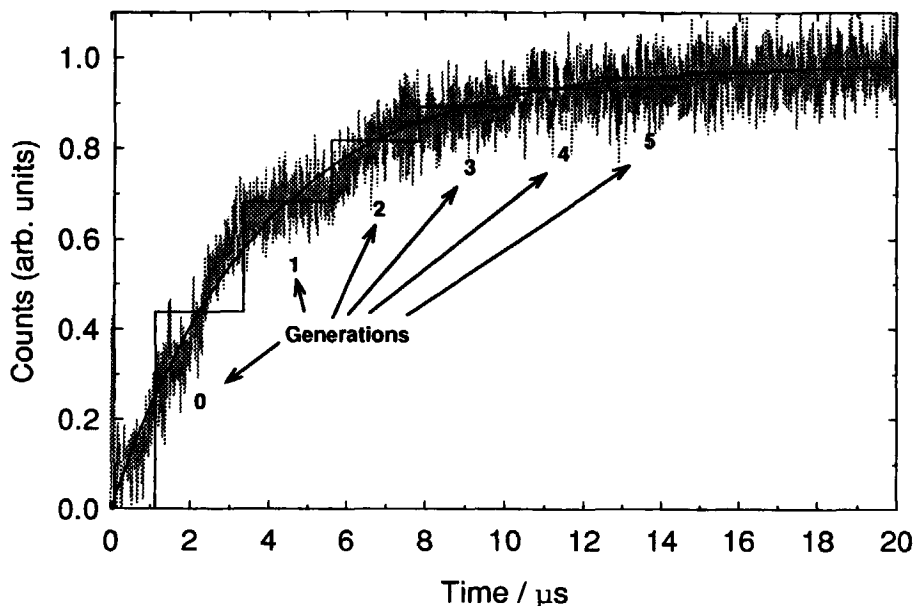
Fig.6.5. Time of annihilation for re-emitted positrons after activating a potential barrier (+ 5 V) at a distance of 1.15 m from the target. The incident energy of the primary positron beam was 1 keV giving rise to a continuous background (zero level). The smooth line through the data is the fit to the data. The step function line is for the ideal case of 2.5 eV mono-energetically emitted positrons with no energy loss during reflection.

$$f(t) = 1 - \exp\left(\frac{\ln(R)}{2\,\tau}\,t\right) \tag{6.1}$$

where R is the reflection coefficient and τ is the characteristic time of the system, indicating the average time of flight for a re-emitted/reflected positron to travel the distance from the grid to the sample. A round trip would thus take 2τ. The best fit was obtained for a reflection coefficient, $R = 0.55$ (± 0.05) and $\tau = 1.2$ μs. The value for τ thus corresponds to an average kinetic energy of the re-emitted positrons of about 2.5 eV travelling over a distance of 1.15 m. If one assumes that all re-emitted positrons have an energy of exactly 2.5 eV and no energy spread occurs, the expected result for R=0.55 and τ=1.2 μs would be the step-function also shown in Fig.6.5, where
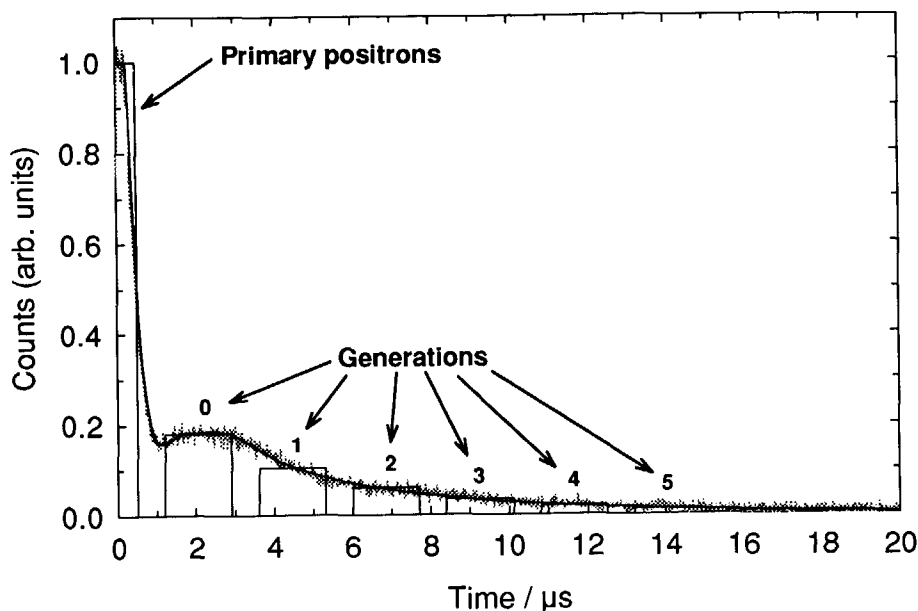
Fig.6.6. Time of annihilation when using an incident energy for the primary positrons of 20 eV and a potential barrier of + 25 V. Now the primary beam is also cut off by the barrier but can still be seen for very small times. The smooth line through the data is the fit to the data (see text for details). The step function line is for the ideal case of 2.5 eV mono-energetically emitted positrons with no energy loss during reflection. The insert shows the same data on a log. scale.

each step indicates a different 'generation'of reflected positrons (see Fig.6.2).

The result of the 20 eV incident positron energy experiment is shown in Fig.6.6. Again the data were fitted with exponentials in the different time regions and the best fit to the reflection time region (above about 3 µs, see below) was obtained with R=0.58 (± 0.04) and $\tau = 1.3$ µs. This fit, as well as a step diagram assuming mono-energetic positrons, are also shown in Fig.6.6. The smaller uncertainty on the value of R in this experiment than in the previous experiment (Fig.6.5) is due to better statistics. The data in this experiment were accumulated over 18 hours, while the data in Fig. 6.5 were accumulated over 1 hour.

When the grid switches from -5 V to +25 V, there is still a 'train' of primary beam positrons that have passed the grid but have not yet reached the sample. That means that these positrons reach the sample within 0.5 µs ($E_{e+} = 20$ eV) after the grid has switched positive though

with a possible tail up to 1 to 1.5 μs due to backscattering of these primary positrons. The annihilation of these positrons can be seen in Fig.6.6 as the high count-rate at very small times. The backscattered tail should be a fast decreasing exponential. Re-emitted positrons with an energy of 2.5 eV that are approaching the grid when the bias switches, will be sent back and reach the sample about 1.2 μs after the grid has switched positive. The last positron in this 'train' of re-emitted generation 0 positrons should then reach the sample 1.7μs later, if they all have an energy of 2.5 eV. Thus if all re-emitted positrons were mono-energetic, there would then be 0.7 μs after each generation with no positrons arriving at the sample. This is not visible in the data, except for the dip between the primary beam positrons and generation 0, thus indicating that the reemitted positrons have a rather broad energy spectrum. This was confirmed by a later retarding field measurement and was to be expected given that the surface of the foil was undoubtedly contaminated. That the lack of dips between the generations is due to a spread in the positron energies and not caused by a poor time-resolution of the detection system, can be seen from the fact that typical time resolutions for Ge counters is in the order of 0.1 μs and thus much too small to explain the observed spread.

The 20 eV experiment was fitted using an exponential for the drop off from the primary beam (0.3-1.0 μs). The reflection time regimen (3 - 20 μs) was fitted using two exponential functions of the form

$$f(t) = A \, \exp\left(\frac{\ln(R)}{2\,\tau} \, (t-3) \right) + B \, \exp\left(\frac{\ln(R')}{2\,\tau'} \, (t-3) \right) \qquad (6.2)$$

Of these two exponentials the dominant one had values R = 0.58 (± 0.04) and τ = 1.3 μs as mentioned earlier. The other exponential was fitted to values of R' and τ' of 0.40 (± 0.20) and 0.68 μs respectively. This last exponential had an amplitude of about 30 % of the total number of re-emitted positrons. That this exponential is needed in order to reproduce the data, can be seen from Fig.6.7 where the data when plotted using a logarithmic scale only fit a straight line for times larger than about 6 μs. The value for τ' corresponds to an average positron kinetic energy of about 8 eV. We therefore conclude that the part of the spectrum described by R' and τ' are caused by epithermally emitted positrons. The fact that such a contribution was not seen in the 1 keV experiment is ascribed to the fact that the fraction of epithermal positrons increases with lower incident energy as the positrons are implanted closer to the surface and thus have a greater
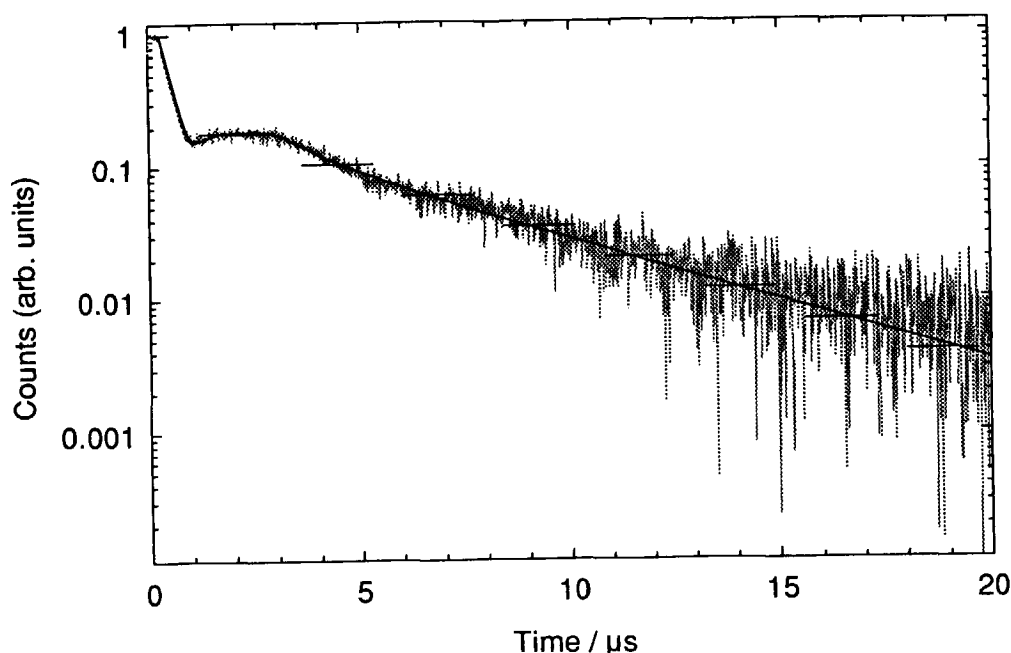
Fig.6.7. The same data as in Fig.6.6 but on a logarithmic scale.

chance of being re-emitted from the surface before they are fully thermalized. The short characteristic time, τ', and low reflection coefficient, R', for the epithermals make that contribution die off very quickly so that above 6 µs the reflection of the thermally emitted positrons is dominating.

The fact that the reflection did not disappear over time even after several days of experiments and the fact that it was also so clearly present in the POSH experiments, with the poorer vacuum conditions of that set-up, shows that the effect is very rugged. The heat treatment the foils received prior to installation, would cause the surface to be predominantly covered with oxide, since this would only leave the surface at a temperature of about 1600°C (Chen *et al.* 1985). There would probably also be traces of C diffusing to the surface from the bulk and maybe N, but the main surface contaminant is thought to be oxide. Such a coverage combined with a possible physisorption of e.g. water, would be in agreement with our results. It is noteworthy that oxygen coverage on W has been shown to increase the positron workfunction for the surface to about 4 eV, depending on the surface orientation (Wilson 1983, Fischer *et al.* 1986). This might

also explain the broad energy spectrum of the re-emitted positrons, as observed by the retarding field experiment. The extra oxide layer, possibly with minor amounts of physisorbed water, would give the emitted positrons ample opportunity to loose energy on the way out through this layer by inelastic scattering or by elastic scattering that cause the positron to be emitted into vacuum under an angle other than perpendicular. Since it is only the perpendicular velocity that is important for the observed characteristic τ value, emittance at an angle would also be observed as a spread in the energy. The average energy of 2.5 eV and large energy spread would be consistent with this, but clearly more knowledge of the details of the process could be obtained by being able to monitor and alter the surface conditions in situ.

Energy loss may also occur repeatedly during multiple reflection. Since the positrons during reflection would approach the surface very closely, this could possibly also lead to some ineleastic scattering events with loss of energy. This should lead to a gradually lower average energy for each new generation of positrons but this has not been observed in the data. This suggests that either the positrons are reflected with negligible or no loss of energy or they are lost due to annihilation after the close encounter with the surface. This annihilation can follow instantaneously or after initial trapping at the surface potential well, or after formation of positronium.

6.4. Conclusion and final remarks

We have observed reflection of very low energy positrons from the surface of tungsten where the surface is most likely covered with oxygen. This was done by monitoring the time of annihilation of re-emitted positrons after implanting 1 keV positrons into such a W sample. A reflection coefficient of 0.55 (± 0.05) was observed. In a second experiment where 20 eV positron impinged on the same surface, a reflection coefficient of 0.58 (±0.04) was observed.

We should note that our results are also in perfect agreement with the results from test experiments of our new reactor based beamline. Here the best fit to the measurements on similar foils yielded a reflection coefficient of about 0.6.

The effect demonstrated here of positron reflection off oxygen covered tungsten surfaces could be utilized to improve the overall efficiency of moderators by allowing geometries not

previously considered. It could also be used to increase the slow positron density in, e.g., atomic scattering experiments by making the positrons bounce back and forth. The effect of reflection shows good promise as an additional tool to increase the overall efficiency of positron moderators.

CHAPTER 7

THE MICROPROBE FACILITY AND THE ELECTROSTATIC POSITRON BEAM

7.1. Introduction

As mentioned in chapter one, one of the main motivations of this work has been the development and construction of a microprobe facility in connection with the new reactor based beamline (POSH) at the Interfaculty Reactor Institute of Delft University of Technology. The development and calculations on the optics for the microprobe facility, as well as a large part of the mechanical design, is described elsewhere (Seijbel 1995, Seijbel *et al.* 1995). In this chapter a brief description of the present status of the POSH beamline and the microprobe facility will be given. Special emphasis will be given to the remoderation section for the microprobe and the design changes it has undergone. The main part of this chapter will concern the design, construction and testing of an electrostatic beamline. This beamline will first be used to test the remoderation section for the microprobe and the injection into the Scanning Electron Microscope.
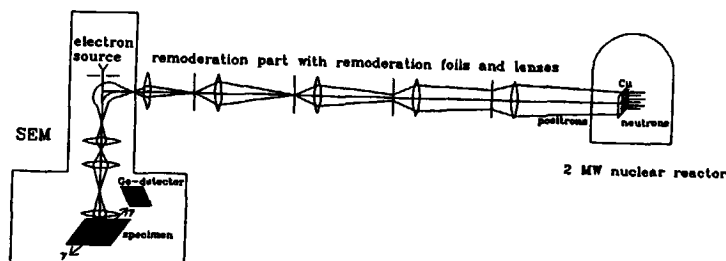
Fig. 7.1. Schematic of the setup for the positron micro-beam. Not to scale (Seijbel 1994).

7.2. A positron microprobe facility

The positron microprobe facility under construction at Delft is centered around a high current reactor based positron beam. This high current beam is converted into a high brightness beam by a 4 stage remoderation process. After injection of these positrons into a modified Philips 535M Scanning Electron Microscope (SEM) they will be used for defect studies in real scale microelectronic devices. The final beamspot is projected to be about 100 nm diameter. The energy of the positrons arriving at the sample will be tunable in the range from 0-25 keV. It is the idea to use the electrons to study the intended sample first and use them to select specific interesting spots where a depth profile can then be made by the positrons. This demands that the positrons and electrons end up in exactly the same position and that the 100 nm positron spot does not move around when the energy of the positrons is varied during the depth scan. These are not simple demands and extended testing and calibration of the facility will therefore be needed. More detailed information about the microprobe facility can be found elsewhere (Seijbel 1995, Seijbel *et al.* 1994, 1995)

7.2.1. Present status of POSH
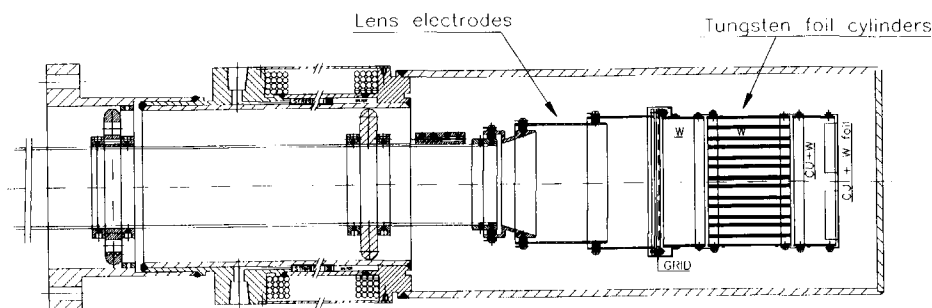
Fig. 7.2. The source end of the POSH beamline.

The POSH (POSitrons at the HOR Reactor) beamline is now nearing completion after having undergone testing in connection with the summer reactor shutdown the last three summers. On the basis of these tests several improvements to the beamline and particularly the source have been made. The original design and calculation for the beamline can be found in van Veen (1989) and van Veen *et al.* (1994, 1997).

The source design has been altered to concentrate more on positrons formed by pair creation from the hard gamma rays from the reactor core. According to calculations 90 % of the positrons in the beam now stems from pair creation and only 10 % come from neutron activated ^{64}Cu under saturation conditions. In line with this, more of the emitting surface of the source end is now made up of tungsten, which because of its higher Z is better for the gamma-pair-creation reaction. Fig. 7.2 shows a drawing of the source configuration as used for the test experiments in the summer of 1997.

The positron yield versus reactor power is shown in Fig. 7.3. The number of positrons at full power (2000 kW), including the last improvements, was found to be 8×10^7 s^{-1}, which makes it the current record holder as the most intense positron beam ever in Europe. It is expected that with improvements based on what was learned during this summers test, it should be possible to increase the yield by a factor of 3-4 putting it well above the original 10^8 positron per second target value. The insert in Fig. 7.3 shows the beam profile at the target. The beam had a FWHM
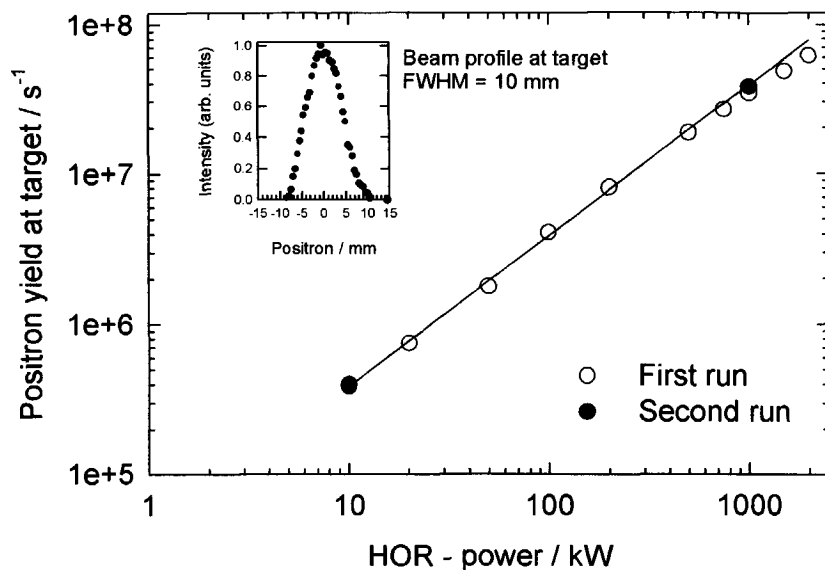
Fig. 7.3. The positron yield of the POSH beam as a function of reactor power at the last tests in Sept. 1997. The insert shows the beam profile.

of 10 mm.

A new experimental hall north of the reactor will house the positron microprobe facility and the 2D-ACAR setup for the POSH beamline, as well as new neutron facilities. This should be ready in early 1998. Fig. 7.4 shows drawing of the part of the new experimental hall where the positron microscope and Ebeam will be placed.

7.3. The remoderation section

The key component in making a high brightness microbeam is remoderation. In our setup we have opted for transmission remoderation. This will be the first time that remoderation is tried in transmission mode. This has traditionally had a lower efficiency and it has been more difficult to get good clean emitting surfaces. However, from an optics point of view it is far simpler than
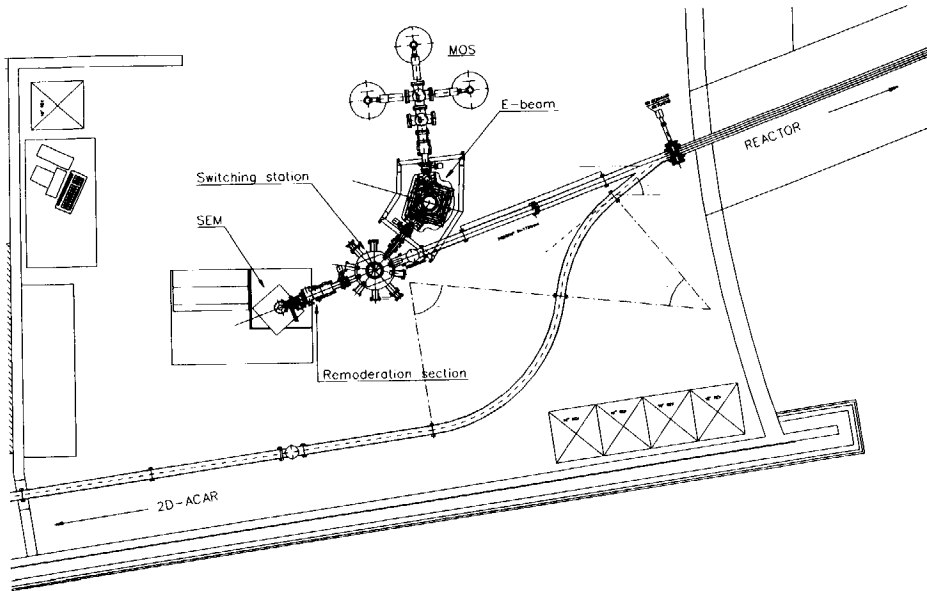
Fig. 7.4. Plan of the part of the new experimental hall containing the microprobe facility, the E-Beam and the SEM.

the backscattering geometry because the focusing optics is separated from the extraction optics. And by utilizing our new rectifier foils (see chapter 5) we hope to achieve the same or better efficiencies than has been achieved in backscattering mode. As described in Seijbel (1995) the remoderation section is about 10 cm long and will be housed inside a μ-metal vacuum chamber to avoid magnetic fields. Although the optical characteristics are still the same as in the original design (Seijbel 1995), the remoderation has been completely revised to make it more rugged and the foil mounting less bulky.

7.3.1. Design changes

The original design for the remoderation section had the lenses suspended and kept in
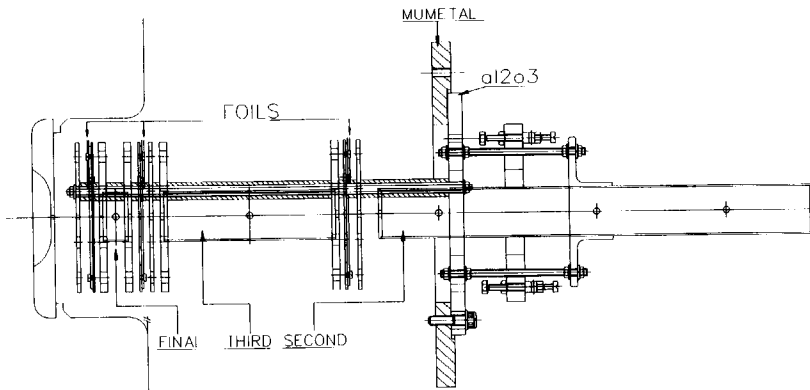
Fig. 7.5. Drawing of the new remoderation stage design.
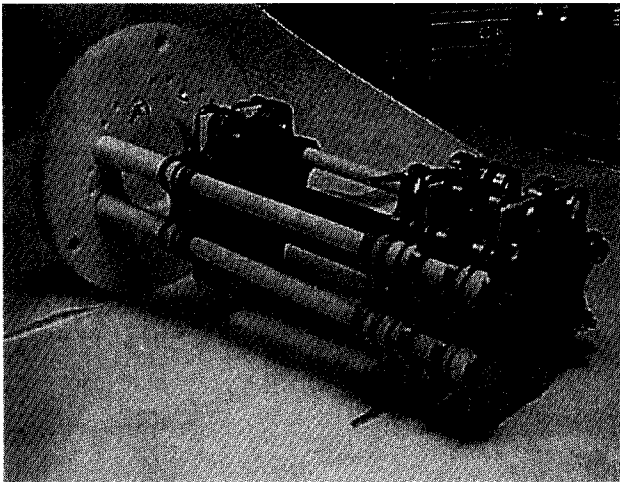
Fig. 7.6. Photo of the remoderation section. The three ceramic plates for mounting the remoderation foils can be clearly seen. Also note the small exit hole through the last lens at the front end of the remoderation stage.

place by thin glass rods. Furthermore the method for placing the thin remoderation foils was rather bulky. Therefore it was decided to make a new design based on metal and ceramic rods and standard metal plates (see Fig. 7.5 and 7.6). The same size lenses and the same distances between the lenses were used as in the original design. The carrier foils with the thin remoderation foils placed over a center hole are now placed on ceramic plates with metal clamps at either end. These metal clamps were also used as electrical connectors to the foils allowing moderate in situ resistive heating. The clamps have thick metal wires attached to the ends that are connected to high current feed-throughs. The ceramic plates with foils clamps and connectors are placed on one of the standard metal plates of the remoderation section. The remoderation section has been assembled and shown to fulfill the tolerances set by Seijbel (1995). These include the need for the lens elements to be well centered, parallel and with strict tolerances on the roundness of the lenses.

7.4. The Electrostatic Positron Beamline

In order to test the remoderation section and injection into the SEM microscope prior to installation at the POSH beamline a new electrostatic beamline (E-beam) was constructed. This beamline will later also be used for MOS studies (Metal-Oxide-Semiconductor) and surface studies. The beam uses the old radioactive source from the VEP beamline. This source had a strength of about 15 mCi when it was installed at the E-beam at the end of July 1997.

Fig. 7.7 shows a cut-up drawing of the E-beam source end and cylindrical mirror with the three ports for experimental stations. In the following subsections the design considerations for this beamline will be discussed and the testing and modeling it has already undergone will be described.

7.4.1. Design considerations

The new beamline was intended to be electrostatic. As such it is necessary to shield for magnetic fields and in particular for the earth magnetic field. This is accomplished by lining the inside of the beamline, just outside the lenses, with μ-metal. This is done all the way from the source to the remoderation section. The only distance with no μ-metal lining inside is the vacuum
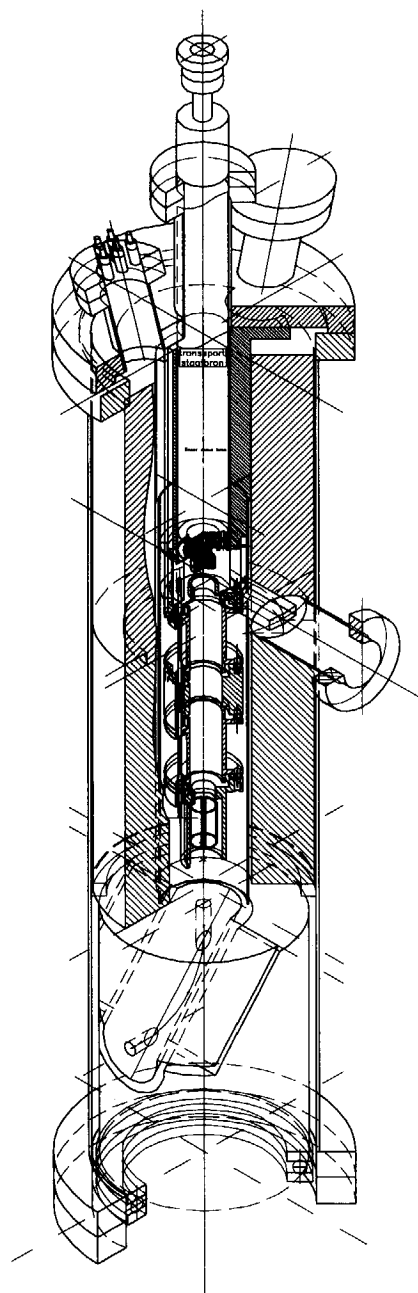
Fig. 7.7. Cut-up drawing of the source end and electrostatic mirror of the E-beam.
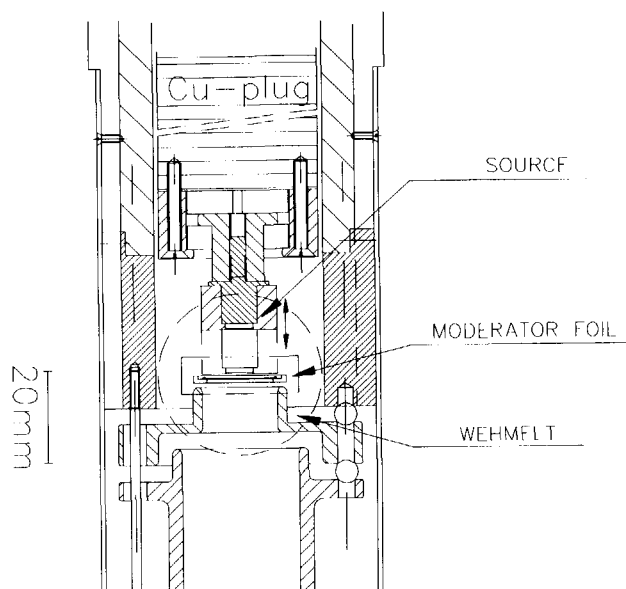
Fig. 7.8. Drawing of the source region showing the electrically isolated retractable source and the moderator foil position.

valve which covers a distance of about 2-3 cm. The source chamber has massive copper cylinders placed inside it, surrounding the electrostatic lenses. This is for radiation shielding purposes. The cylinders have groves cut in them to allow for better pumping. Additional shielding is provided by a double brick lead wall around the entire source end. The cylindrical electrostatic mirror is also made of massive copper to provide shielding from the source in the downward direction. The source is placed on a long copper rod to provide shielding above the source.

The source is electrically isolated from the copper rod. The copper rod and source are placed on a linear motion drive to allow the source to be retracted while the primary moderator foil is heated in situ (See Fig. 7.8). The primary moderator consists of a 3.5 μm thick polycrystalline tungsten foil. It can be heated in situ up to about 1200 °C by resistive heating.

SOURCE

MODERATOR FOIL

WEHMELT

DEFLECTOR PLATES
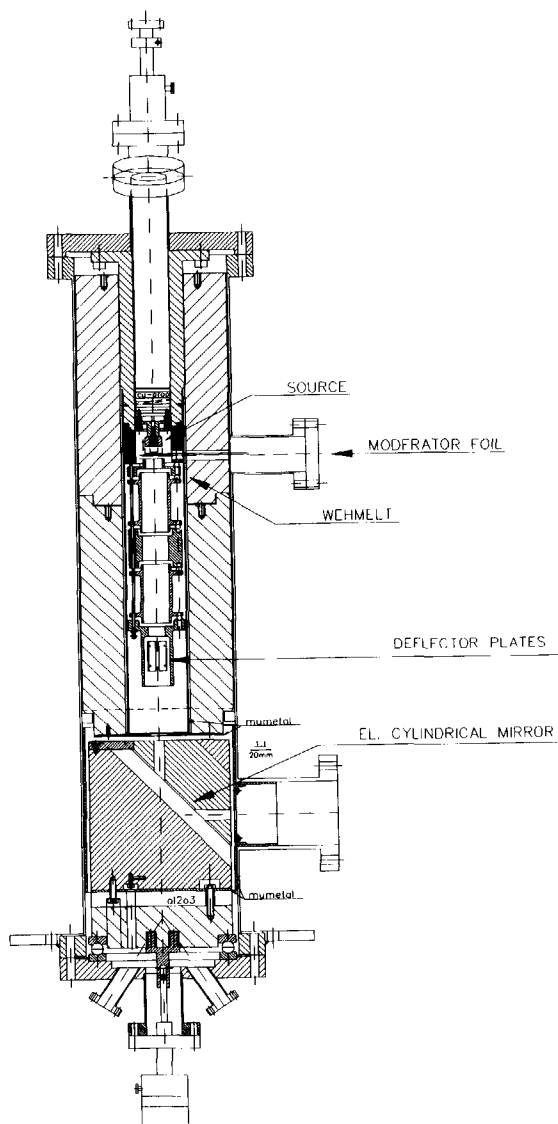
EL. CYLINDRICAL MIRROR

mumetal

1-1
20mm

mumetal

al2o3

Fig. 7.9. Drawing of the source and lenses up to the cylindrical mirror. Also shown are the massive copper cylinders for radiation shielding, the μ-metal magnetic shield, the deflection plates within the last lens and the source guidance cylinder.
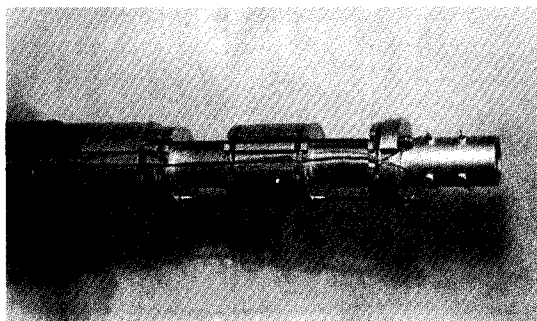
Fig. 7.10. Photo of the source end with all the lenses connected.

A configuration similar to that used by Canter (1989) is used for the extraction of the positrons from the moderator. After the source extraction there is an einzel lens to focus the positrons for the entrance of the cylindrical mirror. To provide positional fine tuning of the beam four quarter-cylinder deflection plates are positioned inside the last grounded element of the einzel lens. In this way it should be possible to get a good focusing and positioning as the positrons enter the cylindrical mirror (see Fig. 7.9). The gun and lens elements were also made of copper, but in order to avoid any charging effects of any oxides on the copper, all lens elements as well as the cylindrical mirror were gold plated (see Fig. 7.10). Also the lens elements directly after the mirror were gold plated.

The remoderated microbeam has been designed to be tunable in the energy range from 0 to 25 keV. The optics of the remoderation section is designed for an incident energy of 5 keV at each remoderation foil. This means that the POSH and, for the tests, also the E-beam should be able to deliver positrons with energies up to 40 keV at the entrance of the remoderation section. For optical reasons we have chosen for a transport energy in the E-beam of 3 keV. The entire beamline up to right before the remoderation section is electrically isolated and can be floated to 40 keV. The source end and its shielding rests on five ceramic insulators. The source region is pumped by two turbo molecular pumps that are electrically isolated from the rest of the set-up.

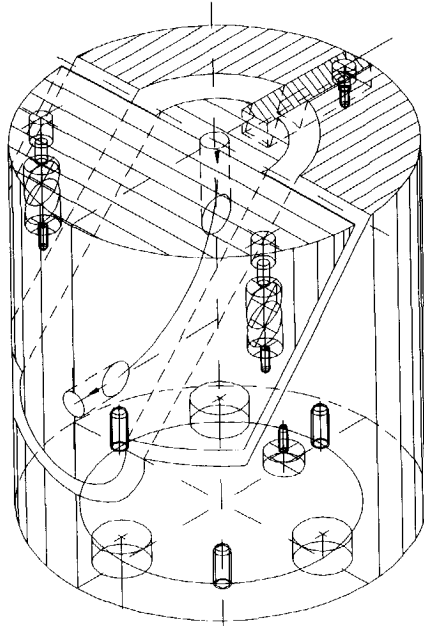The electrostatic cylindrical mirror is, as mentioned earlier, made of goldplated massive

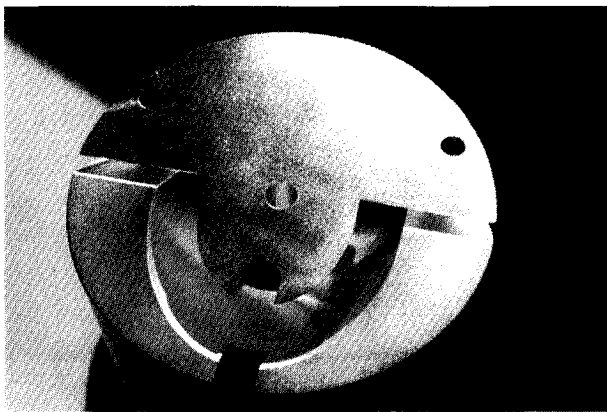Fig. 7.11. Drawing of the cylindrical electrostatic mirror.

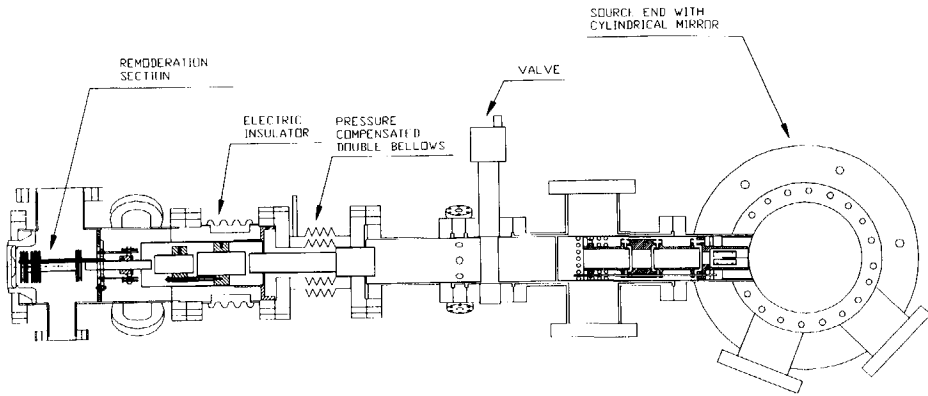Fig. 7.12. Photo of the cylindrical mirror seen from above.

Fig. 7.13. Drawing showing the lenses after the mirror and up to the remoderation section. Note the pressure compensated double bellows. Note also that the final acceleration to the relative incident energy of 5 keV for the first foil takes place directly before this foil.

copper (see Fig. 7.11 and 7.12). It rests on ball-bearings that allow the beam to be switched between three beam ports. Presently the center one of these three ports is being used to monitor the pressure in the source region. The other two are to be used for the microbeam and MOS setup, respectively. In the early phases of testing the MOS will be used for monitoring the beam quality and diagnosing the source optics. The MCP is presently attached to this station.

After the cylindrical mirror, towards the remoderation section, there is first a focusing einzel lens equal to the lens right before the mirror (see fig. 7.13). The lens element closest to the cylindrical mirror has four quarter-cylinder correction plates placed inside it to allow for corrections after exiting the mirror. After this lens, there is a manual vacuum valve. Thus the source end can be kept under vacuum while the rest of the beamline is opened up. This is an advantage not only to prolong the lifetime of the primary moderator foil, but also because the source end takes a long time to pump out properly because of the less than optimal pumping conditions caused by the massive copper cylinders and the µ-metal lining.

After the valve there are a number of transport lenses and a focusing lens right before the first foil of the remoderation section (see Fig. 7.13). In this part the floating of the beamline ends. However, internal lenses protruding through the electrical isolator and all the way to the
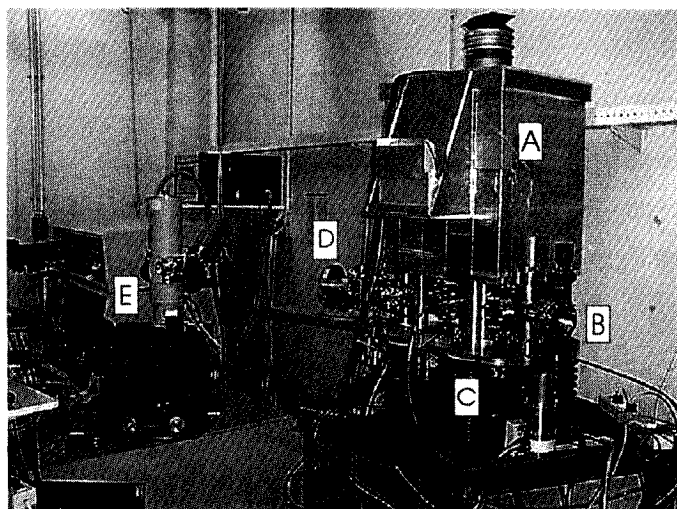
Fig. 7.14. Photo of the beamline. (A) The lead surrounding the source end. (B) Valve for one of the three beamports. (C) The high voltage insulators on which the beamline rests. (D) The beamport for the remoderation section (not mounted when the photo was taken). (E) The modified Scanning Electron Microscope with the microscope column with the valve for the microbeam mounted.

remoderation section mean that the ground potential of the beampipe should never be in view of the positrons in the beam until after the remoderation section.

In this section there is also a pressure compensated double-bellows. The pressure compensation is to keep the bellows soft while the system is under vacuum. In this way we hope to avoid vibrations from the source end (and later from the POSH) interfering with the measurements in the SEM. To further isolate the SEM mechanically from the positron beamline, a counterweight system has been designed. This will compensate the weight of the positron beamline at the entrance of the SEM and keep the SEM spring support soft. Fig. 7.14 shows the beamline as it looked in early November 1997.

The remoderation section itself will be pumped by a turbo molecular pump and the pressure in this region will be continuously monitored by an ion gauge. For the first test of the remoderation section a new small vacuum chamber has been constructed. This chamber will hold
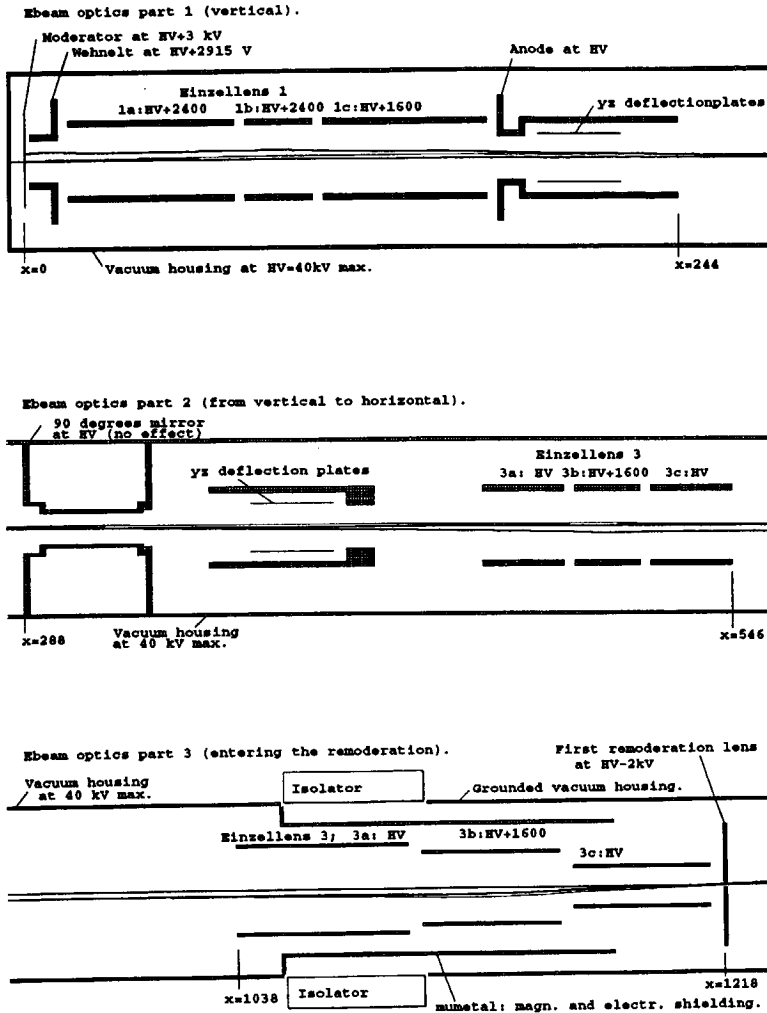
Fig. 7.15. SIMION modelling of the entire beamline showing three positron trajectories for positrons leaving the moderator 3 mm from the axis at angles of +10 degrees, 0 degrees and -10 degrees, respectively. The positrons in the simulation leave the moderator with a relative energy of 2 eV. Note in the last part how the high potential of the housing is extended beyond the isolator and all the way to the remoderation stage. The vacuum tube can be raised to 40 kV. The impact energy on the first remoderation foil has been designed to be 5 keV.
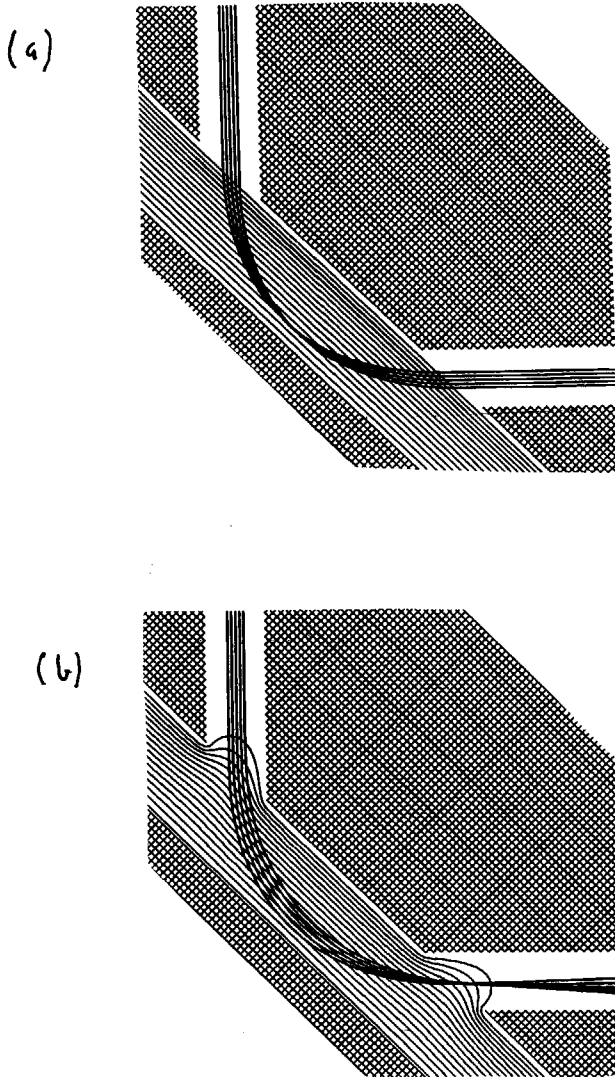
Fig. 7.16. SIMION modelling of the cylindrical mirror. (a) without field penetration and (b) with field penetration through the holes of the cylindrical mirror

a channeltron detector with three retarding grids to measure the yield of the remoderation section as well as the energy distribution of the remoderated positrons. The chamber will be pumped by a separate turbo molecular pump with an ion gauge attached. The opening of the remoderation section is only 1 mm. Therefore separate pumping is required.

7.4.2. Modelling

Prior to construction of the E-beam, the modified design underwent modelling. This was done using the SIMION modelling program for calculation of charged particle trajectories (Dahl and Delmore 1988). The modelling was done to assess the characteristics of the beamline and to find the optimum lens settings. Figure 7.15 shows a modelling calculation for the entire beamline. The modelling is two dimensional in this case so the direction of bending of the mirror is omitted. Fig. 7.16 shows a modelling of this dimension. The effect of penetration of the electric field through the holes of the mirror is shown. This could potentially cause problems to the beam quality but could be corrected by placing metal grids over the holes. This will be discussed further in the next section.

7.4.3. Tests of the E-beam

A number of test experiments have been performed on the E-beam to explore its optical qualities. These experiments were performed using the MCP positioned where the manual vacuum valve is to be. When corrected for detection efficiency a beam strength of 9×10^3 positrons per second was observed. This is close to the expected value given the present strength of the radioactive source (14 mCi). It could, however, probably be increased by further anneals of the primary moderator.

The lens settings were almost exactly as expected, based on the modelling. Intensity plots of the beam were recorded, using one of the einzel lenses after the mirror to focus the beam. In this way it was possible to get a beam spot with a horizontal width of 3.5 mm and a vertical width of 2 mm (see Fig. 7.17). Subsequent modelling has shown that the most likely cause of the non-circular beamspot is the electric field penetrating through the entrance and exits of the cylindrical mirror (see Fig. 7.16). This could perhaps be corrected by placing thin high-transmission metal
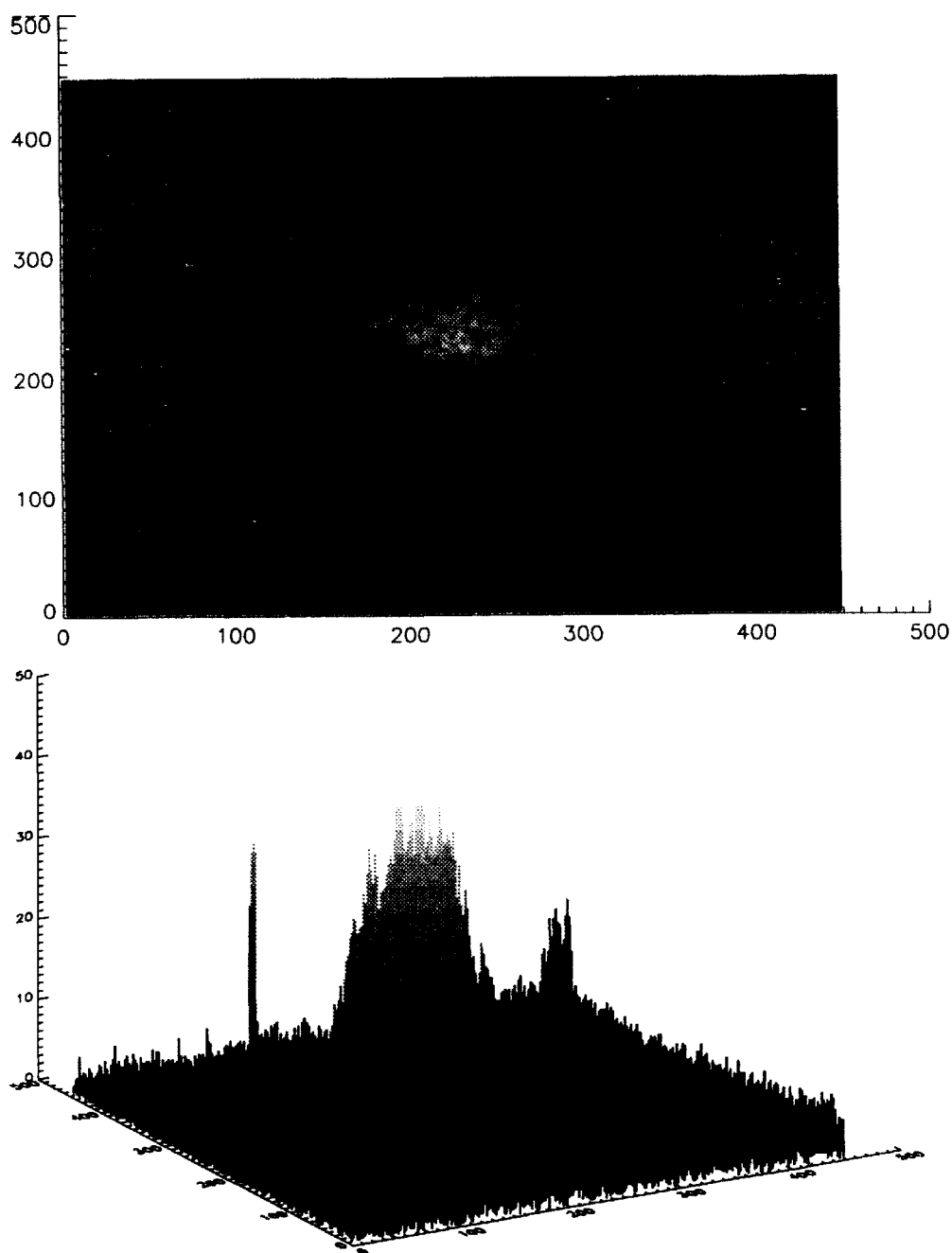
Fig. 7.17(a) The position - intensity plot of beam as recorded by the MCP and (b) contour plot of the same. Note in (a) how the grid directly in front of the MCP is visible. The center to center distance for the grid-holes is about 1 mm. The side spike in (b) is an artifact.

grids over those two openings. Fig. 7.17 also shows a situation where the beam is not in optimum focus. Here the shadow of the retarding grid in front of the MCP is clearly visible. This can also be seen in the in-focus plot, but less clearly. The center-to-center distance of the holes in that grid is 1 mm.

7.5. Conclusion and final remarks

The microprobe facility under construction at Delft is now reaching the test phase. The reactor based POSH beamline has reached an intensity of 8×10^7 positrons per second, making it the highest intensity positron beamline in Europe. An experimental hall that will house the microprobe facility is being built. The remoderation section has been redesigned. And finally a new electrostatically guided beamline has been constructed and tested. This will be used to test the remoderation stage for the microbeam in the near future.

An obvious suggestion would be to replace the original W foils in the remoderation section with W-Mo foils like the ones discussed in chapter 5. The remoderation section has been designed to have a transport energy of 5 keV. That means that the positrons after leaving one remoderation foil will be accelerated to 5 keV and inplanted in the next foil with this energy. This energy was chosen because it is the energy with the largest transmission yield when using 100 nm W foils, as the remoderation section was originally intended to use. Thus to maintain this incident energy the W-Mo foils would have to be slightly thicker than the ones studied in chapter 5, since they had a maximum transmission at an incident energy of 3.5 keV. If we assume that the transmission efficiency would be the same, we can give an estimate of the number of positrons present in the probe in this case. The best efficiency found in chapter 5 was 22 %. There will be a remoderation stage at the exit of the POSH source and three stages in the remoderation section. Using a value for the POSH intensity of 1×10^8, expected next year, and allowing for 50 % loss in transport, there should still be 1×10^5 positrons per second in the probe. This is sufficient for the experiments planned for the microprobe facility. As a matter of fact the number of positrons in the probe should not be much higher than that since the Ge detector to be used in the experiments would not be able to handle much higher annihilation rates.

We expect the countrate in the remoderation section test experiment at the E-beam, using

three W-Mo foils as remoderation foils, to be 50-100 positrons per second at the detector. These test experiments will take place shortly, pending the installation of the last lenses prior to the remoderation section.

SUMMARY

The development of brighter and more intense positron beams has been a continuous driving force in positron physics. The process of converting broadband, high energy β^+-particles into a parallel beam of slow, energy tunable positrons through implantation, slowing down and diffusing to an exit surface from which they are emitted is called moderation. Lately the necessity for higher intensity and brightness positron beams has grown if some of the promising emerging positron techniques are to become more than curiosities. The new techniques that need such improved beams are e.g. positron re-emission microscopy (PRM), low energy positron diffraction (LEPD) and three dimensional defect mapping using a positron microprobe. This last application is being pursued at the Interfaculty Reactor Institute at Delft University of Technology. In this thesis some of the possible techniques and materials that might lead to significant increases in the intensity and brightness of positron beams are investigated.

In chapter 3 field assisted moderation of positrons is discussed. In this case the implanted and thermalized positrons are drifted towards the desired exit surface by means of an electric field penetrating the solid. Many attempts have been made to achieve field assisted moderation in semiconductors. All have failed due to the difficulty in getting the positrons out past the gate/semiconductor interface which, due to the vacancy type defects present here, is usually an efficient trapping layer for the positrons. Here we avoid this pitfall by using rare gas solids (RGS) and in particular argon. An electric field is applied to this material by charging the surface. Using this method the first field assisted moderation of positrons was achieved and some of the dynamics of these systems were investigated. The experimental results for re-emission of positrons were

successfully simulated using a simple model for electric drift and energy loss.

In chapter 4 new wide bandgap semiconductors are investigated for their possible use as moderator or remoderator materials. Their possible use in field assisted moderation is also discussed. The investigations concentrate around SiC and GaN that both show very promising potential for positron moderation. The reason why wide bandgap semiconductors might prove valuable for moderation purposes is that they have the possibility of combining the two different characteristics of the two groups of materials that are presently the mainstay in moderator materials. These are epithermal diffusion as seen in the rare gas solids and efficient workfunction emission as seen in the metal moderators such as tungsten. Furthermore they should lend themselves well to field assisted moderation because of their very wide bandgap and high breakdown potentials. Both SiC and particularly GaN were shown to be fulfilling these expectations. Both were thus shown to have negative positron workfunctions and large surface branching ratios to free positrons.

In chapter 5 a method for applying internal potential barriers to positrons in metals is investigated. The internal potential step is made by utilizing the differences in positron affinity between different metals. This, like field assisted moderation, could help direct the positrons towards the desired exit surface. The internal potential barrier results in a preferred direction for the positrons in the material and the result is a positron rectifier or diode with a forward and reverse direction. This method is of particular interest in transmission remoderation because the effect of a potential step inside the metal foil would be bigger for thin foils than for thick ones. However, positron trapping at the interface between the two layers might still be a problem. We therefore chose to start by looking at W-Mo layers because of the extremely good lattice match between these two layers that should correspond to few trapping sites. An increase in the transmission yield of about a factor of two was observed and an almost complete cut-off in the reverse direction, showing that these foils do indeed work as rectifiers.

In chapter 6 a new phenomenon of very low energy positron reflection off tungsten surfaces was investigated and verified. When positrons with an energy less than the absolute value of the negative workfunction of a surface impinge on that surface from the outside they do not have enough energy to enter the solid. Previously it was thought that such positrons would simply annihilate at the surface, but the experiments described in chapter 6 show that a large fraction of them are reflected off tungsten surfaces. The reflection coefficient found was about 0.55.

Finally in chapter 7 the present status of the development and construction of a microprobe facility in connection with a reactor based beamline is reviewed. Special emphasis is devoted to the three stage remoderation section of this facility. The design and construction of a new electrostatic beamline is also discussed. The first experiments on this new beamline will be the testing of the remoderation section of the microbeam and the injection of this beam into the Scanning Electron Microscope (SEM).

SAMENVATTING

Positronmoderatie en reëmissie-experimenten

De zoektocht naar zeer heldere en intense positronenbundels is reeds lange tijd een queeste in de positronenfysica. De implantatie van hoog-energetische β^+-deeltjes in een materiaal, waarna de deeltjes afremmen en diffunderen naar een uittreeoppervlak vanwaar ze worden geëmitteerd, wordt moderatie genoemd. Hierbij wordt een breed energiespectrum van β^+-deeltjes getransformeerd naar een bundel van langzame positronen met een unieke energie. De laatste jaren vragen een aantal nieuwe technieken om intense positronenbundels met grote helderheid. Deze nieuwe technieken zijn o.a.: positron reëmissie microscopie (PRM), lage-energie positron diffractie (LEPD) en het driedimensionaal in kaart brengen van defecten door middel van een microbundel. De laatste toepassing, een positronen micro-analyse faciliteit, wordt op dit moment ontwikkeld op het Interfacultair Reactor Instituut van de Technische Universiteit Delft. In dit proefschrift staat onderzoek naar mogelijke technieken en nieuwe materialen ter verhoging van de intensiteit en helderheid van positronbundels centraal.

In hoofdstuk 3 wordt veld-geassisteerde moderatie van positronen bediscussieerd. Met deze techniek is het mogelijk om geïmplanteerde en daarna gethermaliseerde positronen door middel van een elektrisch veld naar het gewenste uittreeoppervlak toe te trekken. Vele pogingen zijn reeds ondernomen om deze techniek op halfgeleider-materialen toe te passen, deze strandden tot nu toe op de interface tussen gate en halfgeleider. Deze interface is door de aanwezige

defecten, met name vacatures, een zeer efficiënte vangsplaats voor positronen. Dit probleem wordt door ons omzeild door gebruik te maken van gecondenseerde edelgassen ("rare gas solids", RGS), in het bijzonder argon. Door het oppervlak op te laden, wordt over het RGS een elektrisch veld aangelegd. Met behulp van deze methode is de eerste veld-geassisteerde moderatie van positronen gedemonstreerd. Ook is de dynamica van dergelijke systemen onderzocht. De experimentele resultaten van reëmissie van positronen konden worden gesimuleerd met behulp van een eenvoudig model van elektrische drift en energieverlies.

In hoofdstuk 4 wordt onderzoek beschreven naar de moderatie en reëmissie eigenschappen van een aantal nieuwe halfgeleider materialen, die een grote bandkloof hebben. De mogelijkheden voor veld-geassisteerde moderatie met deze halfgeleiders materialen worden ook onderzocht. Met name GaN en SiC blijken veelbelovend te zijn als moderatiemateriaal. De karakteristieke eigenschappen van de twee klassen van de huidige generatie moderatiematerialen komen in deze halfgeleiders samen: de epithermische diffusie van positronen van de gecondenseerde edelgassen en de, door hun hoge (negatieve) werkfunctie voor positronen, efficiënte emissie van positronen uit metalen zoals wolfraam. De hoge doorslagweerstand en zeer grote bandkloof van zowel SiC als GaN maken deze materialen ook geschikte kandidaten voor het gebruik bij veld-geassisteerde moderatie. De beide materialen vertonen een negatieve werkfunctie voor positronen en tevens tredt een hoog percentage van het aantal positronen dat het oppervlak bereikt ook daadwerkelijk uit als vrije positronen.

In hoofdstuk 5 worden experimenten gepresenteerd, waarbij interne potentiaalbarrières voor positronen in metalen worden aangelegd. Deze stap in de potentiaal wordt aangelegd door gebruik te maken van het verschil in positronaffiniteit van verschillende materialen. Dit zou, analoog aan de veld-geassisteerde moderatie, kunnen helpen om de positronen naar een gewenst oppervlak te laten diffunderen. De interne potentiaalbarrière in het materiaal resulteert in een voorkeurs-richting voor de positronen en fungeert zo als een positrongelijkrichter ofwel als een diode met een sper- en doorlaatrichting voor positronen. Omdat het effect van de potentiaalstap groter is voor dunnere folies dan voor dikke, is deze methode is in het bijzonder geschikt voor transmissiemoderatie. Vangst van de positronen aan het grensvlak tussen de verschillende materialen zou nog steeds een probleem kunnen zijn en daarom is begonnen met een W-Mo systeem. Deze lagen sluiten qua roosterconstante extreem goed op elkaar aan, wat zou moeten resulteren in weinig vangstplaatsen voor positronen. Het werken met een materiaal met een

interne potentiaalbarrière heeft een verhoging van de positronentransmissie met een factor twee tot gevolg, terwijl het omdraaien van het systeem een transmissie van vrijwel nul geeft. Dit toont aan dat het systeem inderdaad kan worden gezien als een positrongelijkrichter.

Een nieuw fenomeen waarbij positronenreflectie werd gevonden van zeer-laag-energetische positronen aan wolfraam oppervlakken wordt in hoofdstuk 6 onderzocht en geverifieerd. Als positronen met een energie van minder dan de absolute waarde van de werkfunctie van wolfraam het oppervlak treffen, hebben ze niet voldoende energie om het metaal binnen te dringen. Tot voor kort werd verondersteld dat deze positronen simpelweg annihileren aan het oppervlak. De hier gepresenteerde experimenten tonen echter een reflectie-coëfficiënt van 0,55 van de positronen aan het oppervlak aan.

Uiteindelijk wordt in hoofdstuk 7 de huidige status en de ontwikkeling besproken van een microbundel faciliteit, waarvoor de primaire intense positronenbundel opgewekt wordt bij de kern van de onderzoeks kernreactor anwezig bij de Interfacultair Reactor Instituut. De nadruk wordt gelegd op de drie-staps remoderatiesectie van deze opstelling. Het ontwerp en constructie van een nieuwe elektrostatische positronenbundel, o.a. gebouwd om de microbundel te testen worden ook beschouwd. De eerste experimenten aan deze bundel zullen het testen van de remoderatiesectie van de microbundel en het injecteren van deze bundel in een scanning elektronen microscoop (SEM) zijn.

REFERENCES

Aers, G.C., P. A. Marshall, T. C. Leung and R. D. Goldberg, Appl. Surf. Sci. **85**, 196 (1995)

Anderson, C. D., Science **76**, 238 (1932a)

Anderson, C. D., Phys. Rev. **41**, 405 (1932b)

Anderson, C. D., Phys. Rev. **43**, 491 (1933)

Asoka-Kumar, P., K. G. Lynn and D. O. Welch, J. Appl. Phys. **76**, 4935 (1994)

Asoka-Kumar, P., M. Alatalo, V. J. Ghosh, A. C. Kruseman, B. Nielsen, and K. G. Lynn, Phys. Rev. Lett. 77, 2097 (1996)

Baker, J. A., N. B. Chilton, K. O. Jensen, A. B. Walker and P. G. Coleman, J. Phys.:Condens. Matter **3**, 4109 (1991a)

Baker, J. A., N. B. Chilton, K. O. Jensen, A. B. Walker and P. G. Coleman, Appl. Phys. Lett. **59**, 2962 (1991b)

Beling, C. D., R. I. Simpson, M. Charlton, F. M. Jacobsen, T. C. Griffith, P. Moriarty and S. Fung, Appl. Phys. A **42**, 111 (1987)

Bellotti, E., M. Corti, E. Fiorini, C. Luguori, A. Pullia, A. Sarracino, P. Sverzellati, and L. Zanotti, Phys. Lett. B **124**, 435 (1983)

Brandes, G. R., A. P. Mills, Jr. and D. M. Zuckerman, Mater. Sci. Forum **105-110**, 1363 (1992)

Brandes, G. R., K. F. Canter, A. Krupyshev, R. Xie, and A. P. Mills, Jr., presented at The 11th International Conference on Positron Annihilation (ICPA-11), Kansas City, May 25-30 1997, Conf. Proc.to be published in Mat. Sci. Forum (1997)

Brandt, W., Lett. Nuovo Cimento **33**, 499 (1982)

Brandt, W., and R. Paulin, Phys. Rev. B **15**, 2511 (1977)

Brauer, G., W. Anwand, E. M. Nicht, J. Kuriplach, M. Šob, N. Wagner, P. G. Coleman, M. J. Puska and T. Korhonen, Phys. Rev. B **54**, 2512 (1996)

Brauer, G., W. Anwand, E. M. Nicht, P. G. Coleman, N. Wagner, H. Wirth, and W. Skorupa, Appl. Surf. Sci. **116**, 19 (1997)

Britton, D. T., P. A. Huttunen, J. Mäkinen, E. Soininen, and A. Vehanen, Phys. Rev. Lett. **62**, 2413 (1989)

Brown, B. L., W. S. Crane, and A. P. Mills, Jr., Appl. Phys. Lett. **48**, 739 (1986)

Canter, K. F., P. G. Coleman, T. C. Griffith and G. R. Heyland, J. Phys. B **5**, L167 (1972)

Canter, K. F., G. R. Brandes, T. N. Horsky, P. H. Lippel, and A. P. Mills, Jr., in *Atomic Physics with Positrons*, edited by J. W. Humberston and E. A. G. Armour (Plenum Press, New York, N. Y.) p. 153 (1987)

Canter, K. F., G. R. Brandes, T. N. Horsky, P. H. Lippel, and A. P. Mills, Jr., in "Positron Annihilation", Proc. of the 8th Int. Conf. on Positron Annihilation, Ghent 1988, Eds. L. Dorikens-Vanpraet, M. Dorikens, and D. Segers, World Scientific, Singapore, p. 18 (1989)

Charlton, M., R. A. Cullen, J. Raza and M. S. T. Watts, J. Phys. B: At. Mol. Opt. Phys. **25**, 4351 (1992)

Chen, D. M., K. G. Lynn, R. Pareja and B. Nielsen, Phys. Rev. B **31**, 4123 (1985)

Cherry, W., Ph.D. dissertation, Princeton University, USA, unpublished (1959)

Clement, M., J. M. M. de Nijs, A. van Veen, H. Schut and P. Balk, IEEE Trans. Nucl. Sci. **42** 1717 (1995)

Clement, M., J. M. M. de Nijs, P. Balk, H. Schut, and A. van Veen, J. Appl. Phys. **79**, 9029 (1996)

Coleman, P. G., L. Albrecht, K. O. Jensen and A. B. Walker, J.Phys.: Condens. Matter **4**, 10311 (1992)

Dahl, D. A., and J. E. Delmore, "The SIMEON PC/PS2 User's Manual", Idaho National Engineering Laboratory, Idaho Falls, U.S.A. (1988)

Deutch, B. I., M. Charlton, M. H. Holzscheiter, P. Hvelplund, L. V. Jørgensen, H. Knudsen, G. Laricchia, J. P. Merrison and M. R. Poulsen, Proc. Antihydrogen Workshop, Munich 1992, Hyp. Int. **76**, 153 (1993)

Deutsch,M., Phys. Rev. **82**, 455 (1951)

Dirac, P. A. M., Proc. Roy. Soc. **A126**, 360 (1930a)

Dirac, P. A. M., Proc. Camb. Phil. Soc. **26**, 361 (1930b)

Dupasquier, A., in *"Positron Solid-State Physics"*, Proc. of the International School of Physics Enrico Fermi, Course LXXXIII, North-Holland, Amsterdam, eds. W. Brandt and A. Dupasquier, p.510 (1981)

Dupasquier, A., and A. P. Mills, Jr., Editors, Proc. of the Int. School of Physics "Enrico Fermi", Course CXXV: *'Positron Spectroscopy of Solids'*, Varenna, Italy 6 -16 July 1993 (IOS Press, Amsterdam) (1995)

Fischer, D. A., K. G. Lynn, and D. W. Gidley, Phys. Rev. B **33**, 4479 (1986)

Ghosh, V. J., K. G. Lynn and D. O. Welch, in *Positron Spectroscopy of Solids*, Proc. of the International School of Physics Enrico Fermi, Course CXXV, July 1993, Eds. A. Dupasquier and A. P. Mills, Jr. (IOS Press, Amsterdam) p. 683 (1995)

Gidley, D. W., and W. E. Frieze, Phys. Rev. Lett. **60**, 1193 (1988)

Gullikson, E. M., and A. P. Mills Jr, Phys. Rev. Lett. **57**, 376 (1986)

Gullikson, E. M., A. P. Mills, Jr. and E. G. McRae, Phys. Rev. B **37**, 588 (1988)

Gullikson, E. M., A. P. Mills, Jr. and C. A. Murray, Phys. Rev. B **38**, 1705 (1988)

Gullikson, E. M., and B. L. Henke, Phys. Rev. B **39**, 1 (1989)

Hautojärvi, P., J. de Physique IV, C1-3 (1995)

Howell, R. H., T. E. Cowan, J. Hartley, P. Sterne, and B. Brown, Appl. Surf. Sci. **116**, 7 (1997)

Jääskelääinen, J., T. Laine, K. Fallström, K. Saarinen, and P. Hautojärvi, Appl. Surf. Sci. **116**, 73 (1997)

Jacobsen, F. M., and K. G. Lynn, Phys. Rev. Lett. **76**, 4262 (1996)

Jensen, K. O., A. B. Walker, and N. Bouarissa, in *Positron Beams for Solids and Surfaces*, edited by P. J. Schultz, G. Massoumi and P. J. Simpson (AIP, New York) p. 17 (1990)

Jørgensen, L. V., J. P. Merrison, B. I. Deutch, M. Charlton and G. O. Jones, Phys. Rev. B **52** 12402 (1995)

Jørgensen, L. V., A. C. Kruseman, H. Schut, A. van Veen, M. Fanciulli, and T. D. Moustakas, Mat. Res. Soc. Symp. Proc. **449**, 853 (1997)

Khatri, R., M.Charlton, P. Sferlazzo, K. G. Lynn, A. P. Mills Jr. and L. O. Roellig, Appl. Phys. Lett. **57**, 2374 (1990)

Kruseman, A. C., H. Schut, A. van Veen, P. E. Mijnarends, M. Clement, and J. M. M. de Nijs, Appl. Surf. Sci. **116**, 192 (1997)

Liu, D. C., and W. K. Roberts, Phys. Rev. **132**, 1633 (1963)

Lynn, K. G., J. R. MacDonald, R. A. Boie, L. C. Feldman, J. D. Gabbe, M. F. Robbins, E. Bonderup, and J. Golovchenko, Phys. Rev. Lett. **38**, 241 (1977)

Lynn, K. G., and B. T. A. McKee, Appl. Phys. **19**, 247 (1979)

Lynn, K. G., P. J. Schultz, and I. K. MacKenzie, Solid State Commun. **38**, 473 (1981)

MacKenzie, I. K., C. W. Shulte, T. Jackman, and J. L. Campbell, Phys. Rev. A **7**, 135 (1973)

Madanski, L., and F. Rasetti, Phys. Rev. **79**, 397 (1950)

Madey, J. M. J., Phys. Rev. Lett. **22**, 784 (1969)

Mäkinen, J., S. Palko, J. Martikainen and P. Hautojärvi, J. Phys.: Condens. Matter **4**, L503 (1992)

Marder, S., V. W. Hughes, C. S. Wu and W. Bennett, Phys. Rev. **103**, 1258 (1956)

Marsolais, R. M., and L. Sanche, Phys. Rev. B **38**, 11118 (1988)

Matthews, J. W., J.Vac.Sci.Technol. **12**, 126 (1975)

Merrison, J. P., M. Charlton, B. I. Deutch and L. V. Jørgensen, J. Phys.: Condens. Matter **4**, L207 (1992)

Merrison, J. P., M. Charlton, B. I. Deutch and L. V. Jørgensen, in Proceedings of the Antihydrogen Workshop, Munich, July 1992 (ed. J. Eades), Hyp. Int. **76**, 305 (1993)

Merrison, J. P., H. Bluhme, J. Chevallier, B. I. Deutch, P. Hvelplund, L. V. Jørgensen, H. Knudsen, M. R. Poulsen, and M. Charlton, Phys. Rev. Lett. **78**, 2728 (1997)

Mills, A. P., Jr., Appl. Phys. **23**, 189 (1980)

Mills, A. P., Jr., Phys. Rev. Lett. **46**, 717 (1981)

Mills A. P., Jr and E. M. Gullikson, Appl. Phys. Lett. **49** 1121 (1986)

Mills, A. P., Jr., in Proc. of the Int. School of Physics "Enrico Fermi", Course CXXV: *'Positron Spectroscopy of Solids'*, Varenna, Italy 6 -16 July 1993, Eds. A. Dupasquier and A. P. Mills, Jr. (IOS Press, Amsterdam) (1995)

Mohorovicic, S., Astron. Nachr. **253**, 94 (1934)

Morkoç, H., S. Strite, G. B. Gao, M. E. Lin, B. Sverdlov and M. Burns, J. Appl. Phys. **76**, 1363 (1994)

Moustakas, T. D., and R. J. Molnar, Mat. Res. Soc. Symp. Proc. **281**, 753 (1993)

Nakamura, S., Solid State Comm. **102**, 237 (1997)

Nakamura, S., M. Senoh, S. Nagahama, N. Iwasa, T. Yamada, T. Matsushita, Y. Sugimoto, and H. Kiyoku, Appl. Phys. Lett. **70**, 1417 (1997)

Nielsen, B., K. G. Lynn, A. Vehanen and P. J. Schultz, Phys. Rev. B **32**, 2296 (1985)

Nieminen, R. M., and J. Oliva, Phys. Rev. B **22**, 2226 (1980)

Ore, A., and J. L. Powell, Phys. Rev. **75**, 1696 (1949)

Petkov, M. P., K. G. Lynn, L. O. Roellig, and T. D. Troev, Appl. Surf. Sci. **116**, 13 (1997)

Ponce, F. A., and D. P. Bour, Nature **386**, 351 (1997)

Poulsen, M. R., M. Charlton, J. Chevallier, B. I. Deutch, L. V. Jørgensen and G. Laricchia, J. Phys.: Condens. Matter **3**, 2849 (1991)

Poulsen, M. R., G. Laricchia, M. Charlton, K. O. Jensen and A. B. Walker, Mat. Sci. Forum **105-110**, 1431 (1992)

Puska, M. J., P. Lanki and R. M. Nieminen, J. Phys.: Condens. Matter **1**, 6081 (1989)

Puska, M. J., and R. M. Nieminen, Rev. Mod. Phys. **66**, 841 (1994)

Ruark, A. E., Phys. Rev. **68**, 278 (1945)

Saarinen, K., T. Laine, S. Kuisma, J. Nissilä, P. Hautojärvi, L. Dobrzynski, J. M. Baranowski, K.

Pakula, R. Stepniewski, M. Wojdak, A. Wysmolek, T. Suski, M. Leszczynski, I. Grzegory, and S. Porowski, Phys. Rev. Lett. **79**, 3030 (1997)

Sanche, L., and M. Deschenes, Phys. Rev. Lett. **61**, 2096 (1988)

Schrader, D. M., A. Loewenschuss, J. Y. Jean, K. Nakamoto and B. D. Pollard in "Positron Annihilation", Proc. of the 6th International Conference on Positron Annihilation, eds. P. G. Coleman, S. C. Sharma and L. M. Diana, North Holland, Amsterdam, p.657 (1982)

Schultz, P. J., and K. G. Lynn, Phys. Rev. B **26**, 2390 (1982)

Schultz, P. J., and K. G. Lynn, Rev. Mod. Phys. **60**, 701 (1988)

Schut, H., Ph. D. Dissertation, Delft University of Technology, Delft (1990).

Schut, H., A. van Veen, B. Nielsen, and K. G. Lynn, in *International Workshop on Slow Positron Beam Techniques for Solid State and Surface Studies*, University of East Anglia, Norwich, U. K., July 7-10, 1986, unpublished

Schwinberg, P. B., R. S. Van Dyck, Jr. and H. G. Dehmelt, Phys. Lett. **81A**, 119 (1981)

Seijbel, L. J., Ph. D. Dissertation, Delft University of Technology, Delft (1995)

Seijbel, L. J., P. Kruit, J. E. Barth, A. van Veen, and H. Schut, *"Slow Positron Beam Techniques for Solids and Surfaces"*, AIP Conf. Proc. **303** (American Institute of Physics, New York) p.502 (1994)

Seijbel, L. J., R. F. J. Neelissen, P. Kruit, A. van Veen, and H. Schut, Appl. Surf. Sci. **85**, 92 (1995)

Shan, Y. Y., H. L. Au, C. C. Ling, T. C. Lee, B. K. Panda, S. Fung, C. D. Beling, Y. Y. Wang and H. M. Weng, Appl. Phys. A **59**, 259 (1994)

Simpson, R. I., M. G. Stewart, C. D. Beling and M. Charlton, J. Phys.: Condens. Matter **1**, 7251 (1989)

Störmer, J., A. Goodyear, W. Anwand, G. Brauer, P. G. Coleman and W. Triftshäuser, J. Phys.: Condens. Matter **8**, L89 (1996)

Tong, B. Y., Phys. Rev. B **5**, 1436 (1972)

Triftshäuser, G., G. Kögel, W. Trifthäuser, M. Springer, B. Strasser, and K. Schreckenbach, Appl. Surf. Sci. **116**, 45 (1997)

Uedeno, A., S. Tanigawa, H. Funamoto, A. Nishikawa and K. Takahashi, Jpn. J. Appl. Phys. **29**, 555 (1990)

Uhlmann, K., W. Triftshäuser, G. Kögel, P. Sperr, D. T. Britton, A. Zecca, R. S. Brusa and G. Karwasz, Fresenius J. Anal. Chem. **353**, 594 (1995)

Valkealahti, S., and R. M. Nieminen, Appl. Phys. A **35**, 51 (1984)

van de Walle, C. G., and J. Neugebauer, Mat. Res. Soc. Symp. Proc. **449**, 861 (1997)

van Veen, A., POSH, Internal Report IRI-131-89-01, unpublished (1989)

van Veen, A., J. Trace and Microprobe Techniques **8**, 1 (1990)

van Veen, A., H. Schut, J. de Vries, R .A. Hakvoort and M. R. IJpma in: Positron Beams for Solids and Surfaces, AIP Conf. Proc. vol. **218**, eds. P. J. Schultz, G. R. Massoumi, and P. J. Simpson (AIP, New York, 1990) p. 171

van Veen, A., H. Schut, P. E. Mijnarends, L. Seijbel and P. Kruit, *"Slow Positron Beam Techniques for Solids and Surfaces"*, AIP Conf. Proc. **303** (American Institute of Physics, New York) p.354 (1994)

van Veen, A., H. Schut, M. Clement, J. M. M. de Nijs, A. Kruseman and M. R. Ijpma, Appl. Surf. Sci. **85**, 216 (1995)

van Veen, A., F. Labohm, H. Schut, J. de Roode, T. Heijenga, and P. E. Mijnarends, Appl. Surf. Sci. **116**, 39 (1997)

Vasumathi, D., G. Amarendra, K. F. Canter, and A. P. Mills, Jr., Appl. Surf. Sci. **85**, 154 (1995)

Vehanen, A., K. Saarinen, P. Hautojärvi and H. Huomo, Phys. Rev. B **35**, 4606 (1987)

Walker, A. B., K. O. Jensen, J. Szymanski, and D. Neilson, Phys. Rev. B **46**, 1687 (1992)

Weyl, H., 2nd edition, Gruppentheorie und Quantenmechanick, p.234 (1931)

Wheeler, J. A., Ann. N. Y. Acad. Sci. **48**, 219 (1946)

Wilson, R. J., Phys. Rev. B **27**, 6974 (1983)

Wolfenstein, L., and D. G. Ravenhall, Phys. Rev. **88**, 279 (1952)

Wyckoff, R.W. G., *Crystal Structures*, vol **1**, J. Wiley and Sons, New York (1965)

Xiong, Q., H. Schut and A. van Veen, to be published

ACKNOWLEDGEMENTS

around the VEP bunker. And though they all seemed to leave me behind in the dug-out little by little (and in the end even I left for the comfort of the main building!) they were instrumental in creating a very nice surrounding (the nice view added to that as well!!). I am very grateful to Marten and Bram for all the nice physics discussions (and discussions about just about anything else) we had in those days. I also enjoyed the help and wit of Karl Roos. He is largely responsible for the drawings shown in chapter 7.

During the work with the new electrostatic beamline I also worked extensively with August Winkelman. I enjoyed the cooperation very much and also the f act that he could usually be persuaded to have a beer with me in the IRI-bar. Also it was nice to work with someone NEARLY my own size. A very special thanks should also go to Olof Dankert and Alexander Fedorov for being slightly interested in what I was doing and showing me some interesting things that can be done with vacuum equipment.

Also a thanks to Peter Mijnarends for helping out with some theory and suggestions for interpretations of our data and especially for correcting some of my grammatical errors. Kees Westerduin was always helpful with a comment and occasionally could be persuaded to have a beer in the IRI-bar. Also a thanks to the many people in and around the institute that were always helpful, interested and/or encouraging. I has been nice working with you all.

I have been fortunate during my thesis work to collaborate with many people, also from outside Delft. The part of this thesis concerning rare gas solids was done during my time at the University of Aarhus in Denmark in close collaboration with Jon Merrison and the late Bernie Deutch. The work done there also for a large part involved Mike Charlton and Mogens Rysholt Poulsen. Invaluable technical help was provided by Poul Aggerholm and Knud Aage Haahr Mortensen.

A very special thanks should also go to Jacques Chevallier, who have made the Ag, W and WMo foils I have used for many of the experiments. He was also usually keen to discuss the finer things in life. He put me in contact with Marco Fanciulli, which in turn started off first the work on GaN and the contacts to Ted Moustakas at Boston University and later the work on $Fe_{0.5}Si$ and $Si_{1-x}Sn_x$ in collaboration with Arne Nylandsted Larsen and Gerd Weyer, also at Aarhus.

A long series of interesting experiments on the morphology and growth of $FeSi_2$ was performed in collaboration with Peter Henk Amesz and Jeff de Hosson at the University of Groningen. It was a great pleasure to work with them and they taught me many new and

interesting things about growth mode and methods.

There have been collaborations also with Simon van der Zwaags group at Materials Science and several others. I enjoyed the wide range of materials and methods and all the interesting people I met through these contacts. They all made my work more challenging and fun!

I would also like to thank all the friends (or acquaintances, as some prefer to be called) that were there for a night out when that was needed. Especially I would like to mention the United Nations, Delft Branch. With a profusion of clubs (UNRC, UNBC, TVFC, etc.) and general merriment they succeeded to get the raft swinger out in me! Also the Uncles and all my other friends in Denmark and elsewhere that helped make it all bearable are happily acknowledged. A very special thanks also to Marion for helping to prepare this manuscript for the printer. I am not sure I would have gotten through it without your help.

I am lucky to have a rather large and close knitted family. And though the distances were often large and the phone bills equally so, I always looked (and am still looking) forward to our annual summer vacation together and all the other get-togethers. Always a great occasion to catch up with things and crawl around on the floor with the kids.

Thanks all.

CURRICULUM VITAE

The author of this thesis was born in Bramdrup near Kolding in Denmark on March 3, 1965. Between 1971 and 1982 he received his primary education from a number of fine schools in the eastern and southern part of Jutland, Denmark. During 1982-83 he went to high school in the U.S. and graduated from Eastern High School in Greentown, Indiana. After returning to Denmark he started on Højere Forberedelseskursus, first at Kolding Gymnasium but for the most part at Rosborg Gymnasium in Vejle. He passed the Højere Forberedelseseksamen in 1985 and started taking Gymnasiale Supplerings Kurser in Physics, Mathematics and Chemistry at Riiskov Amtsgymnasium on the outskirts of Aarhus. In 1986 he started studying physics and mathematics at the University of Aarhus. By 1990 he had obtained a B.Sc. in physics and a B.Sc. in mathematics. At the end of 1993 he got his Cand. Scient. degree in experimental physics. He held a position teaching physics and mathematics at Skanderborg Amtsgymnasium for the first half of 1994. From November 1 1994 to November 1 1997 he was employed as a Ph.D. student at the Interfaculty Reactor Institute at Delft University of Technology in the Netherlands. Some of the fruits of that labor can be found in this thesis.